AD-A162 019 CONTRIBUTIONS TO THE OCEANOGRAPHY OF THE WESTERN ALBORAN SEA(U) NAVAL OCEAN RESEARCH AND DEVELOPMENT ACTIVITY NSTL STATION MS R ARNONE ET AL APR 85 1/2

UNCLASSIFIED NORDA-TN-315 F/G 8/3 NL

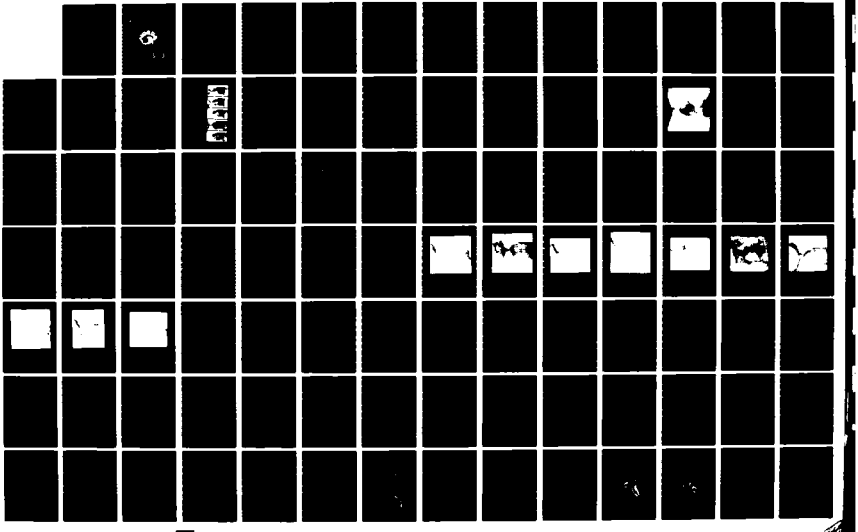

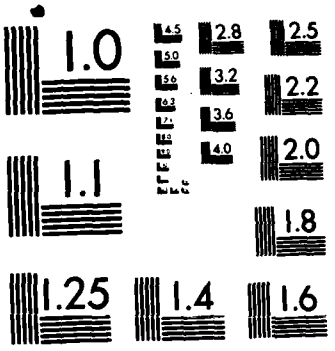

(12)

NORDA Technical Note 315

Naval Ocean Research and Development Activity
NSTL, Mississippi 39529

Contributions to the Oceanography of the Western Alboran Sea

April 1985

CONTRIBUTIONS TO
THE OCEANOGRAPHY OF THE WESTERN ALBORAN SEA

A Selection of Papers Presented at

The XXIXth Congress and Plenary Session of

The International Commission for the Scientific Exploration of

The Mediterranean Sea

Lucerne, Switzerland
October 11-19, 1984

by

R. Arnone (1)
R. Barcala (2)
G. Dawson (1)
R. Fiedler (3)
G. Heburn (1)
T.H. Kinder (1)
P. La Violette (1)
B.E. McDonald (1)
G. Parrilla (4)
H. Perkins (1)
S.A. Piacsek (1)
H. van der Piepen (3)
J.S. van der Piepen (3)
The Donde Va Group (5)

Henry Perkins, Editor

(1) Naval Ocean Research and Development Activity, NSTL, Miss., USA
(2) Deutsche Forschungs- und Versuchsanstalt fur Luft- und Raumfahrt, Oberpfaffenhofen, Federal Republic of Germany
(3) Instituto Nacional de Technica Aerospacial, Madrid, Spain
(4) Instituto Espanol de Oceanografia, Madrid, Spain
(5) Members of the Donde Va Group are listed on page 22

PREFACE

This volume includes papers presented during the XXIXth Congress and Plenary Assembly of the International Commission for the Scientific Study of the Mediterranean Sea (CIESM) in Lucerne, Switzerland, October 11-19, 1984. The authors are a loose association of scientists from the Donde Va? project and from NORDA. The papers will also be reported in the Rapports et Process-Verbaux of CIESM, where they will be condensed to meet the prescribed two-page limit of that report. Their format here is enlarged primarily by the inclusion of the figures that accompanied the original presentations.

Recent activities in the Mediterranean included the international Donde Va? experiment in 1982, which focused on the Alboran Sea gyre. The extensive data collected at that time have now undergone preliminary processing and form the basis for a number of papers, including the first five in the present collection. Further exploitation of this data is still underway, as is development of the numerical studies associated with it.

A number of studies are presently planned for the Mediterranean. Observational efforts will reach a peak in 1986, and analysis and modeling will likely continue through the end of the decade. The total list of planned work is impressive: multinational, multidisciplinary programs are scheduled in the Eastern and in the Western Mediterranean Basins; a comprehensive study of the Strait of Gibraltar will be supported by ONR; and continuing NORDA programs (Chemical Fronts, Fine Scale Variability) anticipate component programs in the Western Mediterranean. The final three papers presented here are the first of NORDA's contributions to these programs.

Present emphasis on the Mediterranean reflects its importance in international affairs and its value as a natural laboratory where the same physical processes that control the large ocean basins may be conveniently studied. The present volume is thus a small step toward a grand objective. In this spirit, we submit it to our colleagues and our sponsors.

The Editor

Contents:

DONDE VA? AN OCEANOGRAPHIC EXPERIMENT IN THE ALBORAN SEA

The Donde Va Group

This article appeared in
the Ocean Report, EOS, 65, 682-684
September 4, 1984

INTRODUCTION

During June-October 1982 an international consortium of oceanographers (see Table) studied the circulation of the western Alboran Sea in an experiment entitled "Donde Va?". Although the English translation of this title is "Where does it go?", our goals were more ambitious than the name implies. In this overview of Donde Va? we will discuss the oceanographic background of the region, the objectives of the experiment, and the preliminary results.

OCEANOGRAPHIC BACKGROUND

The Alboran Sea is the westernmost of the many basins that comprise the Mediterranean Sea. A narrow (10-30 km) current of Atlantic Water (fresher than 36.5 salinity) flows eastward through the Strait of Gibraltar with a volume transport of about 1.4×10^6 m^3/sec, while saline Mediterranean Water (38.4 salinity) flows westward beneath it with a transport that is about 4% less. This two-layer flow maintains the salt and water balance of the Mediterranean which annually loses about 1 m over its surface through the excess of evaporation over river runoff and precipitation (Lacombe, 1984). While intuition might lead one to anticipate that the Atlantic Water entering the Mediterranean would be found along the Moroccan coast (i.e., turning to the right upon exiting the Strait), in fact the inflow is found near Spain, where it forms the northern half of a basin-wide anticyclonic gyre (Lanoix, 1974; Cheney and Doblar, 1982; Parrilla and Kinder, 1984). There have been several model studies of the gyre (Whitehead and Miller, 1979; Nof, 1978; Preller and Hurlburt, 1982), and it is nearly always detectable in satellite infrared images (Phillipe and Harang, 1982).

OBJECTIVES

The primary objective of the experiment was to understand the dynamics and the variability of the anticyclonic gyre using numerical modeling, remote sensing, and field measurements. Our hypothesis was that the the Atlantic inflow is the primary forcing mechanism for the gyre, so that if we made synoptic measurements of the inflow and of the gyre, and compared these measurements to numerical model simulations, then we could increase our understanding of the the gyre dynamics.

The experiment addressed numerous secondary questions including:

What is the structure of the Intermediate and Deep Water flows, and how do these waters contribute to the Mediterranean outflow?

What is the biological and chemical influence on the gyre's strong ocean color signal, and how is this signal related to the physical structure of the gyre?

How does the strong front along the northern limb of the gyre affect the atmospheric marine boundary layer, and how does the marine boundary layer then affect remote sensing data?

How are the surface signatures of the gyre, as measured by satellite and aircraft sensors, related to the subsurface structure of the gyre?

How does atmospheric forcing influence the gyre, both directly and through changes in the Atlantic inflow?

PRELIMINARY RESULTS

The experiment had three overlapping phases, all ending in late October 1982. The first phase began in October 1981, and consisted of satellite monitoring (about 2 processed images per month) of the thermal surface features. The second phase began in June 1982, when five current meter moorings were deployed, a small hydrographic grid was occupied, and satellite image processing increased to about once weekly. During the final phase in October 1982, four ships occupied

OBJECTIVES

The primary objective of the experiment was to understand the dynamics and the variability of the anticyclonic gyre using numerical modeling, remote sensing, and field measurements. Our hypothesis was that the the Atlantic inflow is the primary forcing mechanism for the gyre, so that if we made synoptic measurements of the inflow and of the gyre, and compared these measurements to numerical model simulations, then we could increase our understanding of the the gyre dynamics.

The experiment addressed numerous secondary questions including:

What is the structure of the Intermediate and Deep Water flows, and how do these waters contribute to the Mediterranean outflow?

What is the biological and chemical influence on the gyre's strong ocean color signal, and how is this signal related to the physical structure of the gyre?

How does the strong front along the northern limb of the gyre affect the atmospheric marine boundary layer, and how does the marine boundary layer then affect remote sensing data?

How are the surface signatures of the gyre, as measured by satellite and aircraft sensors, related to the subsurface structure of the gyre?

How does atmospheric forcing influence the gyre, both directly and through changes in the Atlantic inflow?

PRELIMINARY RESULTS

The experiment had three overlapping phases, all ending in late October 1982. The first phase began in October 1981, and consisted of satellite monitoring (about 2 processed images per month) of the thermal surface features. The second phase began in June 1982, when five current meter moorings were deployed, a small hydrographic grid was occupied, and satellite image processing increased to about once weekly. During the final phase in October 1982, four ships occupied

stations in the Alboran Sea, the Strait of Gibraltar, and the Gulf of Cadiz (the area of the Atlantic Ocean just west of the Strait); four aircraft performed remote sensing and AXBT flights; a shore-based current-measuring radar (CODAR) operated; additional meteorological and aerosol data were collected; and all available NOAA-7 (Advanced Very High Resolution Radiometer, AVHRR) and NIMBUS-7 (Coastal Zone Color Scanner, CZCS) images were obtained. The meeting report from an October 1983 workshop contains a detailed account of the experiment and some early results (Parrilla, 1984). We will briefly discuss the preliminary results of the intensive October 1982 phase.

The Structure of the Gyre and The Atlantic Inflow. During October 1982 the gyre was fully developed, filling most of the western Alboran Sea. Figure 1 shows the salinity at 100 dbar, based on data taken over 2 weeks from two ships. The deep part of the inflowing current can be inferred from the closely packed isohalines in the northwest, and the gyre as the low salinity (<37) water centered near $35^{o}30'N$, $4^{o}00'W$. This depiction of the salinity distribution is probably close to the mean for the period, but the gyre displayed considerable variability during these two weeks. Satellite infrared images (see cover) showed large surface temperature changes, and three synoptic aircraft AXBT surveys showed that the thermal center of the gyre at 100 m moved 30 km within 10 days.

Near the Strait of Gibraltar, geostrophic estimates of the Atlantic inflow relative to 200 dbar were about 1.4×10^{6} m^{3}/sec in transport and maximum speeds were 140 cm/sec. Hydrographic stations within 25 km of the Moroccan coast showed unexpectedly high gradients, and currents computed from these data exceeded 100 cm/sec.

Current measurements also showed high speeds with strong variability in the gyre and the inflow. Five short-period (4-5 hour) surface measurements of sonobuoy drift tracks showed that the core of the inflow was associated with a cool sea surface temperature and speeds of 120 cm/sec. South of the inflow, the speeds in the gyre averaged 60 cm/sec, although some higher speeds were measured. Surface currents measured by radar (CODAR) over a region extending 60 km south of Marbella (depending on interference and propagation conditions) were well correlated with geostrophic estimates and current meter data. CODAR measurements showed that the center of the inflow current had a width of 15-30 km, that it moved more than 30

km farther offshore in 4 days, and that it had multiple velocity maxima of 5-15 km width (Janopaul and Frisch, 1984). During October, the current meters (Fig. 2) showed the subsurface velocity core shifting between moorings 14 and 15, with the highest speeds at the shallowest meters (depths of 67-124 m) exceeding 80 cm/sec. The best-resolved velocity section, taken with the CTD/velocity profiler south of Estepona, revealed a current of about 25 km width, 100 m depth (20 cm/sec isotach), and surface speeds of 120-140 cm/sec (Fig. 3). This section also showed that in the highest horizontal shear regions of the current, large along-section velocities made the non-linear terms in the momentum equations nearly as large as the Coriolis term. Generally, the geostrophic estimates appear valid, but details on scales of 10 km or less in the high shear regions may be inaccurate.

Optical, Biological and Chemical Measurements. Simultaneous measurements of visible and infrared radiation from both aircraft (Multi-Spectral Scanner and Ocean Color Radiometer) and satellite (CZCS and AVHRR) sensors clearly pictured the gyre and the Atlantic inflow (Fig. 4). The CZCS images were geometrically registered to a Mercator projection and atmospherically corrected for quantitative chlorophyll concentration and for the diffuse attenuation coefficient. These results and the aircraft data indicated that high chlorophyll concentrations were correlated with cool sea surface temperatures. Surface thermal fronts were coincident with ocean color fronts on the large scale, although differences appeared at smaller scales. Results of the CZCS showed surprisingly large daily changes in chlorophyll concentration and attentuation coefficient across the entire sea.

Along the northern front formed by the gyre and the Atlantic inflow, chlorophyll changed from 1.05 to 0.45 mg/m^3 and the attenuation coefficient from 0.15 to 0.07 within 24 hours. The cause of these changes is still under scrutiny. If the cause is either biological or physical, then the rapidity, areal extent, and size of the changes will be a significant new result.

In situ optical and biological measurements were concentrated along the mooring line (Fig. 2). These measurements showed large temporal and spatial changes in the optical and thermal structure. Correlation with satellite images and other data showed that much of the temporal change was associated with variations in the structure of the Atlantic inflow and gyre (Arnone and La Violette, 1984).

Biological and nutrient concentrations also had a complicated and variable structure. Phosphate concentrations were higher (0.3-0.7 g at P-P04) than previously found, and some high nitrate concentrations also suggested that upwelling or mixing may have been supplying nutrients to the photic zone. High chlorophyll concentrations were associated with the high nitrate. Diatoms were strongly dominant, with Rhizosolenia Stolterfothii the most abundant.

Submesoscale Thermal Features. Examination of the the twice-daily infrared images (see cover) and visible CZCS images (Fig. 4) revealed tongues of colder and more turbid water that were pointed toward the center of the gyre. They appeared first near the Strait, and then apparently were advected around the gyre at a mean speed of 40 cm/sec (La Violette, 1984). These features had a horizontal dimension of 10-20 km (compared to the internal deformation radius of 15-30 km), and a vertical extent, measured by AXBT sections, of at least 100 m. Salinity from a CTD cast obtained within one feature was in the range of Atlantic Water. During 15 days of cloud-free satellite images, 9 features could be tracked most of the way around the gyre. Because they appeared to originate near the Strait about twice per day (the same frequency as the NOAA satellite passes), we conjecture that the strong Strait of Gibraltar tides may influence their formation.

Meteorology and Aerosols. Shore stations and shipboard measurements, including soundings and aerosols, provided dense observation of the lower atmosphere. These data were obtained to check the influence of the atmosphere on the gyre (Cheney and Doblar, 1982; Bucca and Kinder, 1984) and on remote sensing measurements. The marine boundary layer was modified by cooling and warming due to the air-sea temperature differences over the water masses on either side of the sea surface thermal fronts: the boundary layer over the colder water was 50 m lower than over the warmer gyre water, had a stable inversion layer overlaying a shallow surface layer, and had a greater concentration of smaller-sized aerosols. Aerosol populations over the Alboran Sea (gathered by ship) were characterized by large diurnal variations in concentration, size, and chemical composition. On the average, submicron-sized particle concentrations were approximately 50% greater over the colder water (probably trapped in the low level inversion), while concentrations of particles > 1 micron were comparable in both areas. Wave data inferred from aircraft photography also showed smaller wave heights in the colder water. The correlations of these atmospheric parameters with oceanographic

features can both complicate interpretation of remote sensing images and offer clues to useful analysis.

Internal Waves. Non-linear internal waves (often described as bores) have been known in the Strait of Gibraltar for decades. For the first time, however, our data show that these eastward-propagating waves often form ordered groups of short period (about 30 minutes) waves in the Alboran Sea, apparently as internal solitons (Osborne and Burch, 1980). These waves have sufficient amplitude (exceeding 50 cm/sec in eastward velocity) to affect measurement programs, and perhaps directly influence larger scale dynamics as well. The waves were common, forming during most semi-diurnal tidal cycles but with varying strength.

Gulf of Cadiz. Hydrographic observations in the Gulf of Cadiz showed Atlantic Water near the Spanish coast flowing eastward toward the Strait. The Mediterranean outflow appeared to move down five submarine canyons along the Iberian slope, mixing with the surrounding waters. There were several gyres or eddies in the dynamic topographies, including an anticyclonic gyre (near $36^{o}20'N$ and $7^{o}10'W$) that has been detected in CZCS images. Velocity profiling south of Cape St. Vincent (extreme southwestern Portugal) indicated that the Mediterranean Water was moving at speeds of less than 10 cm/sec. In these data and companion CTD data, the temperature and salinity at the core of the Mediterranean Water fluctuated as much as $1^{o}C$ and 0.2 over either distances of a few kilometers or periods of a few days (spatial and temporal fluctuations on these scales could not be separated because of ship movement).

Numerical Modeling. Reduced gravity models (single active layer above a quiescent lower layer) used by Preller and Hurlburt (1982) demonstrated the importance of both the magnitude and direction of the inflowing Atlantic Water in the determination of the gyre dimensions. Inflow directed north of east, and thus conforming to the orientation of the Strait of Gibraltar, enlarged the north-south extent of the gyre. Increasing the magnitude of the inflow intensified the gyre and shifted it farther east.

When a westward-flowing lower layer was included, the importance of the bottom topography became apparent. In cases of large inflows ($>1.7 \times 10^{6}$ m^{3}/sec) with an initial northward component, the submarine ridge system near Alboran Island

deflected the flow northward. This deflection eliminated the anticyclonic gyre west of the Island. Smaller inflows, such as the 1.4×10^6 m^3/sec estimated for October, resulted in a large anticyclonic gyre west of the Island.

Deep and Intermediate Water. Hydrographic sections showed that the Deep and the Intermediate Water took separate paths through the Alboran Sea. The Deep Water flowed as a narrow (20 km) current against the base of the Moroccan continental slope and then appeared at the eastern end of the Strait along the southern side, much as predicted by Bryden and Stommel (1982). The Intermediate Water, however, appeared to flow preferentially in the northern two-thirds of the Alboran Sea, arriving at the eastern end of the Strait along the northern side. The Deep Water flow was thus anticyclonic, like the shallow Atlantic Water Gyre, while the Intermediate Water flow was cyclonic. Two-layer numerical model experiments suggested that this pattern resulted from the influence of rotation on the Intermediate Water, and of bathymetry on the Deep Water.

REFERENCES

Arnone, R.A. and P.E. La Violette. Bio-optical variability in the Alboran Sea as assessed by NIMBUS-7 coastal zone color scanner. Submitted to J. Geophys. Res., 1984.

Bryden, H.L. and H.M. Stommel. Origin of the Mediterranean outflow. J. Mar. Res. 40 (suppl):55-71, 1982.

Bucca, P.J. and T.H. Kinder. An example of meteorological effects on the Alboran Sea Gyre. J. Geophys. Res. 89(C1):751-757, 1984.

Cheney, R.E. and R.A. Doblar. Structure and variability of the Alboran Sea frontal system. J. Geophys. Res. 87(C1):585-594, 1982.

Janopaul, M.M. and A.S. Frisch. CODAR measurements of surface currents in the northwest Alboran Sea during the Donde Va experiment. Annales Geophysicae, in press, 1984.

Lacombe, H. General physical oceanography of the Mediterranean Sea. In Proceedings of NATO Advanced Research Workshop, La Spezia, H. Charnock, ed., in press, 1984.

Lanoix, F. Projet Alboran. Etude Hydrologique et Dynamique de la Mer d'Alboran. NATO Tech. Rept. 66, Brussels, 39 pp, 1974.

La Violette, P.E. The advection of submesoscale thermal features in the Alboran Sea Gyre. J. Phys. Oceanogr. 14(3), in press, 1984.

Nof, D. On geostrophic adjustment in sea straits and estuaries: theory and laboratory experiments. Part II. J. Phys. Oceanogr. 8:861-872, 1978.

Osborne, A.R. and T.L. Burch. Internal solitons in the Andaman Sea. Science 208(4443):451-460, 1980.

Parrilla, G. (editor) Donde Va? Meeting Report, Fuengirola, October 1983. Instituto Espanol de Oceanografia (extended abstracts in English, short abstracts in Spanish and English), 1984.

Parrilla, G. and T.H. Kinder. The physical oceanography of the Alboran Sea. In Proceedings of NATO Advanced Research Workshop, La Spezia, H. Charnock ed., in press, 1984.

Philippe, M. and L. Harang. Surface temperature fronts in the Mediterranean from infrared imagery. In Hydrodynamics of Semi-Enclosed Seas, J.C.J. Nihoul, ed., Elsevier, pp. 91-128, 1982.

Preller, R. and H.E. Hurlburt. A reduced gravity model of circulation in the Alboran Sea. In Hydrodynamics of Semi-Enclosed Seas, J.C.J. Nihoul, ed., Elsevier, pp. 75-89, 1982.

Whitehead, J.A. and A.R. Miller. Laboratory simulation of the gyre in the Alboran Sea. J. Geophys. Res. 84:3733-3742, 1979.

Cover. NOAA-7 Advanced very high resolution radiometer (AVHRR) infrared images of the Alboran Sea collected as part of the Donde Va? experiment during October 1982. The dot and V in the images show the advection of two submesoscale features about the Alboran Sea gyre (the line designates a key section near the current moorings, cf. Fig. 2). A close examination of the images shows that other unmarked features were also being advected. Continuous monitoring of these cold-water features was possible because of the twice-daily (about every 12 hours) spacing of the NOAA-7 overpasses. After registration to a mercator projection (accuracy $\pm$1 km) and an atmospheric correction to arrive at absolute temperatures, analysis of the displacement of the cold water features in successive images show their apparent origin east of Gibraltar, their average speeds of 40 cm/sec around the gyre, and their apparent entrainment into the incoming Atlantic Water east of Gibraltar.

1432 GMT 6 OCTOBER

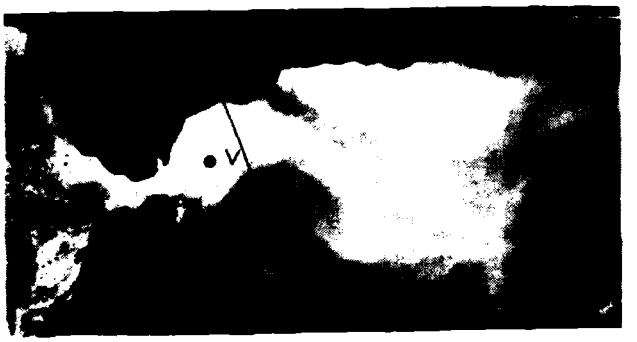

0256 GMT 7 OCTOBER

1422 GMT 7 OCTOBER

0244 GMT 8 OCTOBER

1408 GMT 8 OCTOBER

Figure 1. Salinity at 100 dbar, showing the structure of the Atlantic inflow and gyre at depth.

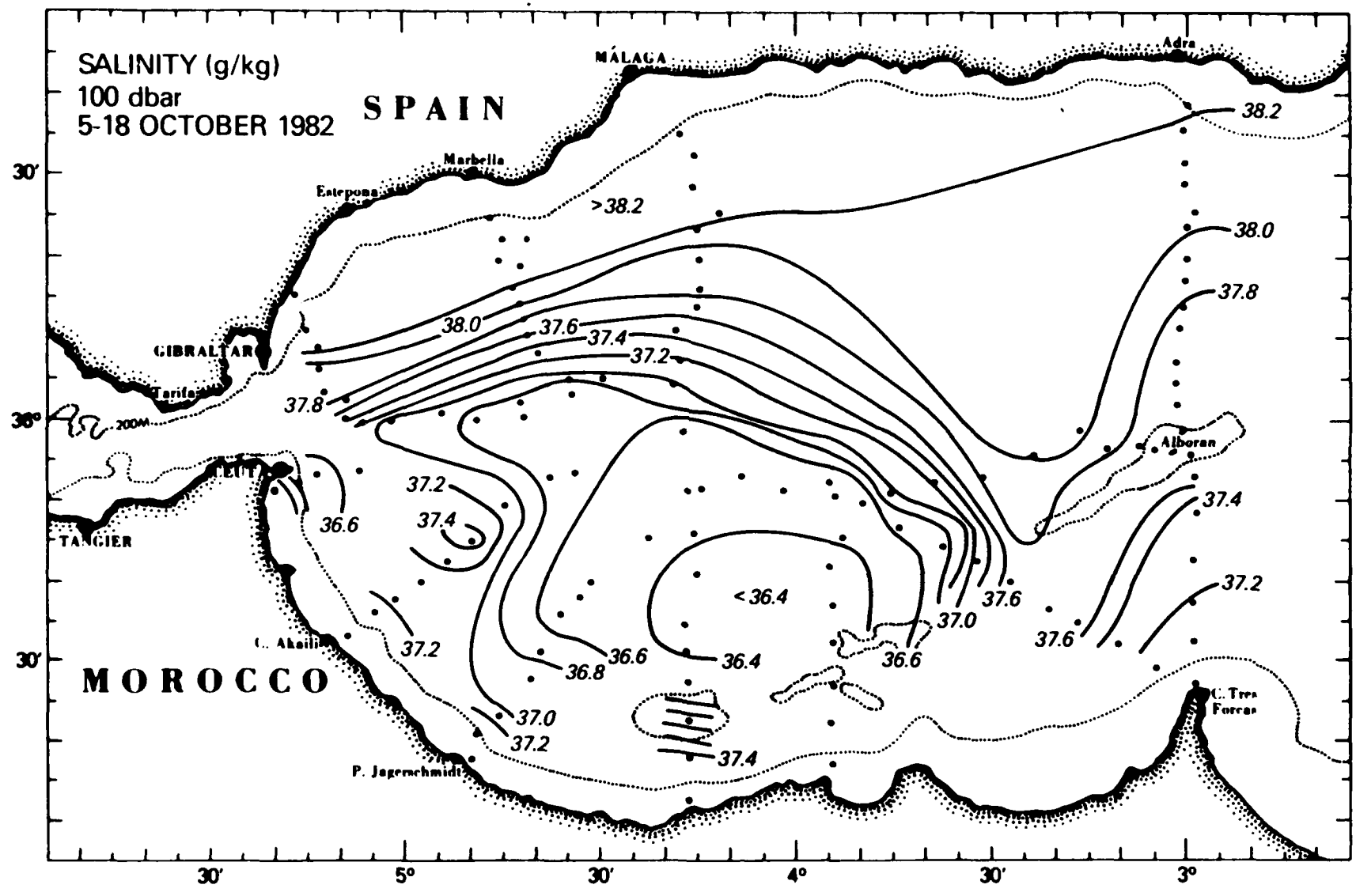
SALINITY (g/kg)
100 dbar
5-18 OCTOBER 1982
SPAIN
MÁLAGA
Adra
Marbella
Estepona
GIBRALTAR
Tarifa
TANGIER
MOROCCO
Alboran
C. Tres Forcas
P. Jaguenschmidt
38.2
>38.2
38.0
37.8
37.6
37.4
37.2
37.0
36.8
36.6
36.4
<36.4
30'
36°
5°
4°
3°

Figure 2. Mean velocities from the current meters. The solid arrows are from instruments in the Atlantic inflow or gyre, while the dashed arrows (note scale change) were in the lower part of the Mediterranean Intermediate Water.

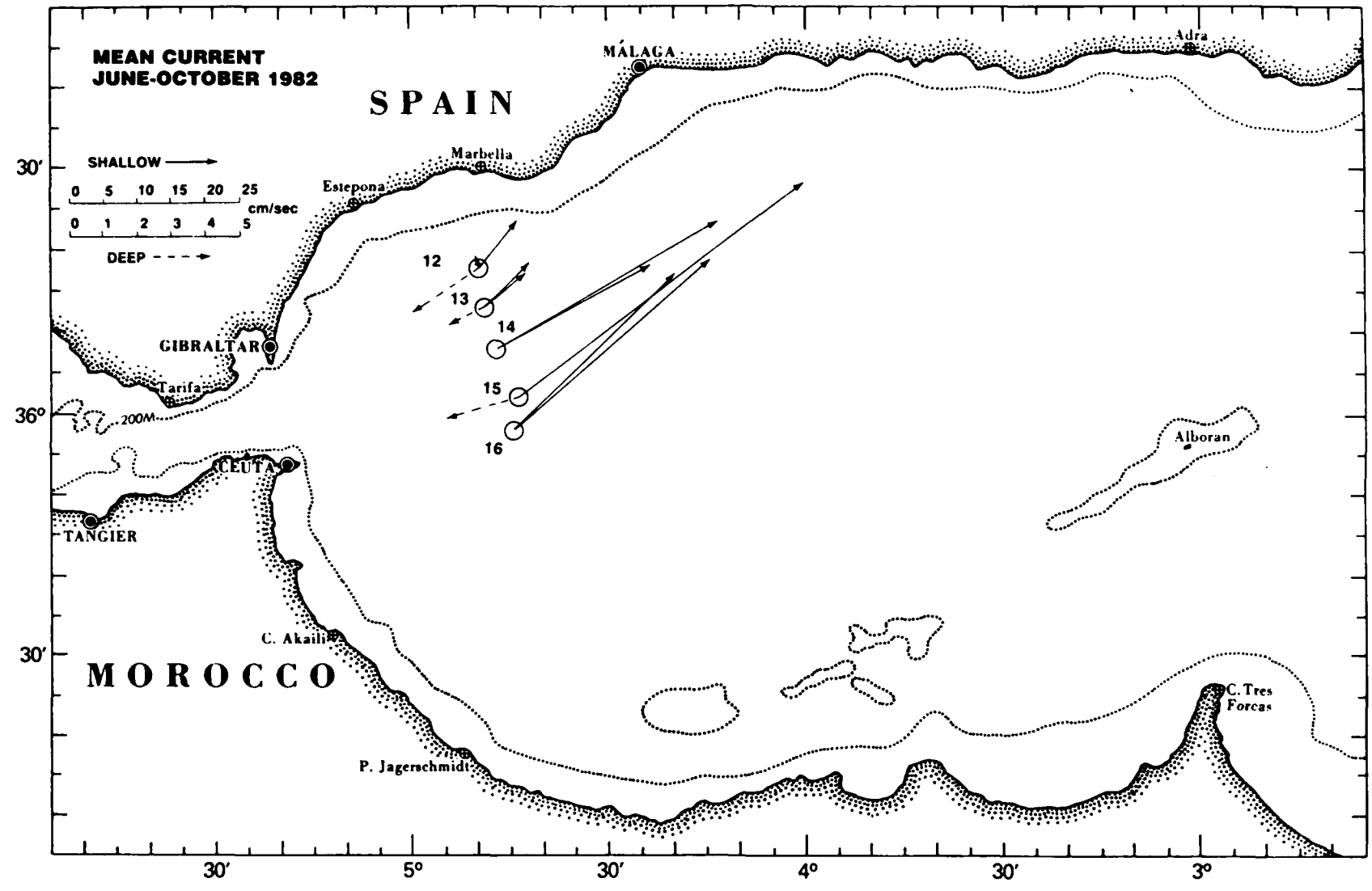
MEAN CURRENT
JUNE-OCTOBER 1982
SPAIN
MOROCCO
SHALLOW
0 5 10 15 20 25
cm/sec
0 1 2 3 4 5
DEEP
MÁLAGA
Adra
Marbella
Estepona
GIBRALTAR
Tarifa
200M
CEUTA
TANGIER
C. Akaili
P. Jagerschmidt
Alboran
C. Tres Forcas
12
13
14
15
16
30'
36°
30'
30'
5°
30'
4°
30'
3°

Figure 3. CTD/current profiles measured south of Estepona during 16-17 October. The currents were measured, and not inferred from the hydrography. (a) Temperature (^{o}C). (b) Salinity. (c) Eastward velocity (cm/sec). (d) Northward velocity (cm/sec). The bottom axis is distance south of 36^{o}24'N, and the top axis station location.

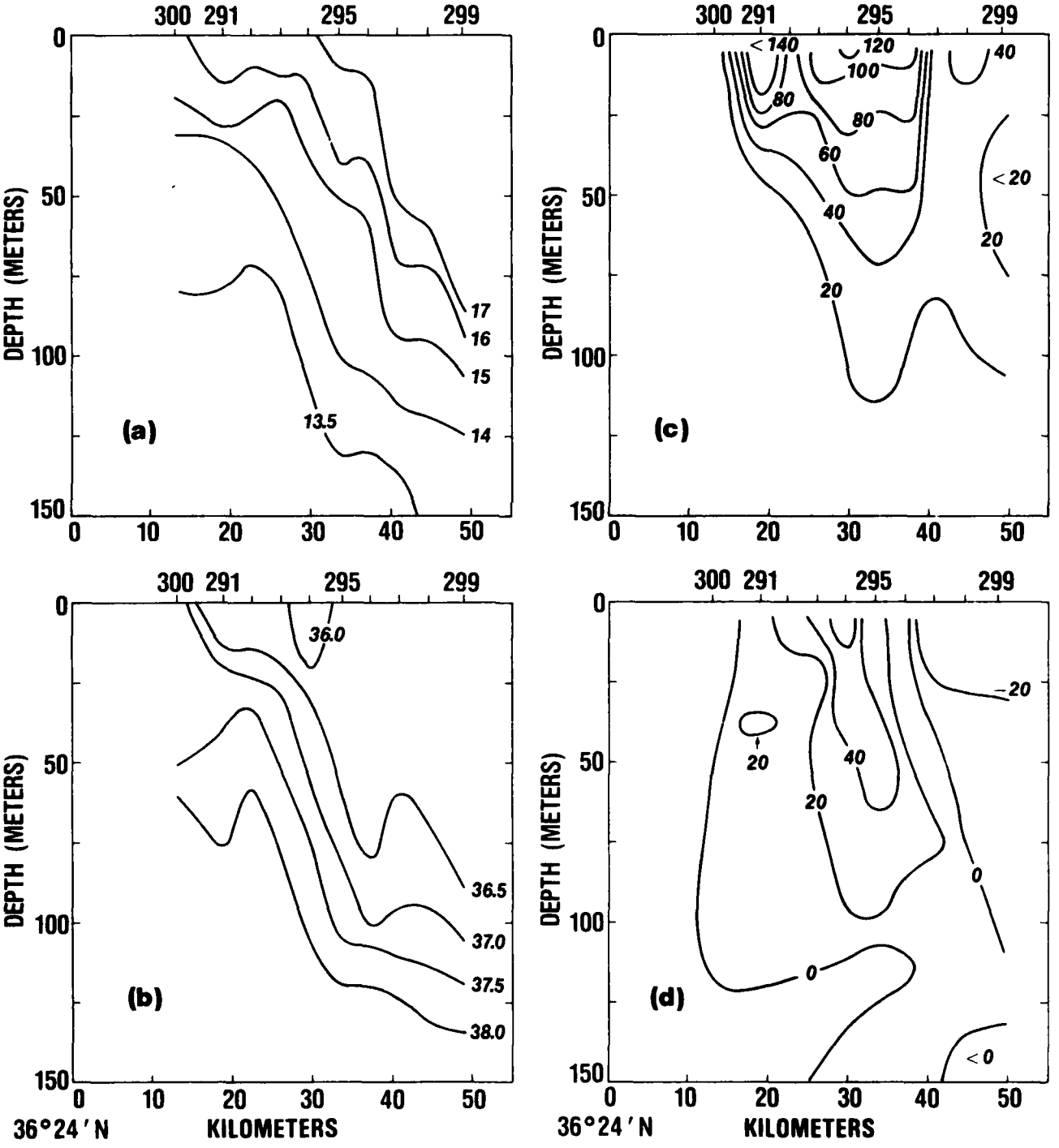
300 291 295 299
DEPTH (METERS)
0
50
100
150
0 10 20 30 40 50
(a)
17
16
15
14
13.5
(b)
36.0
36.5
37.0
37.5
38.0
(c)
< 140
120
100
80
80
60
40
20
40
< 20
20
(d)
20
20
40
20
0
0
< 0
36°24 ' N
KILOMETERS

Figure 4. CZCS image on 7 October 1982. Darker shades correspond to higher phytoplankton pigment concentrations (cf. cover).

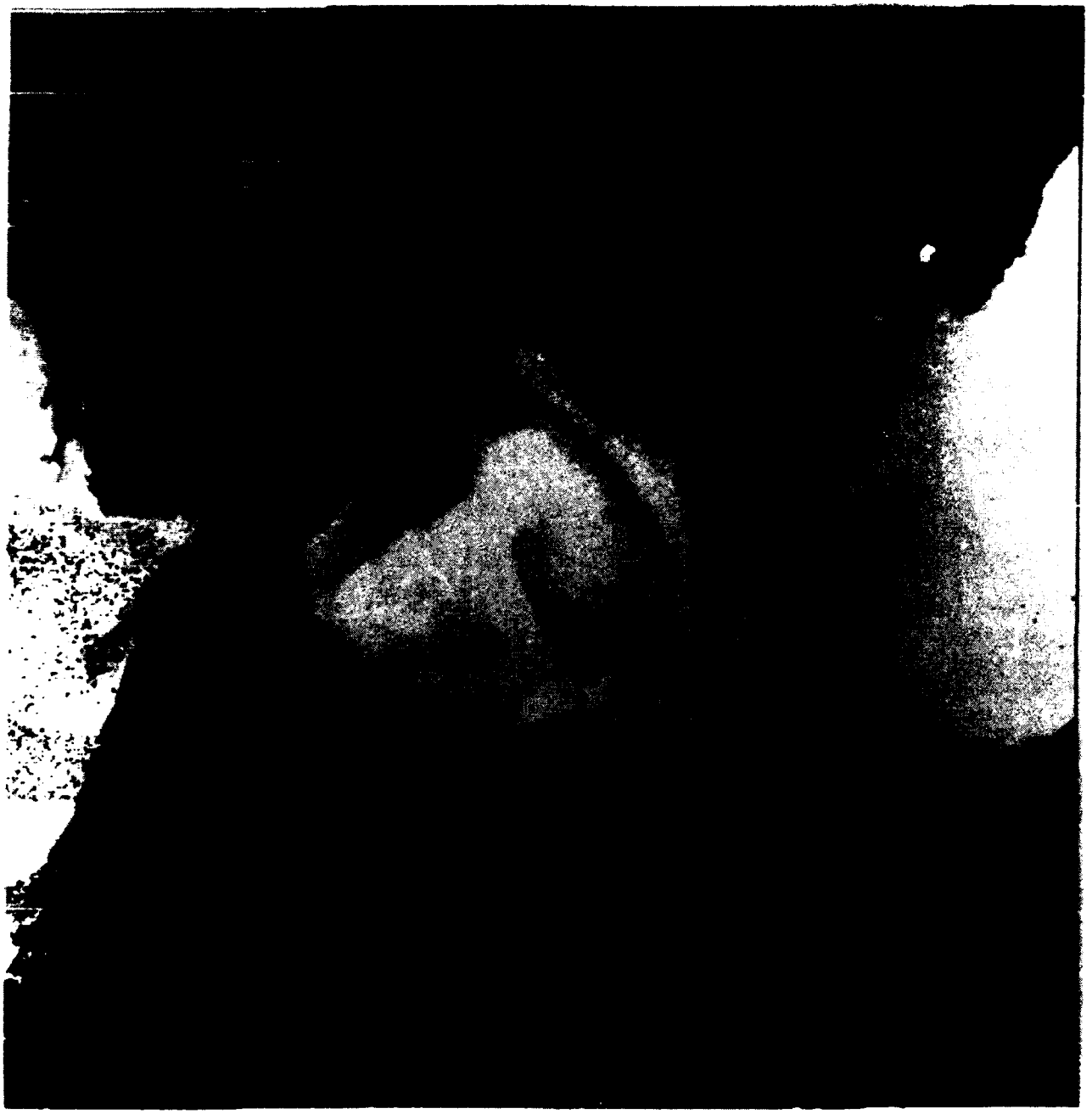

Figure 4.

Figure 5. Pycnocline anomaly for a steady state two-layer model experiment. Upper layer inflow was 30 cm/sec angled 21^{0} north of east, and lower layer inflow was a uniform 0.2 cm/sec across the eastern boundary. Positive contours denote a thickening of the upper layer (contour interval is 4 m).

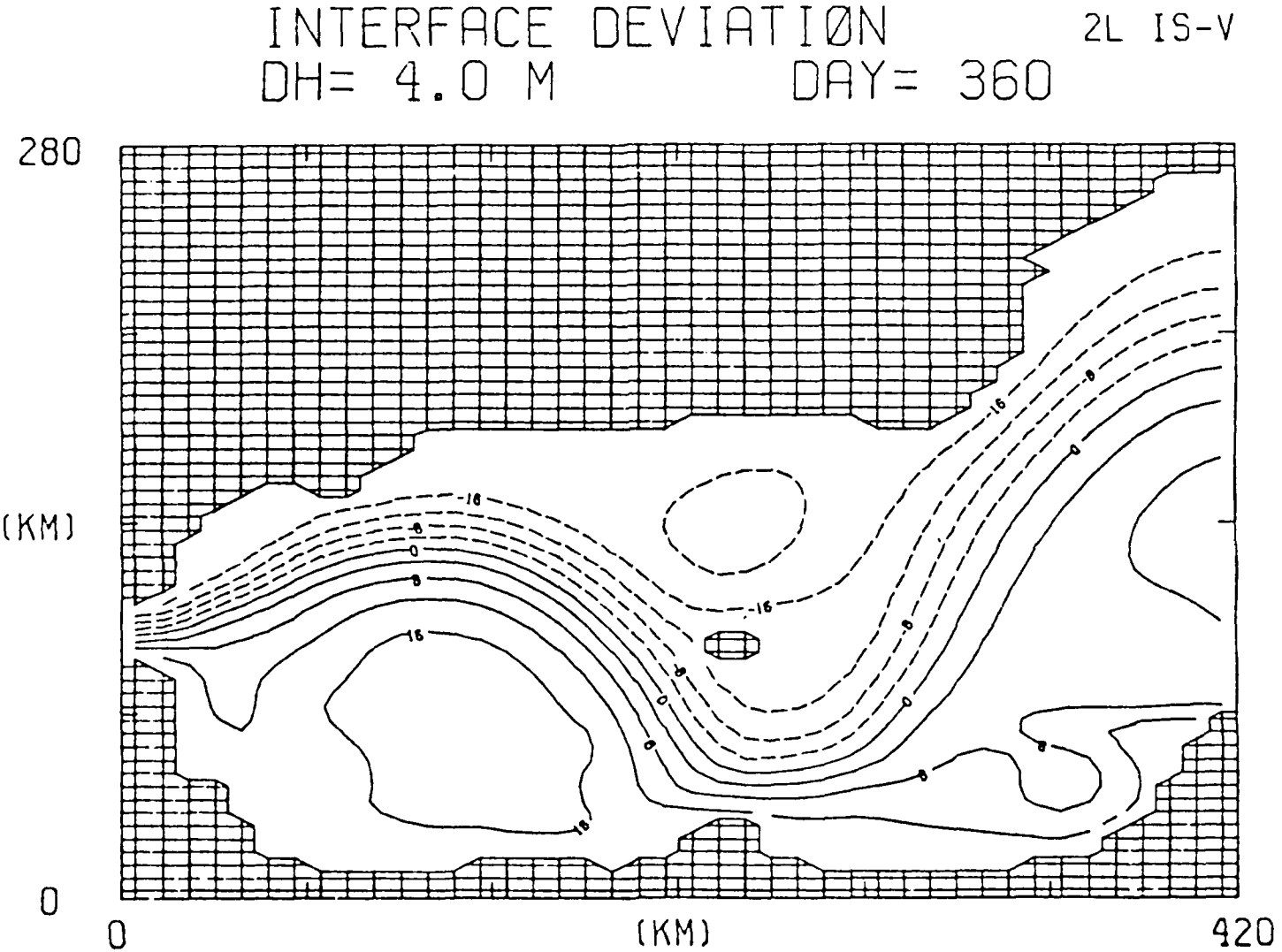

Figure 5.

LIST OF PARTICIPANTS

Name	Institution	Program
G. Parrilla	Instituto Espanol de Oceanografia, Madrid	CTD/XBT
J.M. Cabanas	Instituto Espanol de Oceanografia, La Coruna	Chlorophyll, Nutrients, Total Dissolved Solids
D. Cortes	Instituto Espanol de Oceanografia, Fuengirola	
C. Garcia	Instituto Espanol de Oceanografia, Madrid	
J.M. Fernandez Lopez E. Ortega Serrano	Instituto Hidrografico de la Marina, Cadiz	CTD/XBT
I. Tato J. Torralbo R. Barcala V. Moreno	Instituto Nacional de Tecnica Aerospacial, Madrid	Visible and Infrared Measurements from Aircraft and Satellite
H. van der Piepen V. Amann R. Fiedler H. Helbig	Institut fur Optoelektronik Deutsche Forschungs - und Versuchsanstalt fur Luft - und Raumfahrt e.v. Oberpfaffenhofen, Federal Republic of Germany	Visible and Infrared Remote Sensing from Aircraft and Satellite
M. Champagne-Philippe T. Phulpin	Etablissement d'Etudes et de Recherches de la Meteorologie Centre de Meteorologie Spatiale Lannion, France	Satellite Infrared
R.W. Fett	Naval Environmental Prediction Research Facility, Monterey, CA	Meteorology and Aerosols
S.A. Hsu	Louisiana State University, Baton Rouge, LA	
E.J. Mack	Arvin Calspan, Buffalo, NY	
A.R. Miller W.R. Wright	Associated Scientists at Woods Hole, Inc. Woods Hole, MA	CTD

Name	Institution	Program
M.M. Janopaul A.S. Frisch	Wave Propagation Laboratory (NOAA/ERL) Boulder, CO	H.F. Radar (CODAR) Surface Currents
R.A. Arnone	Naval Ocean Research and Development Activity (NORDA) NSTL, MS	Satellite Visible and In situ Optical
H. Perkins K.D. Saunders	NORDA	Vertical Profiling of Horizontal Velocity, CTD/XBT
R.H. Preller H.E. Hurlburt	NORDA	Numerical Modeling
P.E. La Violette	NORDA	Visible and Infrared Measurements from Satellite and Aircraft; AXBT
T.H. Kinder	NORDA	Moored Current Meters; CTD/XBT

Donde Va? was organized by Thomas H. Kinder, Paul E. La Violette and Gregorio Parrilla.

THE HYDROGRAPHIC STRUCTURE OF THE ALBORAN SEA GYRE, JUNE AND OCTOBER 1982

Thomas H. Kinder

Naval Ocean Research and Development Activity, NSTL, MS 39529
also at Woods Hole Oceanographic Institution, Woods Hole, MA 02543

Gregorio Parrilla

Instituto Espanol de Oceanografia, Alcala 27-4°, 28014, Madrid, Spain

---

In 1982 we did two CTD surveys of the western Alboran Sea as part of the Donde Va experiment (Donde Va Group, 1984; Parrilla, 1984). A rapid two-ship survey during 5-13 October encompassed the entire western Alboran, and a single-ship survey during 22-30 June covered the northern half only.

We use the hydrographic distributions and geostrophic calculations to compare the gyre found in 1982 to that present during summer 1962. Lanoix (1974) used data gathered by four ships during 15 July-15 August 1962 to comprehensively describe the anticyclonic gyre which is formed by the inflowing Atlantic Water. The summer 1962 and October 1982 surveys are the two best realizations of the gyre to date. This gyre is always present, but its size and location vary (Parrilla and Kinder, 1984).

We used two working definitions for the gyre boundary. Both the 15 dyn cm (1.5 J/kg) contour on the 0/200 dbar dynamic topography and the 140 dbar isobar on the 37.5 isohaline distribution were closed isolines that appeared to separate the gyre from the inflowing Atlantic Current during both years (see figures).

The 1962 gyre was larger and stronger than the 1982 gyre (see table). In 1962 the center was about 14 km farther north, and the periphery about 20 km farther north and 30 km farther east. This resulted in more than twice the surface area and volume of Atlantic water (defined as salinity < 37.5). The 1962 gyre was also about 25 percent deeper and had a stronger dynamic high. During October 1982 transport around the gyre (i.e., recirculation) was similar to the inflow, but in 1962 it was about 50 percent greater than the inflow (based on Lanoix Sections 8 and 9).

The partial survey in June 1982 suggested that the gyre may have been larger than in October, although probably smaller than in 1962. The diminution may have occurred during a major episode of low eastward flow that appeared in

current meter records north of 35°58'N along 4°45'W in mid-September (Kinder, 1984). During this episode the Atlantic inflow current was either absent or flowing far south where the gyre is normally found. To transform from a 1962-size gyre to an October 1982-size gyre over the ten day low-flow episode would require the gyre to lose about 1.1×10^6 m^3/sec of water with salinity < 37.5, or about the normal eastward transport.

References

Donde Va Group (1984). Donde Va? An oceanographic experiment in the Alboran Sea. EOS 65 (36):682-683.

Kinder, T. H. (1984). Net mass transport by internal waves near the Strait of Gibraltar. Geophys. Res. Lett., in press.

Lanoix, F. (1974). Projet Alboran. Etude hydrologique et dynamique de la Mer d'Alboran. NATO Technical Report 66, 39 pp. and 32 Figs.

Parrilla, G. (ed) (1984). Preliminary Results of Donde Va? Inst. Espan. Ocean. Inform. Tech. 24-1984, 267 pp.

Parrilla, G., and T. H. Kinder (1984). The physical oceanography of the Alboran Sea. In: Proceedings of NATO Advanced Research Workshop, La Spezia, H. Charnock, ed., in press.

TABLE: Gyre comparisons

		July–August 1962	October 1982	June 1982	Notes
Area (km^2)		11,800	4,900	–	15 dyn cm
		10,300	4,900	–	37.5 at 140 dbar
Volume (km^3)		1,650	725	–	Salinity < 37.5
Center:	North	35°50'	35°40'	–	dynamic height
		35°45'	35°39'	–	37.5 isohaline
	West	4°08'	4°10'	–	dynamic height
		4°08'	4°10'	–	37.5 isohaline
Penetration:	North	36°08'	36°03'	36°04'	15 dyn cm
		36°08'	35°51'	36°05'	37.5 at 140 dbar
	West	3°21'	3°43'	–	15 dyn cm
		3°18'	3°35'	–	37.5 at 140 dbar
Depth of 37.5 isohaline (mean, m)		160	148	–	
(maximum, m)		220	174	$\geq$ 183	
Maximum Dynamic Height (dyn cm)		33	25	$\geq$ 25	
Inflow ($10^6 m^3$/sec)		1.6	1.3	1.2	
Gyre ($10^6 m^3$/sec)		2.5	1.4	2.3	

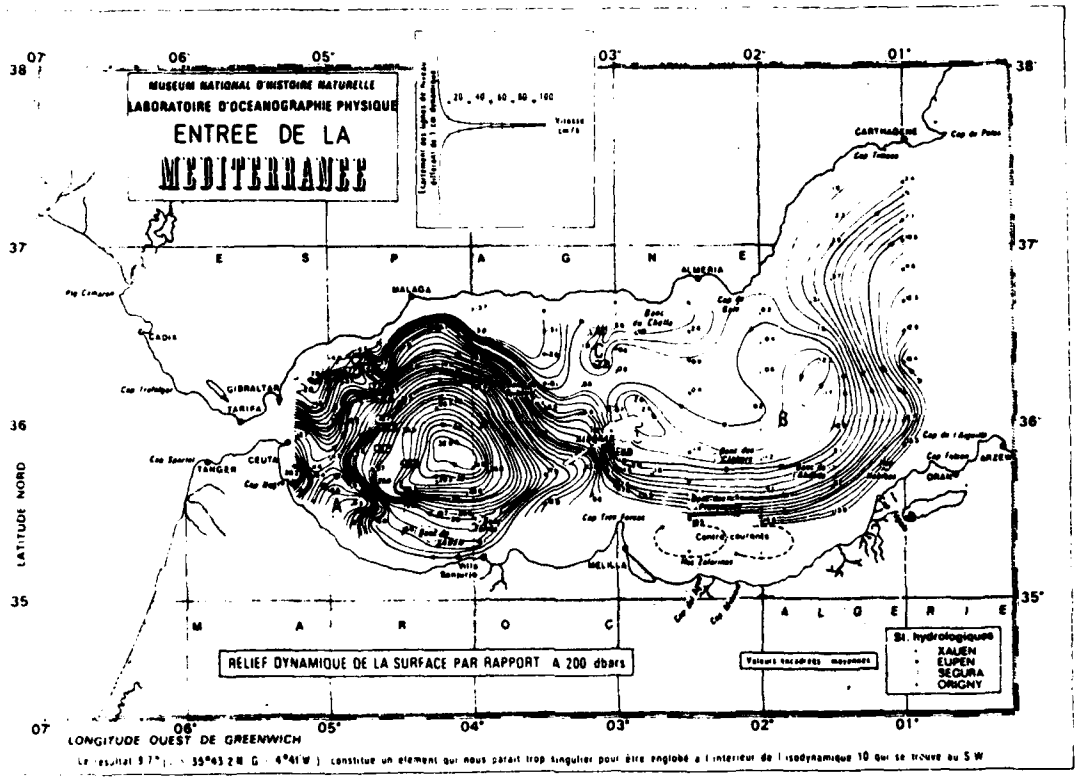

FIG 25

Figure 1. Dynamic topography, summer 1962 (Lanoix, 1974). Contour interval 1 dyn cm (0.1 J/kg), range +33 to -7.

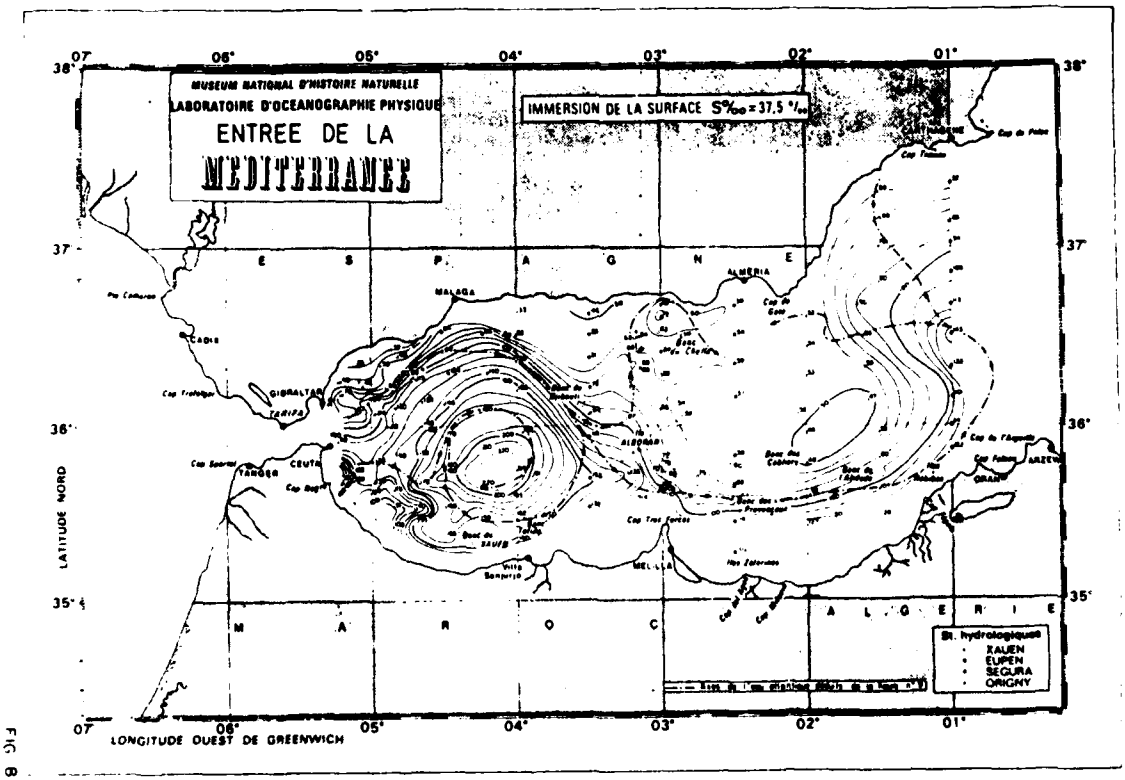

FIG 8

Figure 2. Depth of 37.5 isohaline, summer 1962 (Lanoix, 1974). Contour interval 10 m, range 30 to 220 m.

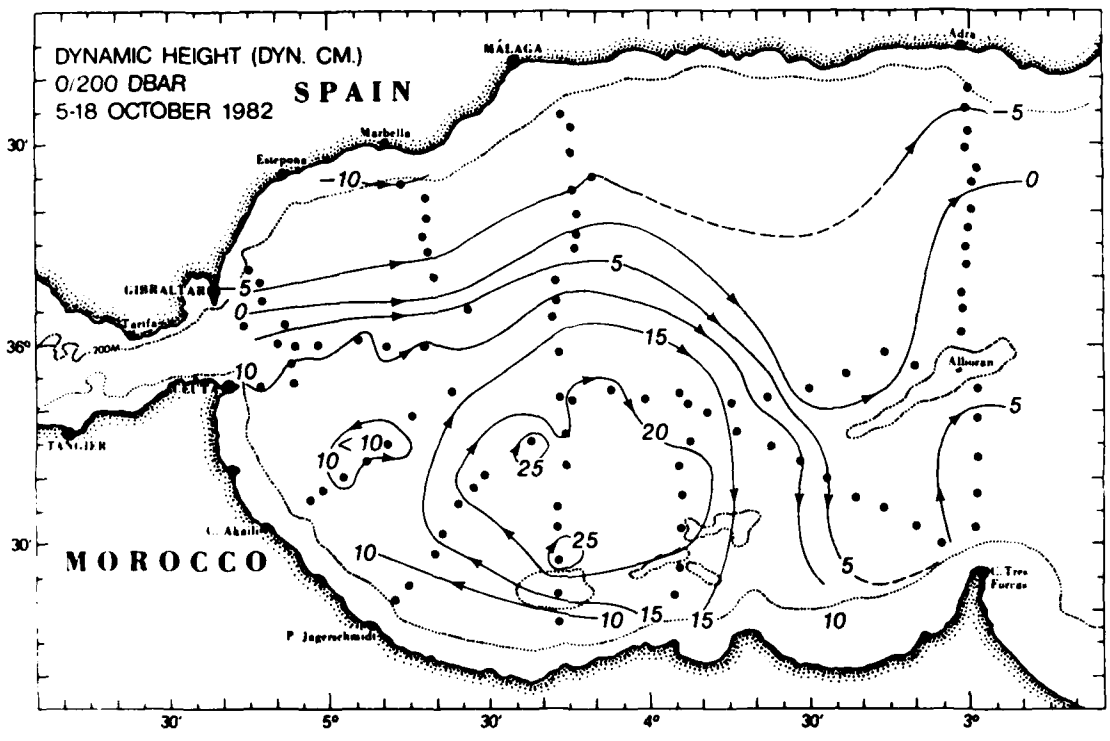

Figure 3. Dynamic topography, October 1982.

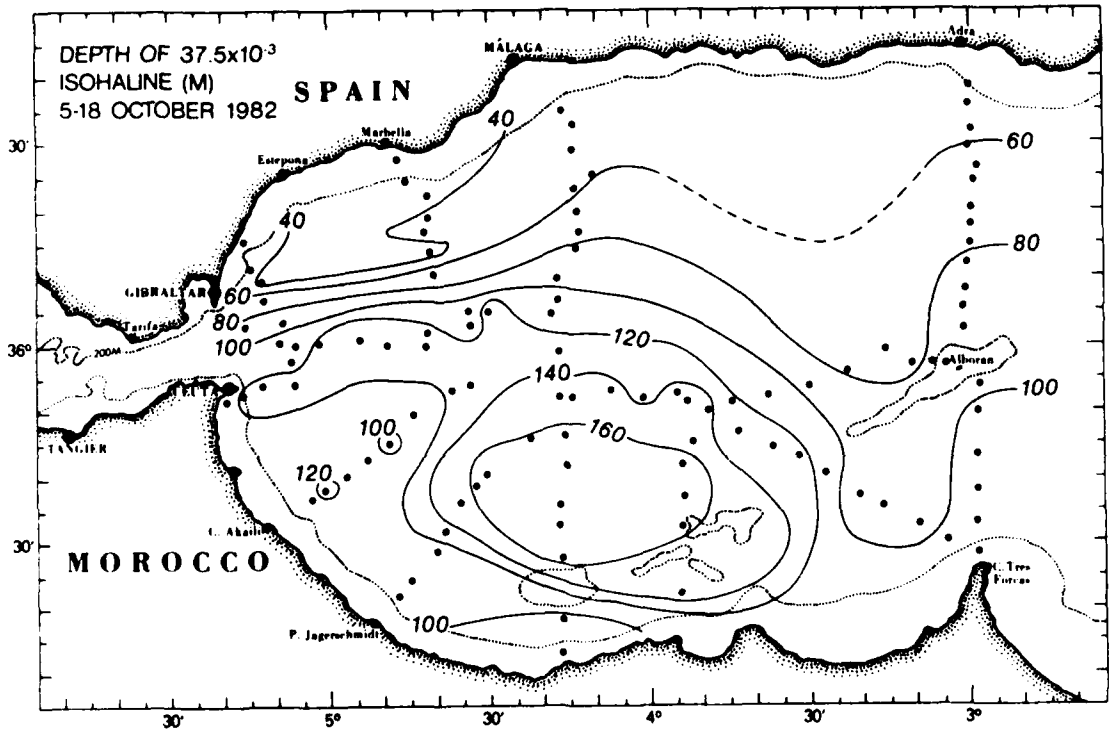

Figure 4. Depth of 37.5 isohaline, October 1982.

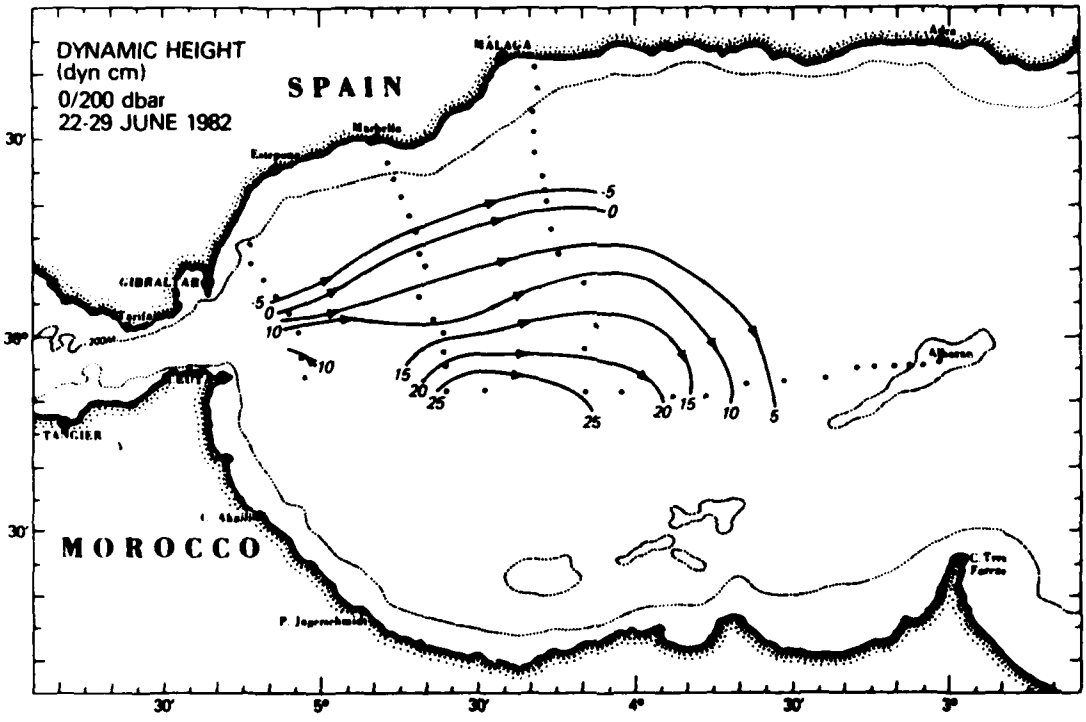

Figure 5. Dynamic topography, June 1982.

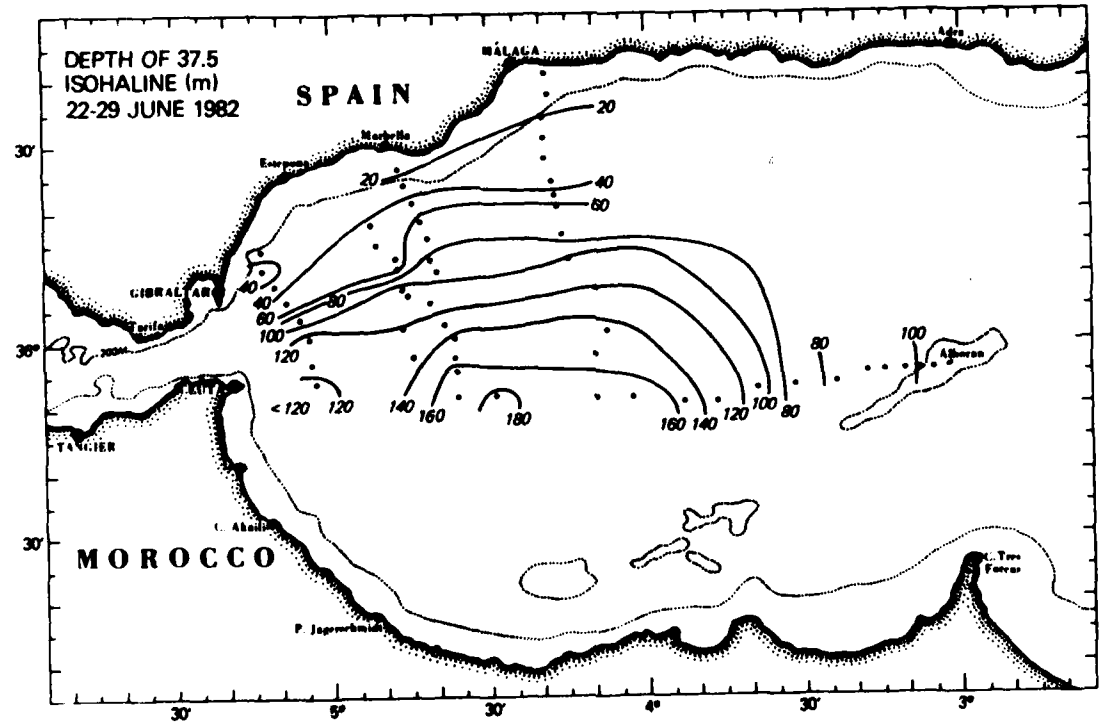

Figure 6. Depth of 37.5 isohaline, June 1982.

INTA/DFVLR

ALBORAN SEA EXPERIMENT 1982 ("DONDE VA?")

NIMBUS-7 / CZCS - DERIVED MAPS OF NEAR - SURFACE CHLOROPHYLL

by

H. van der Piepen[+], R. Barcala[++], J. S. van der Piepen[+], R. Fiedler[+]

[+] DFVLR, Institut für Optoelektronik D8031 Oberpfaffenhofen, BRD

[++] INTA, Paseo del Pinto Rosales 34, Madrid 8, Espana

Summary

Data from the Coastal Zone Color Scanner (CZCS) on the Nimbus-7 satellite have been processed geometrically and radiometrically so as to map the distribution of near-surface pigments in the Alboran Sea during October 1982.

1. Introduction

During 1982 a major oceanographic experiment - the Alboran Sea Experiment ("Donde Va? ") took place in the western Mediterranean Sea in which a number of research organizations from the United States and from European countries participated. The objective of the Experiment was the study of the jet-like Atlantic inflow into the Mediterranean Sea through the Strait of Gibraltar and the associated anti-cyclonic circulation in the Alboran basin.

Since particular emphasis during the Experiment was given to the verification and application of remote sensing methods, relevant data were not only collected from ships but also from aircraft, satellites and ground-based stations in an attempt to achieve a synoptic view of the complex and rapidly varying oceanic phenomena in this region.

Because of its significance for investigations concerning both ocean dynamic processes and especially marine biology and ecology, this report deals with the remote sensing of ocean color from space and its evaluation in terms of the pigment distribution in the Alboran Sea during October 1982. In Europe these investigations were done jointly by INTA and DFVLR.

2. Ocean color phenomenon

2.1 General

Visible light may penetrate the water body to a certain depth. Through processes like absorption, fluorescence and scattering caused by natural and man-made suspended and dissolved substances as well as by the water itself, it is modulated in intensity and spectral composition. The backscattered portion of the light as observed by a remote sensor above the water may thus render information on the type, distribution and concentration of many biochemical water parameters. (Because of the limited transparency of both the water and the atmosphere, only the spectral region between approximately 400 nm and 700 nm can generally be used.)

The rather complex physical and biological processes involved have been studied in much detail during the past (1). Nevertheless further research in this field is still needed before the

interpretation of water color can be used routinely for a quantitative monitoring of coastal zones. In particular, the combined collection of data from satellite, aircraft and ship is expected to support the development and verification of algorithms and atmospheric correction methods.

2.2 Optical properties of water

Radiative transfer theory (2) shows that the spectral diffuse reflectance R of macroscopically homogeneous, optically deep water is determined at each wavelength by the ratio of its diffuse back scattering coefficient b^+ to its diffuse absorption coefficient a^+, as follows:

$$R = \frac{b^+/a^+}{1 + (b^+/a^+) + \sqrt{1 + 2(b^+/a^+)}} \quad \ldots\ldots (1)$$

Normally, $b^+/a^+ < 1$.

The spectral reflectance of typical arid (blue) water results from combined effects of a^+ and b^+, since both vary to some extent with optical wavelength across the spectrum. When any type of living phytoplankton is added to such water, the spectral reflectance rises in the green and falls in the blue part of the spectrum. (Compare water-leaving radiances in Fig. 1) The rise in the green is caused by the increased backscatter of the plankton particles increasing b^+ in the above equation. In the green, the absorption coefficient a^+ is not changed appreciably by the addition of phytoplankton because chlorophyll does not absorb green light appreciably. Thus the green reflectance R increases with b^+. In the blue, however, chlorophyll absorbs so strongly that the addition of phytoplankton causes the absorption coefficient a^+ to increase much more than does the back scattering coefficient b^+. Thus R is decreased in the blue region of the spectrum. (Compare water-leaving radiance - dashed line - in Fig. 1)

Sediments in suspension scatter light strongly, thereby increasing b^+ throughout the spectrum, but they ordinarily have only weak effects on a^+. Thus an addition of sediments tends to raise the spectral reflectance of ocean water at all wavelengths.

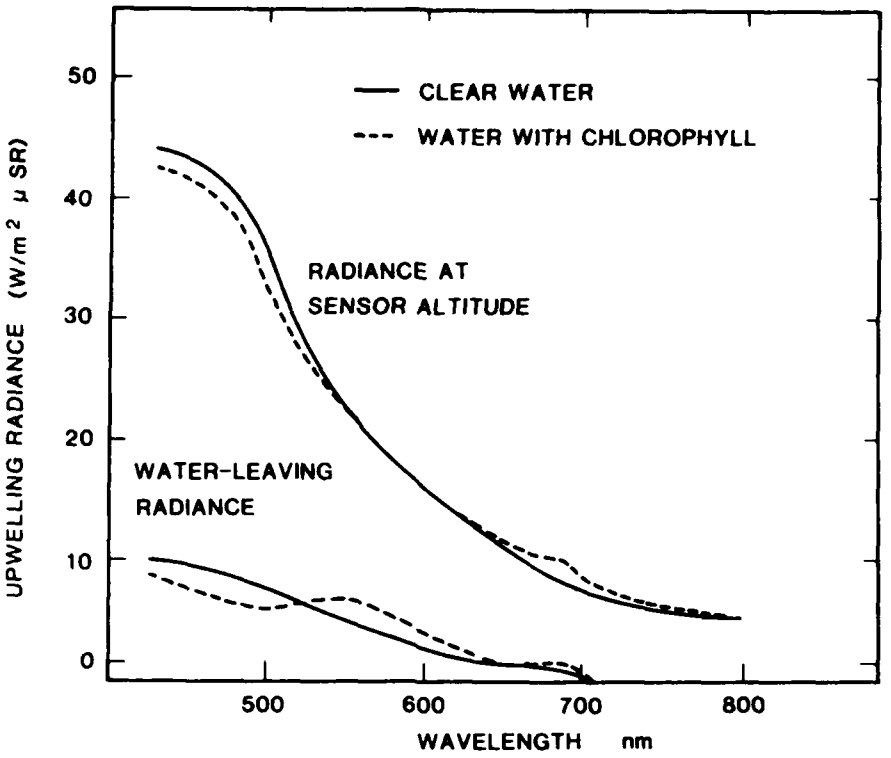

Fig. 1 Upwelling radiance above the water and above the atmosphere for clear (solid line) and for case I * water containing some chlorophyll (dashed line)

Consequently the presence of suspended sediments can be distinguished from chlorophyll-bearing plankton by the shape of their respective reflectance curves. Decomposing organic materials produce solutes (yellow substance) which increase a^+ primarily in the blue and violet spectral region and thus lower the spectral reflectance at those wavelengths in a manner which at least theoretically could be distinguished from the spectral effects of living chlorophyll.

---

* Case I waters (2) are those water masses for which phytoplankton and their derived products play a dominant role in determining the optical properties. They are not influenced by terrigenous influx. Case I waters range from oligotrophic and deep blue waters ($C < 0.1$ mg/m^3) to moderately productive green waters ($C \approx 1$ mg/m^3) and even to some eutrophic, dark green waters ($C > 10$ mg/m^3) which can be encountered in upwelling regions along arid coasts.

2.3 Radiative transfer through the atmosphere

In order to retrieve the water-leaving radiance (or reflectance R_w) from the data collected at satellite altitude, these have to be corrected for the influences of the atmosphere in between, i.e., for absorption processes and for scattering by the molecules (Rayleigh scattering) and the aerosols (Mie scattering).
The correction scheme is based on the following equation (3):

$$R_{Sat}(\lambda) = T_{O_3}(\lambda) \cdot \left\{ R_R(\lambda) + R_A(\lambda) + R_W(\lambda) \cdot T_R(\lambda) \cdot T_A(\lambda) \right\} \quad \ldots\ldots \quad (2)$$

where

$R_{Sat}(\lambda)$	reflectance measured by satellite
$R_R(\lambda)$	reflectance due to Rayleigh scattering
$R_A(\lambda)$	reflectance due to aerosol scattering
$R_W(\lambda)$	water-leaving reflectance
$T_R(\lambda)$	Rayleigh transmission losses
$T_A(\lambda)$	aerosol transmission losses
$T_{O_3}(\lambda)$	ozone transmission losses

Equation (2) means that the reflectance $R_{Sat}(\lambda)$ at satellite altitude is the sum of two atmospheric terms, $R_R(\lambda)$ and $R_A(\lambda)$, respectively caused by Rayleigh and by aerosol scattering, and of the water reflectance $R_W(\lambda)$. This last term is attenuated by Rayleigh and aerosol transmission losses $T_R(\lambda)$ and $T_A(\lambda)$; the entire term is in addition further attenuated by the factor $T_{O_3}(\lambda)$ accounting for the ozone absorption.

Further, equation (3) indicates that the aerosol contribution $R_A(\lambda)$ at any wavelength λ can be proportionally derived from a value of $R_a(\lambda_o)$ at a reference wavelength λ_o,

$$R_A(\lambda) = E(\lambda) \cdot R_A(\lambda_o) \quad \ldots\ldots\ldots\ldots\ldots\ldots \quad (3)$$

The atmospheric correction is the inversion of equation (2) which transforms the satellite reflectance $R_{Sat}(\lambda)$ into the water-leaving reflectance $R_W(\lambda)$ by using equations (2) and (3) and computations of Rayleigh and aerosol scattering $R_R(\lambda)$ and $R_A(\lambda)$, and transmissions $T_R(\lambda)$ and $T_A(\lambda)$.

This inversion procedure begins by computing $R_c(\lambda)$, i.e. the reflectance corrected for ozone and most Rayleigh effects.

$$R_c(\lambda) = \frac{1}{T_R(\lambda)} \cdot \left\{ \frac{R_{Sat}(\lambda)}{T_{O_3}(\lambda)} - R_R(\lambda) \right\} \quad \ldots\ldots\ldots\ldots \quad (4)$$

Compared to $R_{Sat}(\lambda)$ in which $R_R(\lambda)$ plays a major role, this term has the advantage to be nearly independant of the view angles. Since the Rayleigh and ozone effects change monotonically across the image (in contrast to aerosol effects), only one set of conversions from $R_{Sat}(\lambda)$ and $R_c(\lambda)$ has to be computed and applied for all the pixels of a given image sub-set. The size of this sub-set has to be decided according to a balance between correction accuracy and economy regarding computer time. For the images processed at DFVLR, conversion tables were computed for sub-sets of 512 x 512 pixels.

The introduction of equation (2) into equation (4) yields two further equations:

$$R_A(\lambda) = T_R(\lambda) \left\{ R_c(\lambda) - R_W(\lambda) \cdot T_A(\lambda) \right\} \quad \ldots\ldots\ldots\ldots \quad (5)$$

$$R_W(\lambda) = \frac{1}{T_A(\lambda)} \left\{ R_c(\lambda) - \frac{R_A(\lambda)}{T_R(\lambda)} \right\} \quad \ldots\ldots\ldots\ldots\ldots\ldots \quad (6)$$

A Rayleigh term $R_R(\lambda)$ still appears, however, its effect is minor in comparison to that one removed in the previous step. The aerosol transmittance T_A has a second order influence. Subsequently $R_A(\lambda)$ can be derived from equation (5) assuming $R_W(\lambda)$ is known or preferably negligibly small. This latter assumption is well established for higher wavelengths (red and infrared region) especially for case I waters, and thus allows the determination of $R_A(\lambda)$. Once $R_A(\lambda)$ has been determined at a higher wavelength it can be extrapolated towards the shorter wavelengths (equation (3)) making feasible the retrieval of $R_W(\lambda)$ by using equation (6).

The factor E() in equation (3) can be determined from the following relationship:

$$E(\lambda) = \left(\frac{\lambda}{\lambda_0} \right)^{-n} \quad \ldots\ldots\ldots\ldots\ldots \quad (7)$$

where n is the so-called Angstrom exponent. Because n was not yet known at the time of the processing, a value of n=1 was applied.

3. Nimbus-7 / CZCS

3.1 Instrument and orbit specifications

The CZCS on the Nimbus-7 satellite is the first multispectral image scanner of high sensitivity dedicated to the measurement of ocean color from space in five narrow spectral bands. (The sixth band for the measurement of sea surface temperature failed in late 1981.) The instrument specifications for the CZCS are listed in Table 1; Nimbus-7 orbit parameters are listed in Table 2.

FOV	78.68 °	
SWATH WIDTH	1566 km	
IFOV	0.865 m rad	
PIXEL SIZE (nadir)	825 m	
SPECTRAL BANDS:	Centre	Halfwidth
Visible/near i.r.	443 nm	20 nm
	520 nm	20 nm
	550 nm	20 nm
	670 nm	20 nm
	750 nm	100 nm
Thermal i.r.	11.5 μ	2 μ

Tabl. 1 CZCS instrument specifications

ALTITUDE	955 km	INCLINATION ...	99.2 °
NODE	ascending	EQUAT. CROSS ...	noon
RE-VISIT TIME	6 days	ORBIT TIME ...	104 min
ORBIT	sunsynchronous	ORBITS/DAY	13.8
SEPARATION	26 °		

Tabl. 2 Nimbus-7 orbit specifications

3.2 Data acquisition

The area of the Alboran Sea was covered once daily by the CZCS around noon with the exception of 4, 5, 10, 15 October 82. However, not all of the imagery collected was suitable for further processing. Data which have been processed into chlorophyll maps in this report are listed in Table 3.

DATE:	ORBIT NR.	APPROX. SCAN ANGLE ABOVE ALBORAN SEA
1 Oct. 82	19932	9° left
6 Oct. 82	19946	22° left
7 Oct. 82	19960	5° left
8 Oct. 82	19974	20° right
11 Oct. 82	20015	35° left
12 Oct. 82	20029	18° left
13 Oct. 82	20043	6° right
16 Oct. 82	20084	40° left
19 Oct. 82	20126	15° right
20 Oct. 82	20140	35° right

Tabl. 3 CZCS data from Oct. 82 which have been processed at DFVLR

4. Data processing

4.1 General

Raw data from the CZCS are pre-processed at the Goddard Space Flight Center according to NASA standard (Tape Specs. T 744041) into so-called Calibrated Radiance and Temperature Tapes (CRTs) which are in a format suitable to be processed further on a digital image processing system. The same standard is used at ESA's receiving station in Lannion and in Maspalomas.

The processing of CRT tapes was done jointly by staff members of INTA and of DFVLR at the Digital Interactive Image Processing System (DIBIAS) of the Institute for Optoelectronics at the DFVLR in Oberpfaffenhofen. For this purpose a special software package consisting of 12 different programmes has been developed and installed during the past years. This consists of special read-in programmes, programmes for additional data extraction, programmes for radiometric and geometric manipulations and the programmes for the generation of derived products like.e.g., chlorophyll maps (4).

Each CRT contains up to three different 2 minute scenes. Each scene consists of both, image data (6 channels) plus the additional housekeeping and geographic data. These are essential for the

radiometric and geometric processing and can be listed or printed upon request. After this, processing is usually done on a smaller, cloud-free sub-scene of the complete image (approx. 512 x 512 pixels) and involves essentially the steps described briefly in the following sections.

4.2 Geometric corrections

The geographic reference data (anchor points) provided for each scan line are chosen in such a way that they correspond to the selected sub-scene (10 x 10 reference points). These are automatically extracted and used for the transformation of the scene into a mercator projection. With this data set a second order polynomial is calculated so as to rectify the sub-scene geometrically on a pixel-to-pixel base.
Further, a suitable longitude / latitude grid is generated within the image processing system which can be superimposed onto the sub-scene.

4.3 Atmospheric corrections

In order to recover the water-leaving reflectance R_W from the recorded radiance values at satellite altitude in the way as described in section 2.3, the following steps are used:

- Calculation of CZCS sensitivity decay (according to (3))
- Calibration of raw data
- Conversion into reflectance through solar constant
- Computation of ozone and Rayleigh attenuation
- Computation of aerosol reflectance in channel 4
- Atmospheric correction of channel 4
- Atmospheric correction of other channels
- Computation of water-leaving reflectances

4.4 Calculation of pigment distribution

A functional form which relates the chlorphyll-a concentration C to the reflectance at zero altitude is:

$$C\ (mg/m^3) = A \times R^B,$$

where R is the reflectance ratio of two CZCS channels, while A and B are constants (1).

For the processing of the chlorophyll maps in this report, the ratio of CZCS channels 1/3 were used for R, while for the constants A and B the values 0.47 and -1.27 were used respectively.

The resulting chlorophyll maps are generated so as to cover a large dynamic range and show the chlorophyll distribution in a logarithmic scale (white = high, grey = medium, black = low concentration). The range covered in the imagery corresponds to chlorophyll values of

$$0.03 \text{ mg/m}^3 = \text{black}$$
$$1.00 \text{ mg/m}^3 = \text{white}$$

The boundary between land (and clouds) against water is masked with a white line. Grey values above land and clouds are in addition modulated with the data derived from channel 5, however, they are not significant in regard to the information above water.

The chlorophyll maps are shown in Figures 2 to 11.

5. Results and discussion

Within the Alboran Sea, chlorophyll appears around the warm, anti-cyclonic gyre, especially north and east of it. This area seems to represent either the jet-like Atlantic inflow, or an upwelling zone associated with the interaction of the inflow with the bottom topography near the Spanish coast (5, 6).
A more detailed comparison with ship and aircraft data is expected to reveal the exact origin of this pigment accumulation and its association with specific water masses.

Within the period during which CZCS data have been processed, rapid changes in the abundance and especially in the geographic distribution of pigments can be observed (7). These rapid changes are probably caused by a period of strong, north-westerly winds and the corresponding displacement and vertical mixing of water from 5 to 9 October 82. Also in this case, a more detailed comparison with bio-chemical (R/V Naucrates) and hydrographic data (R/V Bartlett) will be required before an explanation for these phenomena can be found.

Generally speaking, the concentration at which chlorophyll

appears in the imagery does not vary considerably during the period of observations. However, there is one exception to this, namely the image from 16 October 1982 (Fig. 9). In this image no chlorophyll at all can be found with the exception of the coastal area in the Gulf of Cadiz (river effluent). Since in the chlorophyll maps from the dates before as well as from the dates after 16 October chlorophyll is clearly visible, it is very unlikely that physical or biochemical processes in the water are responsible for this dramatic change. Instead, it is more likely that the atmospheric conditions were such that the "standard" correction procedure applied to all data was not sufficient any more. From Table 3 it is evident that during the orbit on 16 October 82 the Alboran Sea was observed at a comparatively large scan angle of almost 40 ^{o}. Under these conditions apparently special steps have to be undertaken so as to derive corrected water-leaving reflectance values through the increased air mass.

6. Acknowledgement

These investigations are based on a number of specific image processing programmes which have been developed and implemented in cooperation with Mr. H. Helbig, DFVLR and Dr. M. Viollier, Roscoff. Their work but also their support and advice in the use of these programmes is greatly acknowledged.
The participation in the Alboran Sea Experiment 82 and the subsequent data processing was made possible due to a cooperation agreement between INTA in Spain and DFVLR in Germany on behalf of their respective governments. The interest and support by the heads of those organizations and especially the support by the coordinators of this cooperation programme is highly appreciated.

7. Literature

(1) ESA, OCWG "Progress report to ESA Earth Observation Advisory Committee from the Ocean Color Working Group" (ESA BR-20, June 1984)

(2) Duntley, S. Q. et al "Ocean color analysis" (SIO Ref. 74-10, April 1974)

(3) Viollier, M. "Radiometric calibration of the Coastal Zone Color Scanner on Nimbus-7: a proposed adjustment" (Appl. Optics 21(6), 1142-45 (1982))

(4) Triendl, E. et al "Dibias Handbuch" (Internal Report: DFVLR, NE-OE-14-9-82)

(5) Kinder, T. H. et al "Hydrographic measurements in the western Alboran Sea." (NORDA Technical Note 202 (1983))

(6) La Violette, P. E. "Short term measurements of surface currents associated with the Alboran Sea during "Donde va?"." (NORDA Technical Note 241 (1983))

(7) Arnone, R. A. Personal communication (1983).

Fig. 2 Chlorophyll-a distribution on 1 Oct. 1982 (orbit 19932)

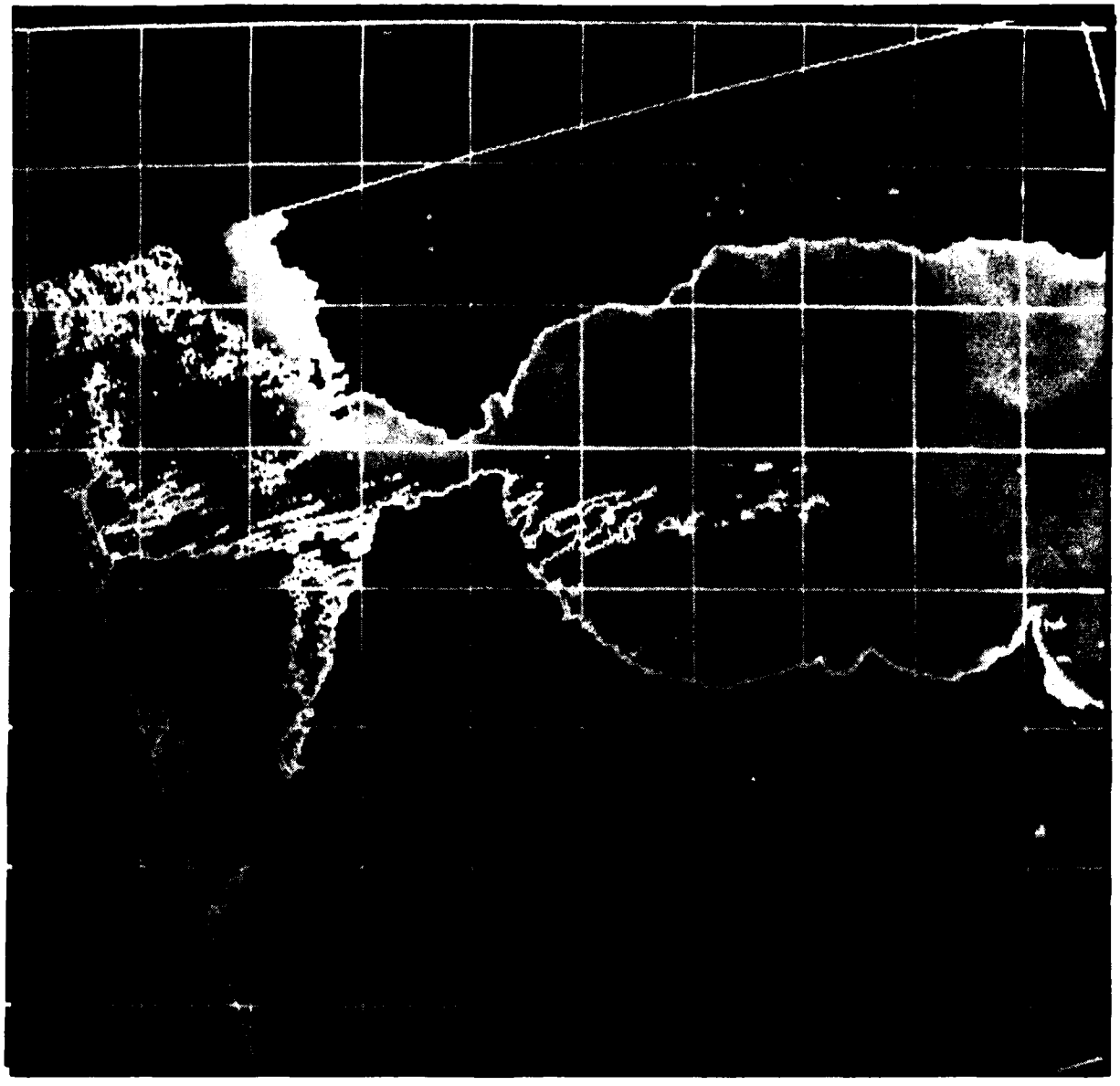

Fig. 3 Chlorophyll-a distribution on 6 Oct. 1982 (orbit 19946)

Fig. 4 Chlorophyll-a distribution on 7 Oct. 1982 (orbit 19960)

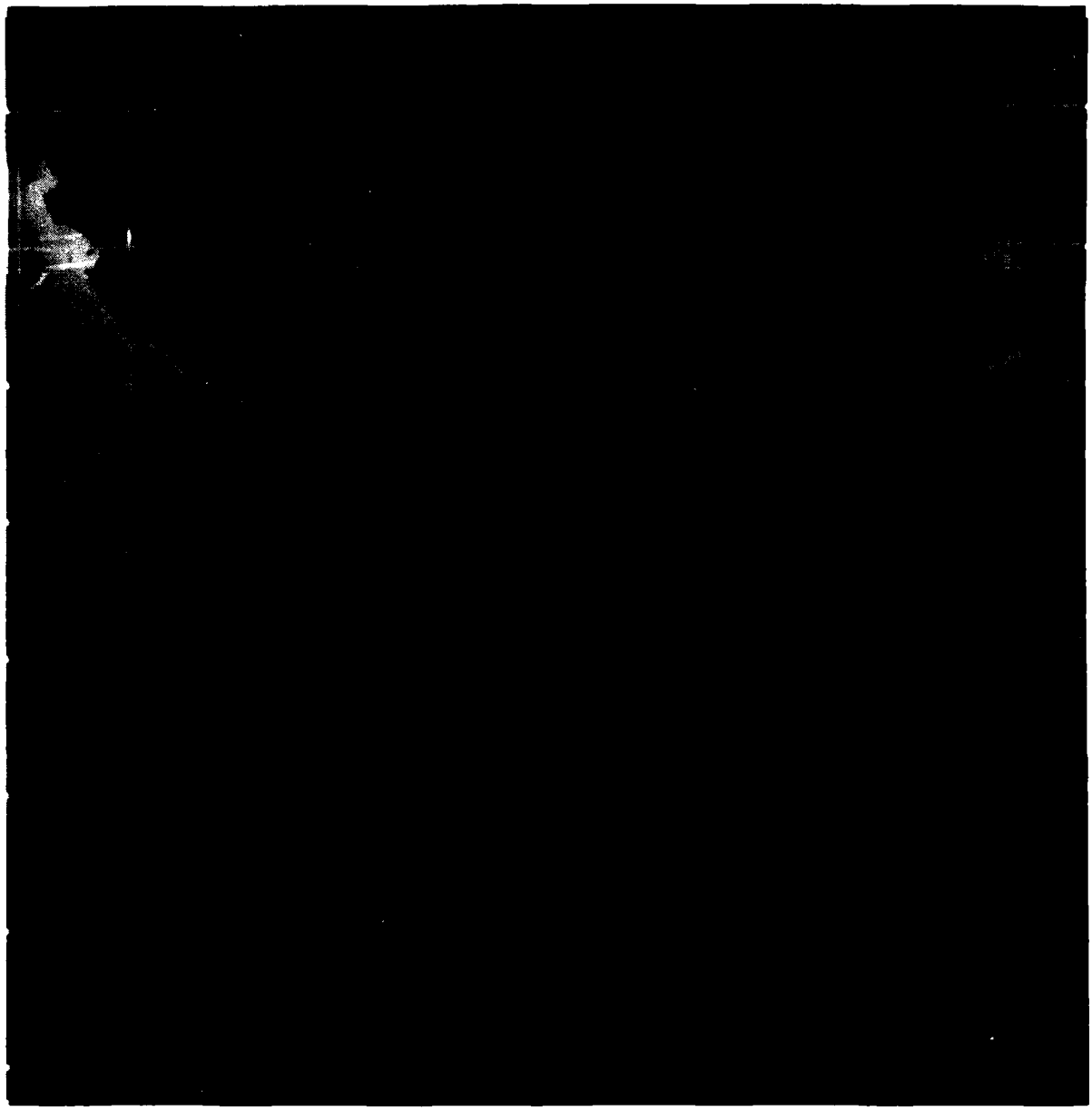

Fig. 5 Chlorophyll-a distribution on 8 October 1982 (orbit 19974)

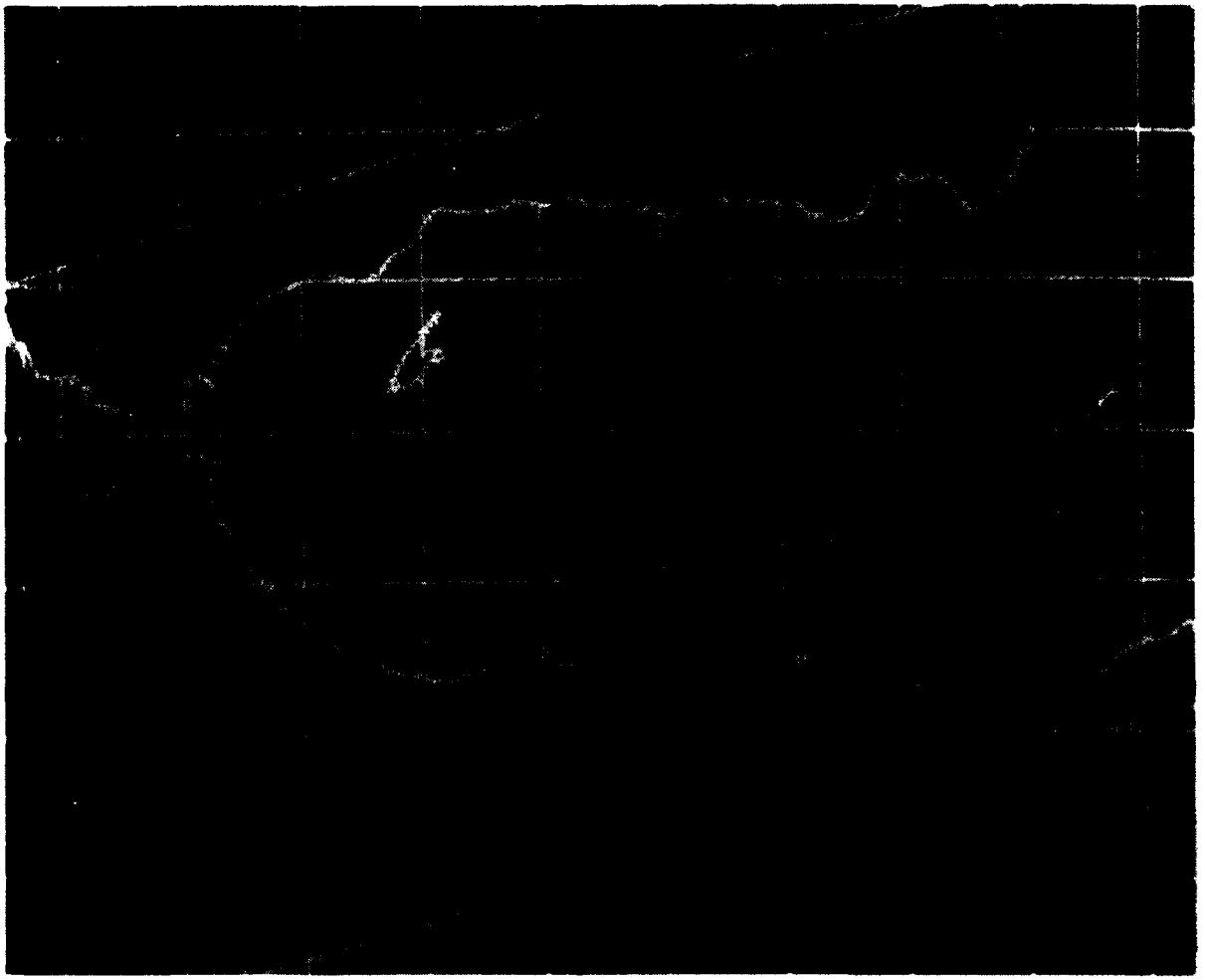

Fig. 6 Chlorophyll-a distribution on 11 October 1982 (orbit 20015)

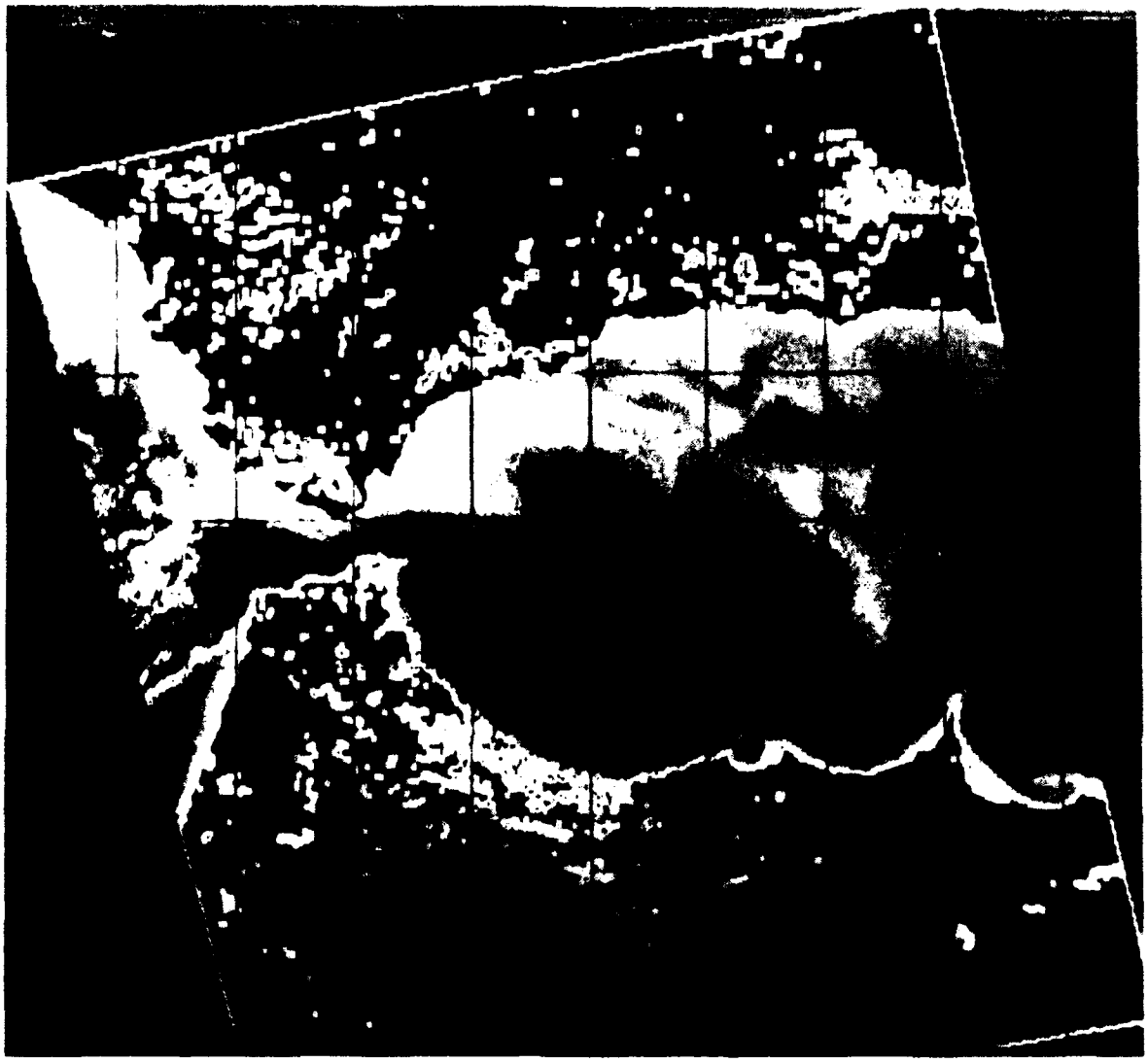

Fig. 7 Chlorophyll-a distribution on 12 October 1982 (orbit 20029)

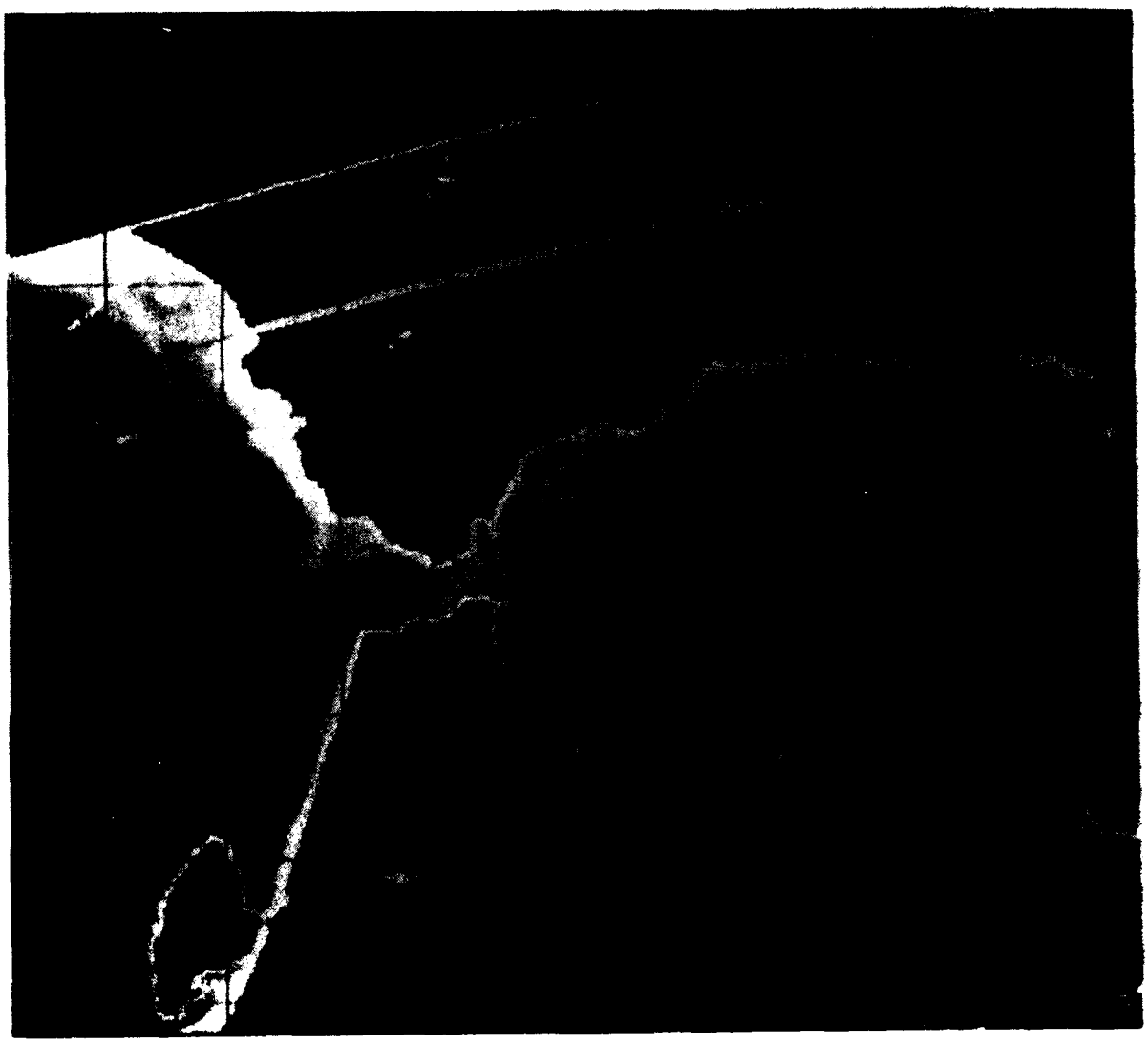

Fig. 8 Chlorophyll-a distribution on 13 October 1982 (orbit 20043)

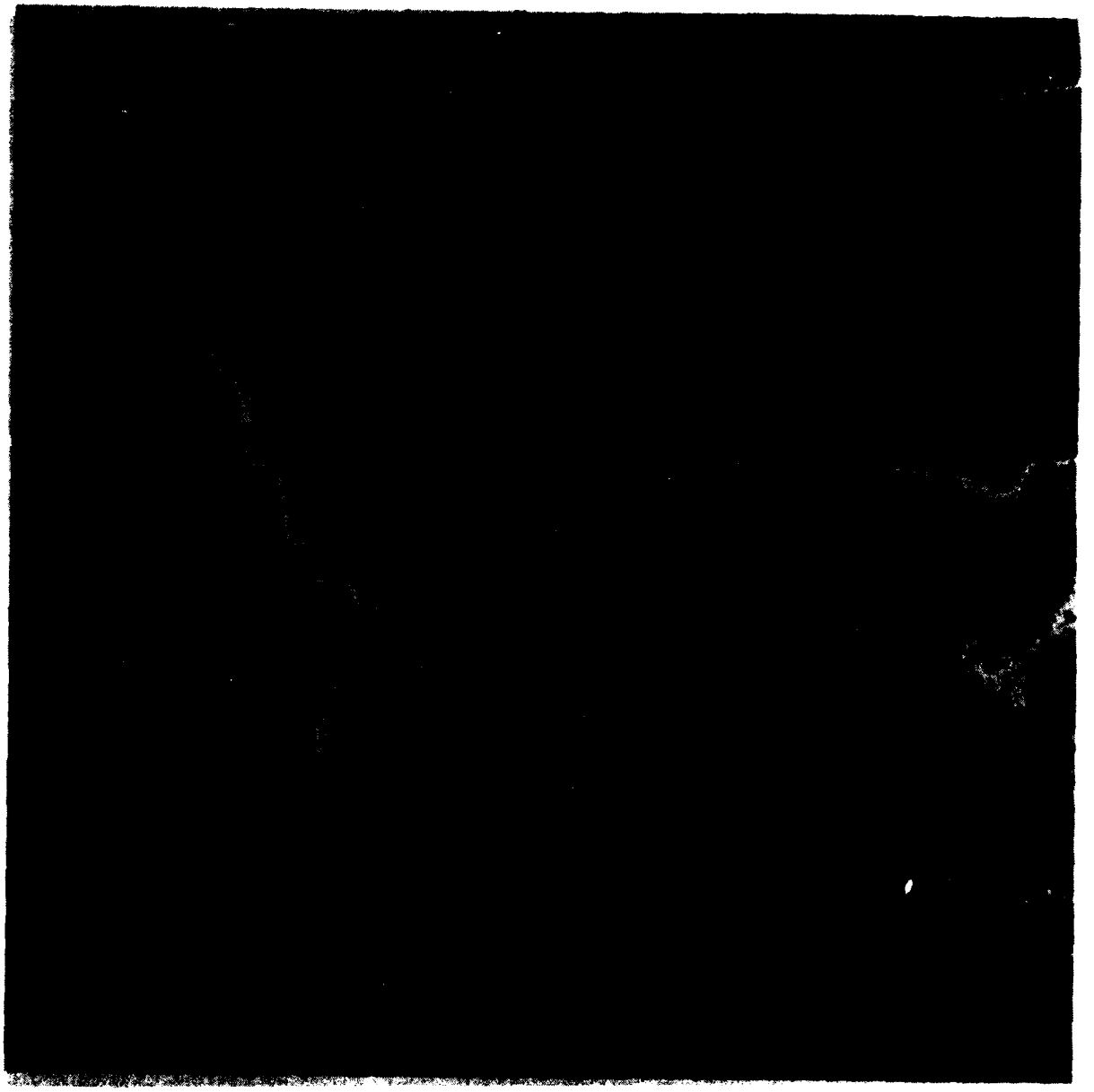

Fig. 9 Chlorophyll-a distribution on 16 October 1982 (orbit 20084)

Fig. 10 Chlorophyll-a distribution on 19 October 1982 (orbit 20126)

Fig. 11 Chlorophyll-a distribution on 20 October 1982 (orbit 20140)

THE FLOW OF ATLANTIC WATER INTO THE ALBORAN SEA DURING DONDE VA

Henry Perkins and Thomas H. Kinder

Naval Ocean Research and Development Activity
NSTL, Mississippi 39529, U.S.A.

Extensive environmental measurements were made in the western Alboran Sea during 5-13 October as part of the Donde Va? experiment. These provide a multi-disciplinary and nearly synoptic view of the area between the Strait of Gibraltar and a section between Adra and Cape Tres Forcas. An overview of the experiment has been given by Parrilla (1984) and by The Donde Va Group (1984). Evident in the dynamic topography is a large anti-cyclonic gyre, similar to that reported by Lanoix (1974) but of lesser intensity (Kinder and Parrilla, 1984). The gyre circulation during Donde Va? was also clear in satellite infrared images and drifter trajectories (La Violette, 1984).

Calculation of geostrophic transport in the upper 200 m (Fig. 1) indicates a satisfactory balance between the inflow through the Strait of Gibraltar and the outflow to the east past Alboran Island. The transport in the northern portion of the gyre along the section south of Malaga (2.7x106 m^3/sec), splits into two approximately equal parts, one continuing on towards the east, the other returning westward to form the southern half of the gyre. The transport at the eastern boundary of the study area passes in nearly equal amounts to the north and south of Alboran Island.

Characteristics of the region in the northwest where the gyre and Atlantic inflow join were determined by a series of stations (Fig. 2) made with an instrument combining the features of a lowered current meter and CTD (VCTD). Even at the westernmost of these sections, near Estepona, the geostrophic adjustment of the inflowing water appears nearly complete, the transport (1.5x106 m^3/sec) of the observed current (Fig. 3) agreeing well with that determined by geostrophy.

The inflowing water from the Atlantic consists of North Atlantic Central Water (NACW) modified by mixing during its travel through the Strait of Gibraltar (Lacomb and Richez, 1982). However, characteristics of the original NACW can still be detected within the Alboran Basin. Fig. 4 shows T-S curves from selected

VCTD stations along the Estepona section. Station 300 on the northern edge of the current indicates normally deep water brought to the surface through geostrophic adjustment, while station 299 on the southern edge is more representative of the gyre interior. The remaining stations, 294-296, correspond to the strongest portion of the current (see Fig. 3) and show a range of variability expected from incompletely mixed NACW.

In contrast, T-S curves on the southern side of the gyre, given in Fig. 5 for the CTD section near Punta Jagerschmidt, represent a well-defined water mass. Elevated surface temperatures of up to 20.8^{o}C are presumed to be the result of surface heating. Similarly prepared figures from other sections show a progressive development of this water mass as it sweeps around the gyre.

References

Donde Va Group (1984). Donde Va? An oceanographic experiment in the Alboran Sea. EOS, 65, 682-683.

Kinder, T.H. and Parrilla, G. (1984). The hydrographic structure of the Alboran Sea gyre, June and October 1982. Rapports et Proces Verbaux des Reunions, CIESM (in press).

Lacombe, H. and C. Richez (1982). The regime of the Straits of Gibraltar. In: Hydrodynamics of Semi-Enclosed Seas, J. Nihoul, ed., Elsevier Oceanography Series, 34, 13-73.

Lanoix, F. (1974). Projet Alboran. Etude hydrologique et dynamique de la Mer d'Alboran. NATO Technical Report 66, 39 pp. and 32 figs.

La Violette, P.E. (1984). The advection of submesoscale thermal features in the Alboran Sea gyre. J. Phys. Oceanogr., 14, 550-565.

Parrilla, G. (ed) (1984). Preliminary Results of Donde Va? Inst. Espan. Ocean. Inform. Tech. 24-1984, 267 pp.

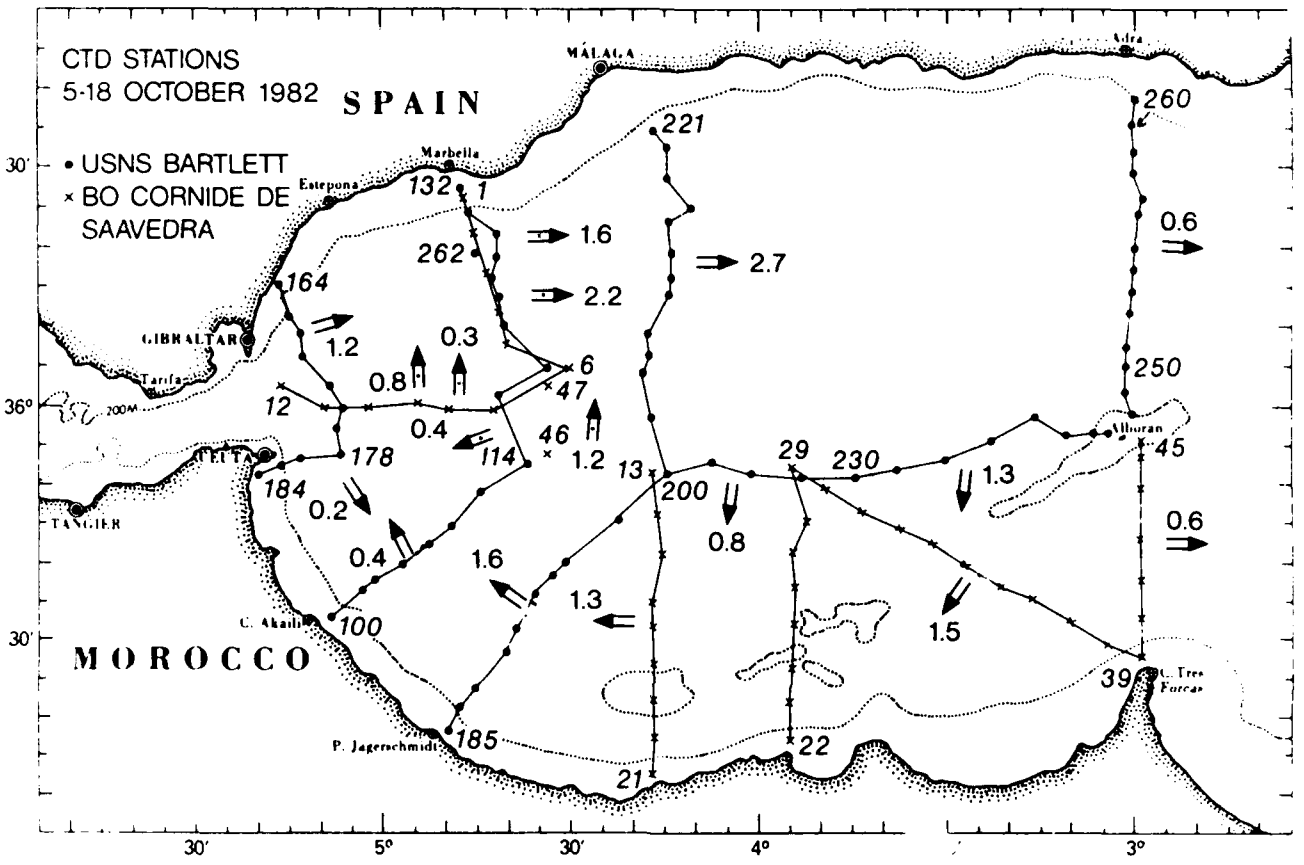

Figure 1. Distribution of hydrographic stations and geostrophic transports. Transports are given in 10^6 m^3/sec for currents between the surface and the reference depth of 200 m.

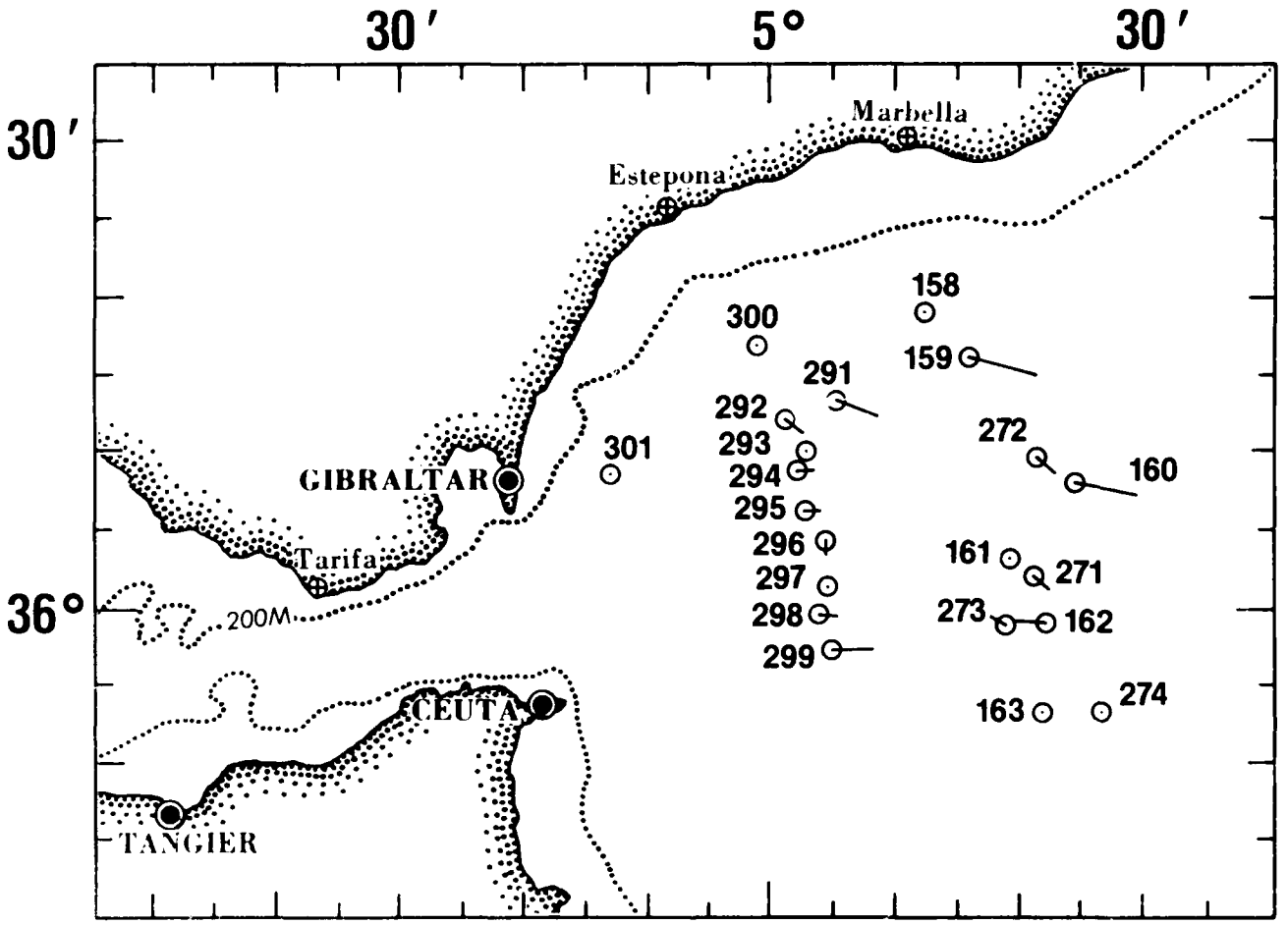

Figure 2. Distribution of VCTD stations. Circles indicate ship position at the start of each station and a line indicates its drift during the station. Directly measured current profiles, as well as hydrographic parameters, were measured at these stations.

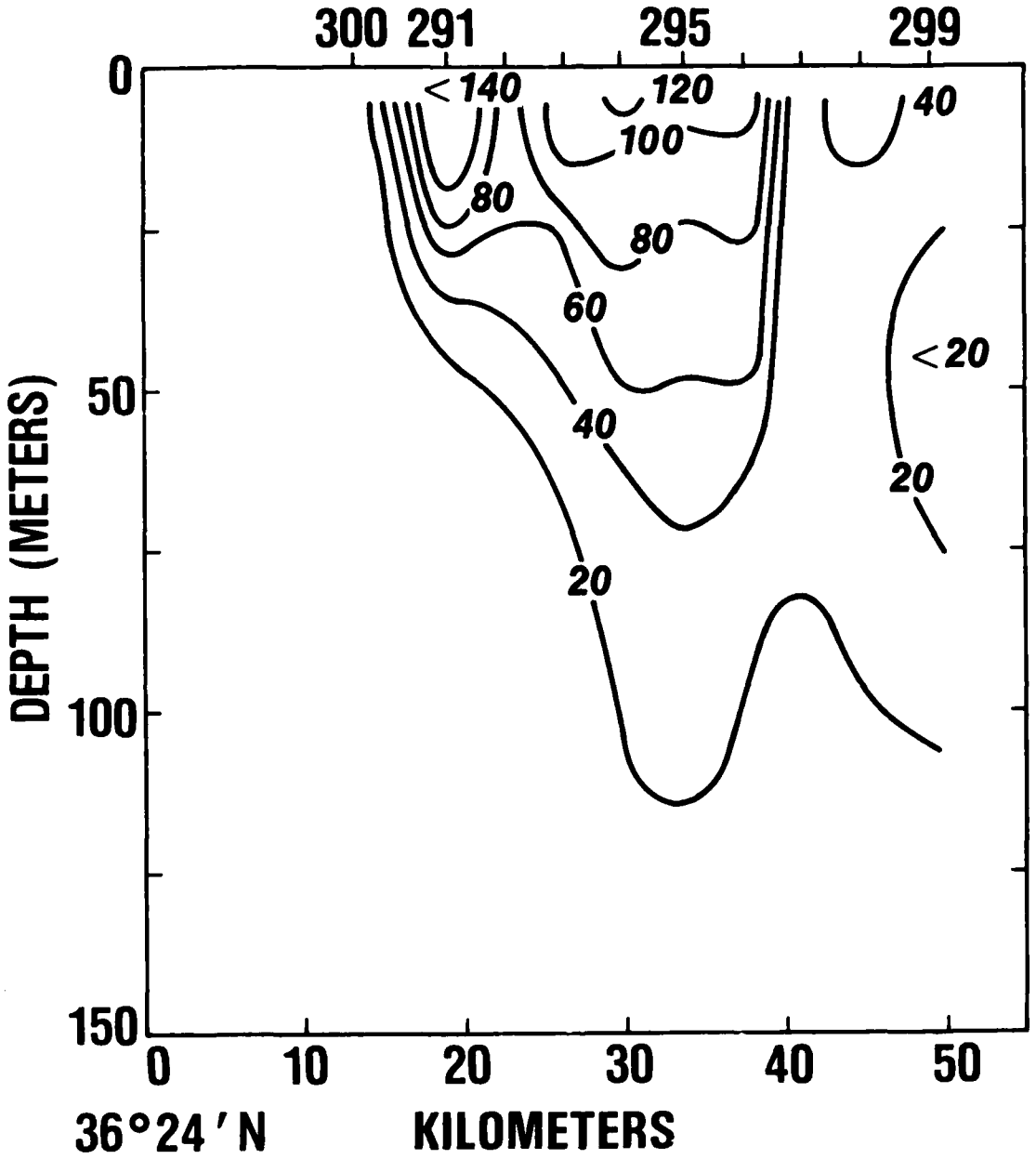

Figure 3. Section of eastward current component for VCTD stations south of Estepona during 16-17 Oct. Station numbers are given on the upper axis.

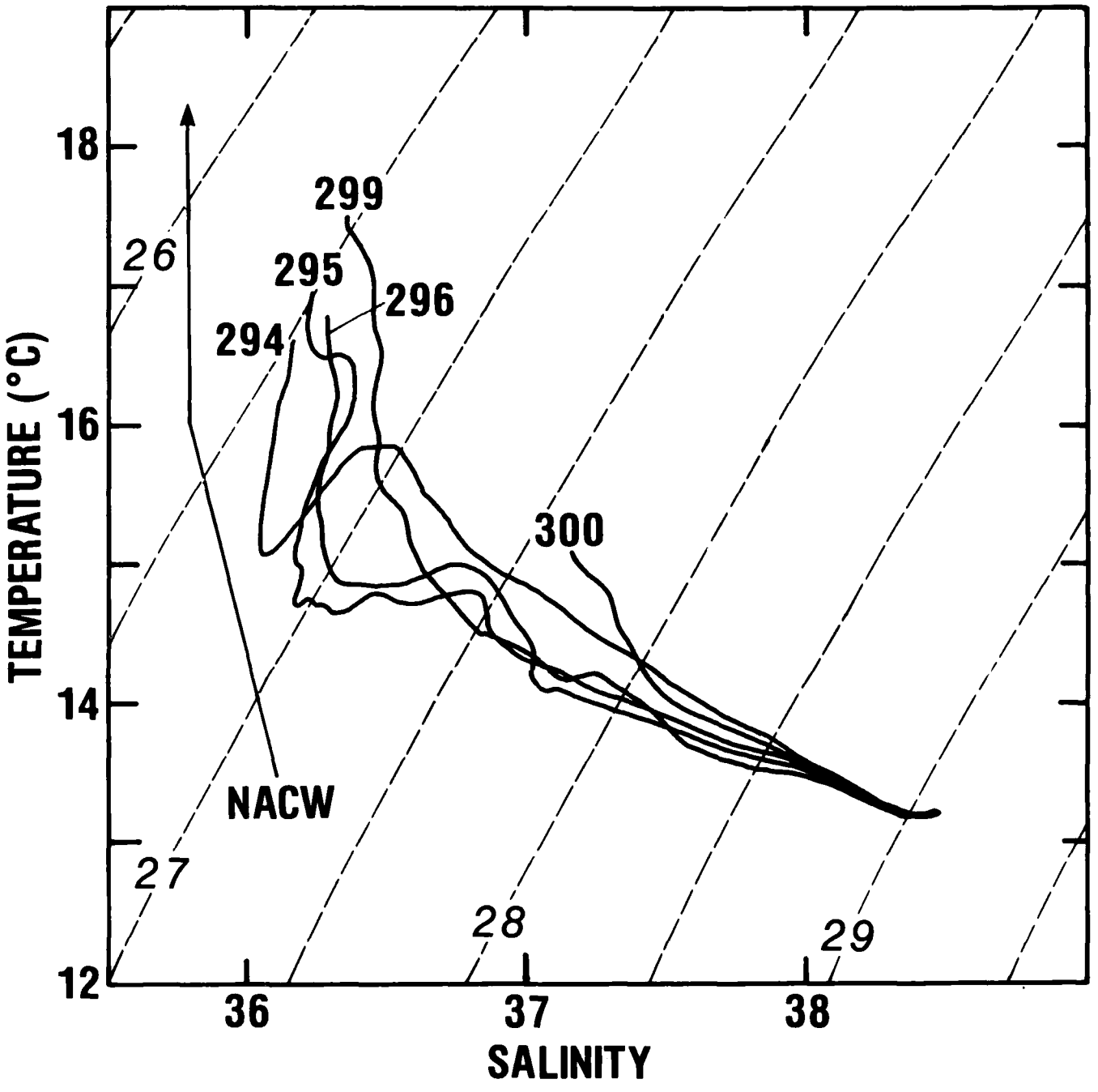

Figure 4. Temperature-salinity characteristics for selected stations along the Estepona VCTD section and for the NACW.

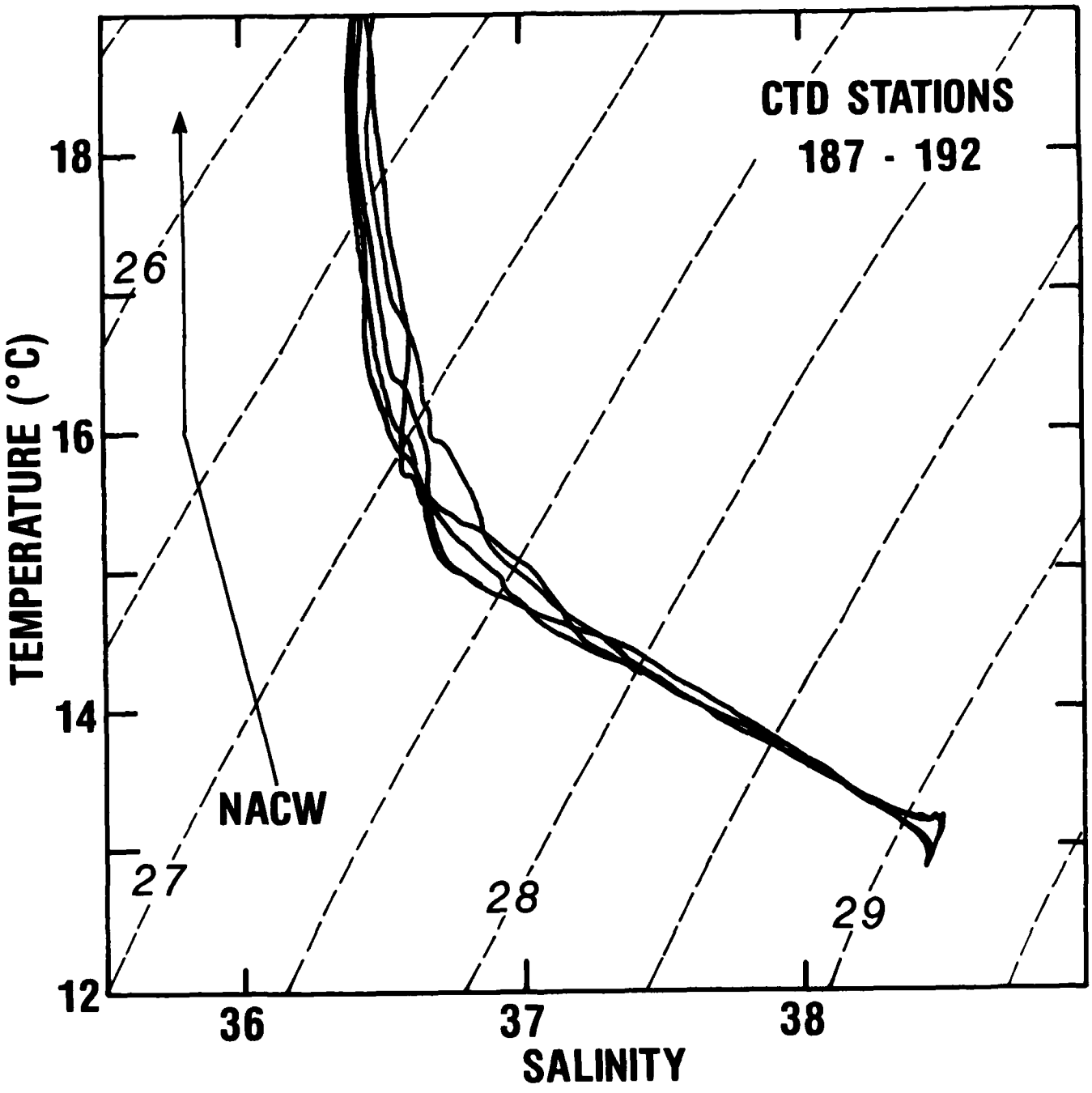

Figure 5. As in Figure 4, but for CTD stations along the P. Jagerschmidt section.

A TIME SERIES STATION AT THE EASTERN ENTRANCE OF THE STRAIT OF GIBRALTAR

GREGORIO PARRILLA
Instituto Espanol de Oceanografia
Alcala 27, 4° 28014 Madrid, Spain

SUMMARY

During the Donde Va? experiment in October 1982, a station located near 36°02'N, 5°14'W in an average water depth of 830 m was occupied for 20 hours. Ten casts were made with a continuously recording CTD. The interval of the survey included the occurrence of two low tides and two high tides at the Strait. The sampling rate permitted the detection of high frequency oscillations only in those occasions when the down and up cast could be compared.

The isolines showed the wave-like shape, found by others (Lacombe and Richez, 1982; Cavanie, 1973), which is related to the tides in the Strait. A description of the variations of temperature and salinity with time is given, as well as an interpretation of the isolines pattern in relation with the flow variations through the Strait.

INTRODUCTION

As part of the Donde Va? experiment in October 1982 (Donde Va? report, 1983; Parrilla, 1984), a time series of CTD profiles was made in the eastern entrance of the Strait of Gibraltar. It was located around 36°02'N and 5°13'W (Fig. 1), close to the point C2 of Lacombe and Richez (1982) and point G of Cavanie (1973). It lasted some 20 hours (October 7, 16.00 h to October 8, 12.30 h) during a period of neap tides. The average bottom depth was 830 m.

METHODS

A Neil Brown MK III CTD was used and calibrated in situ against water samples. Due to the familiar difficulties of working in the Strait, the casts were made

about one hour apart, ten lowerings in total. The time series (Fig. 2a, b) were drawn using the data from both the down and up records for each cast (dashed vertical lines). The time difference between them varied from some 60 minutes at surface to 5 minutes at 700 m. The series are refered to the tides at Tarifa (solid vertical lines).

RESULTS

The sampling rate is well suited to resolve oscillations of approximately tidal frequency only. Occasionally it is possible to notice differences between the down and up record of a cast, indicating the presence of unresolved higher frequency oscillations.

Figures 2a and 2b respectively show variations of potential temperature and practical salinity with time. A wave-like pattern is seen in the whole water column, although it is more uniform in the upper layer. Its period conforms to that of the semidiurnal tidal component in the Strait (Lacombe and Richez, 1982).

The interface, *defined by salinity* 37×10^{-3} *and temperature* $14.5^{o}C$, reached its shallowest value some 4 or 5 hours after high water at Tarifa (HWT) and sank very fast for about 1 or 2 hours before low water (LWT), reaching the lowest depth some 8 h after HWT. The mean of the salinity interface oscillation was around 80 m. The depth of the interface diminished slowly, taking almost 8 h from trough to crest, but it increased relatively rapidly, sinking 80 m in 3 hours.

In the upper layers, during the last part of the ascent and abrupt sinking of the interface, low salinity intrusions ($<36.10 \times 10^{-3}$) and temperature inversions (Ziegenbein, 1969) can be seen. During the subsequent gradual ascent, low salinities were not found, having been replaced by salinities higher than 36.30×10^{-3}, and the potential temperature inversions disappeared.

In the lower layer, the amplitude of the variations of the isolines was larger where the Levantine Intermediate Water (LIW) was manifest. At casts 123 and 129, the LIW signature was especially strong between 200 and 800 meters depth, with peak salinities and potential temperatures of 38.47×10^{-3} and $13.15^{o}C$ at the first of two extrema and 38.45×10^{-3} and $13.10^{o}C$ at the second. The upper 38.43×10^{-3}

isohaline--which together with its lower counterpart bounds the LIW core--raised some 200 m, nearly the same order as the 13°C isotherm. In the rest of the series, the salinity maximum was always less than 38.44×10^{-3} and the depth of the isolines was relatively fixed.

However, note that in some cases (e.g. casts 125 or 127) a variation of some 80 m has been observed between the down and up records in the same cast. This effect may be attributed to internal waves of high frequency that were not detected in upper layers where the time separation between both records was larger.

The Deep Water (DW), that in this part of the Strait occupies a thin layer close to the bottom, was clearly detected at cast 129 where the potential temperature was less than 12.80°C (Fig. 2a).

DISCUSSION

Since there were no current measurements simultaneous with the station, current data from other authors (mainly Lacombe) was used for purposes of interpretation.

According to Lacombe and Richez (1982) the current in the upper layer is strong and always eastward, reaching its maximum near LWT. In the lower layers, it is weaker and reverses direction with the tide. The alternating part of the current seems to be 180° out of phase between the two layers. As a result, during part of the ebb tide there is inflow in both layers reaching a maximum in the lower. A short time before LWT, the current in the lower layer turns again toward the west, while that in the upper continues to increase towards the east, reaching a maximum at about LWT.

During the flood tide, the currents in the upper and lower layers are in opposite directions. After the outflow reaches its maximum, the surface inflow decreases until the reversal of the outflow a short time after HWT, after which the water is again inflowing in both layers with increasing velocity.

Taking in mind this sequence of currents and looking at Fig. 2, an intrusion of North Atlantic Central Water (NACW) (salinity less than 36.20×10^{-3}) is seen to start at ebb tide and to consist of the Atlantic water which had accumulated

between this point and the western entrance of the Strait (Ziegenbein, 1969; Boyce, 1975). The LIW signature was weak at this time as the current there was also inflowing. After the current reversal in the lower layer, the interface became deeper, the most rapid deepening occurring when the upper inflow reached its maximum and the two layers system was no longer in equilibrium (Cavanie, 1973). As the outflow increased, the LIW was more evident.

During flood tide, the inflow in the upper layer decreased and the outflow in the lower layer continued. At the same time, the interface began to rise again and the upper layer was occupied by Atlantic water mixed with some Mediterranean water (salinity greater than 36.40×10^{-3}) and the layer became isothermal ($17^{o}C$). When the ebb tide began again, the lower current became inflowing once more, initiating a new cycle.

The DW was more visible in cast 129 than in cast 123 whereas the reverse is true for the LIW signal. These differences could be a manifestation of the diurnal tidal component.

The brief appearance of the LIW core is puzzling. Why did its signature not persist longer during the flood tide, while the outflow increased and reached a maximum? The sampling rate was barely adequate to resolve these brief pulses, but the fact of their brevity is clear enough.

Acknowledgments. This work was partially funded by Cooperative Project 3044 under the Spanish-American Treaty. M.J. Garcia helped with the data processing and A. Esteban made the drawings.

REFERENCES

Boyce, I.M., 1975. Internal waves in the Strait of Gibraltar. Deep-sea Research, 22: 597-610.

Cavanie, A., 1973. Observations Oceanographiques dans le Detroit de Gibraltar pendant la Campagne PHYGIB (September-October, 1971) Ann. Hydrogr. 5eme series, 1,1: 75-84.

Donde Va?. Report of Field Experiment. June-October, 1982. January 1983.

Lacombe, H. and C. Richez, 1982. The regime of the Strait of Gibraltar. In Hydrodynamics of semi-enclosed seas. Ed. by J. Nihoul. Elsevier O.S.:13-73.

Parrilla, G. (editor), 1984. Preliminary results of the Donde Va? Inst. Esp. Oceanogr., Informes Tecnicos no. 24, 267 pp.

Ziegenbein, J., 1969. Short internal waves in the Straits of Gibraltar. Deep-Sea Res., 16, 5: 479-487.

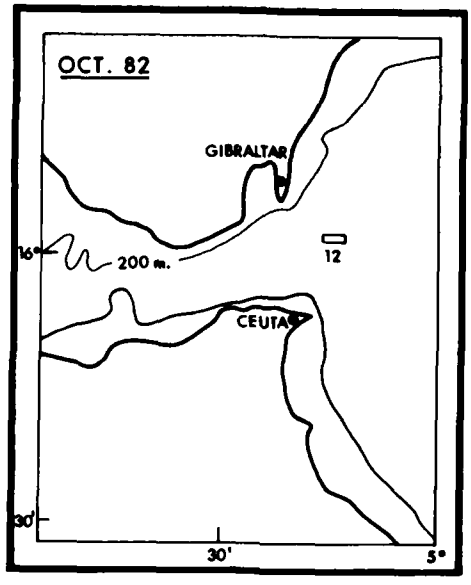

Fig.-1 Location of the time series station

Figure 1. Location of the time series station.

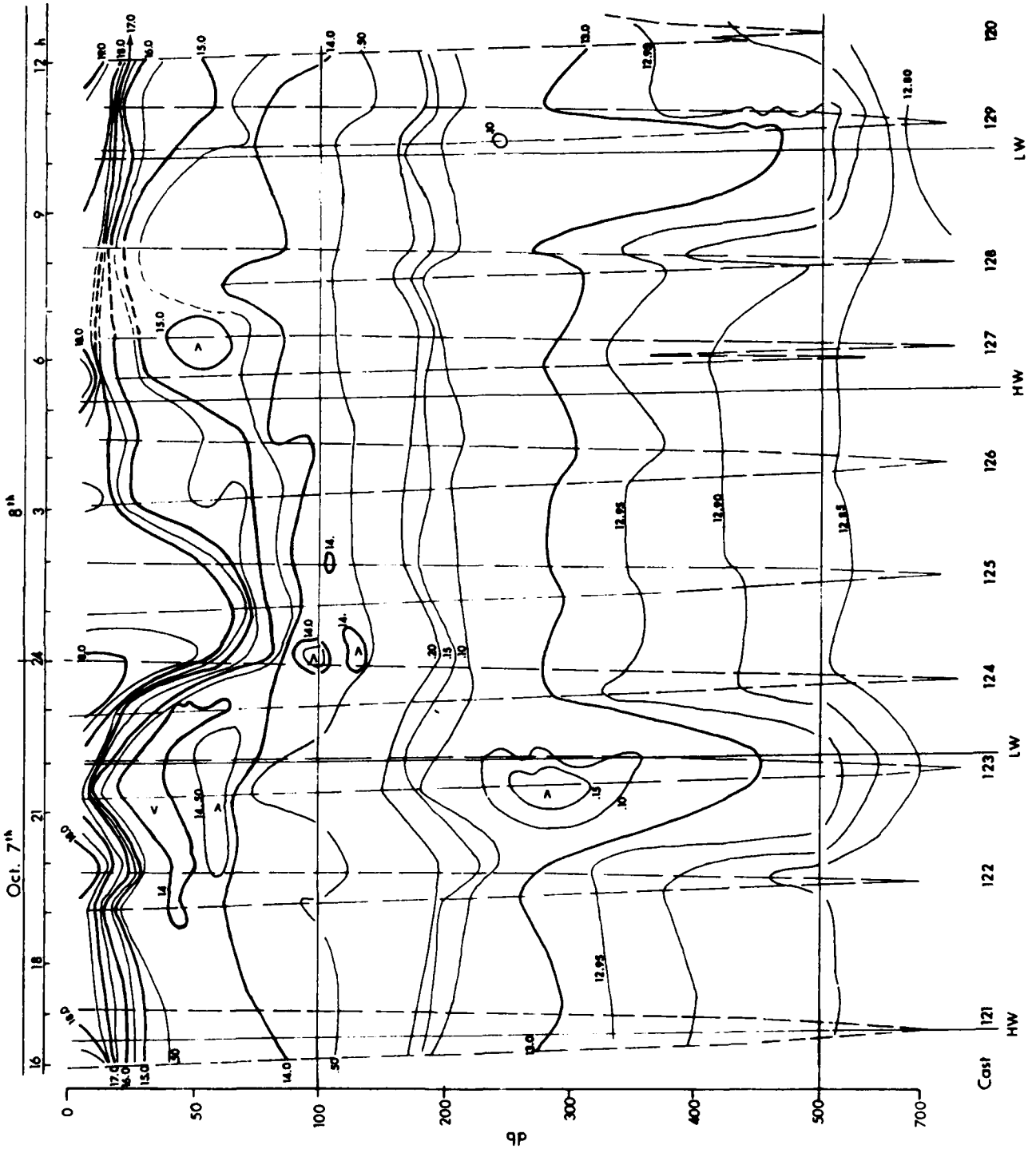

Figure 2a. Variation of potential temperature with time. Vertical solid line, high and low waters in Tarifa. Vertical dashed lines, approximated paths of the CTD lowerings and raisings. Horizontal solid lines, depth scale changes.

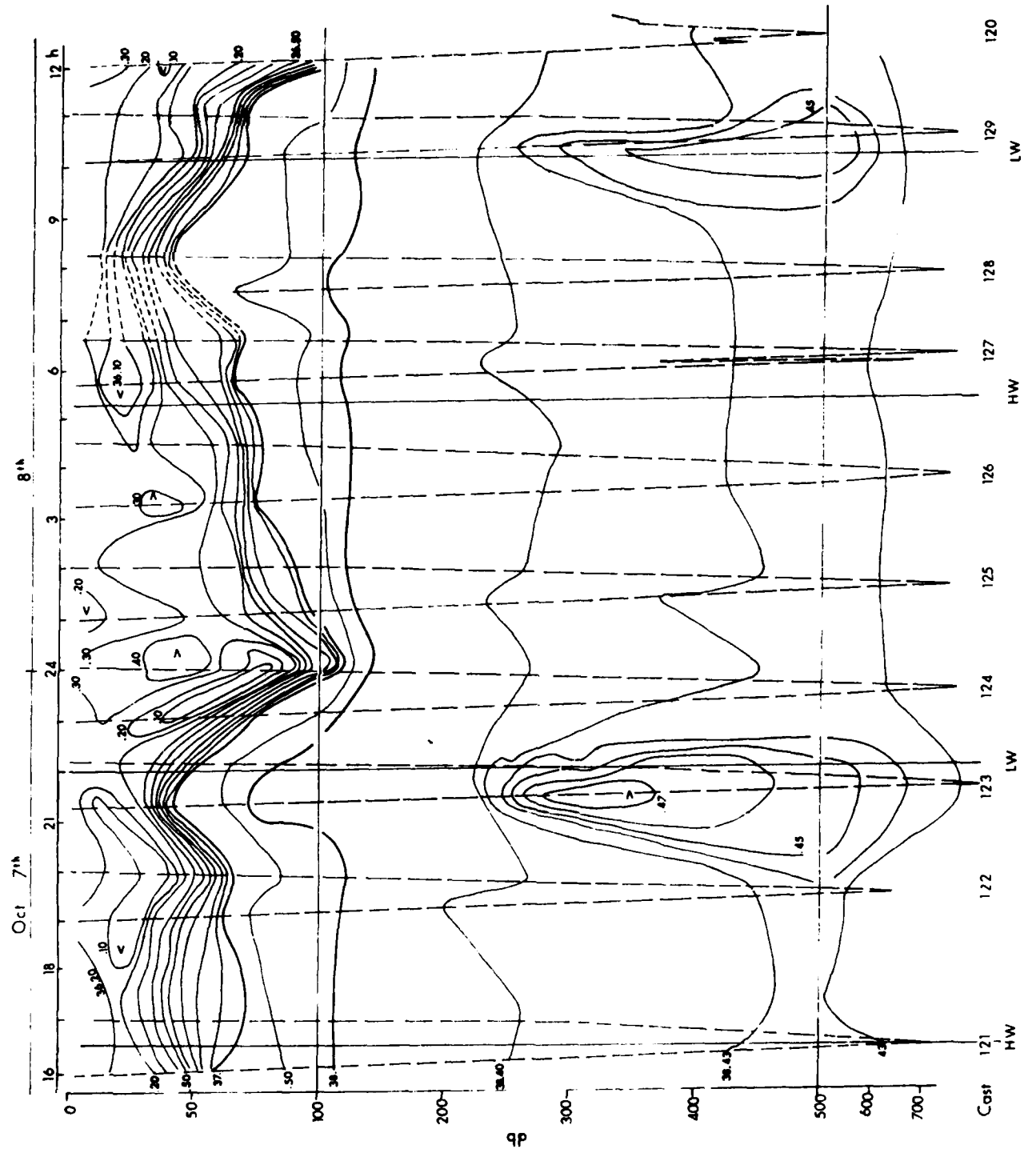

Figure 2b. Variation of salinity with time. Otherwise as in Fig. 2a.

A Preliminary Study of a Standing Internal Wave in the Western Approaches to the Strait of Gibraltar

Paul E. La Violette and Robert A. Arnone
Naval Ocean Research and Development Activity
NSTL, Mississippi 39529-5004

Aircraft flights during the period 6-11 October 1984 provided data which indicate a standing internal wave was continuously present west of the Strait of Gibraltar at 5°50' West. Although the wave appeared to essentially remain at one location--stretching from Spain to Morrocco, its surface appearance--visually and in the aircraft radar and infrared scanner imagery--showed considerable changes in strength that took place within several hours. The surface feature of the wave varied in appearance. However, it normally was shown to have a main portion that consisted of a central 1 kilometer-wide ridge of rapidly moving water with almost no waves. On each side of this central region, the waters were usually agitated with a strong chop. On one occasion, a wave went over the 20 meter high afterbridge of a 100 meter long freighter at the point that the freighter left the centeral comparitavely calm area of the standing wave and entered the region of chop.

AXBT's data showed that horizontal changes of 3°C were present across the feature and that vertical disturbances in temperature extended at least to the depth of the AXBT's (350 meters). Examination of the regional bathymetric charts shows the standing internal wave was associated with the main sill of the Strait of Gibraltar and was evidently a manifestation of the Mediterranean intermediate water flowing westward at depth over the sill into the Atlantic.

Unlike the eastward-moving tidal-induced internal waves normally found in the strait that displayed eastward-oriented bows as their surface configuration, the standing internal surface wave appearance was that of a large westward-oriented bow. On two occasions, eastward-propatating sets of tidal-induced internal waves were found originating from a position south of the center of the standing wave. These appearances occurred approximately 2 hours before local high tide. Although numerous eastward-moving internal waves were seen in the straits during the flights none was noted west of the standing wave.

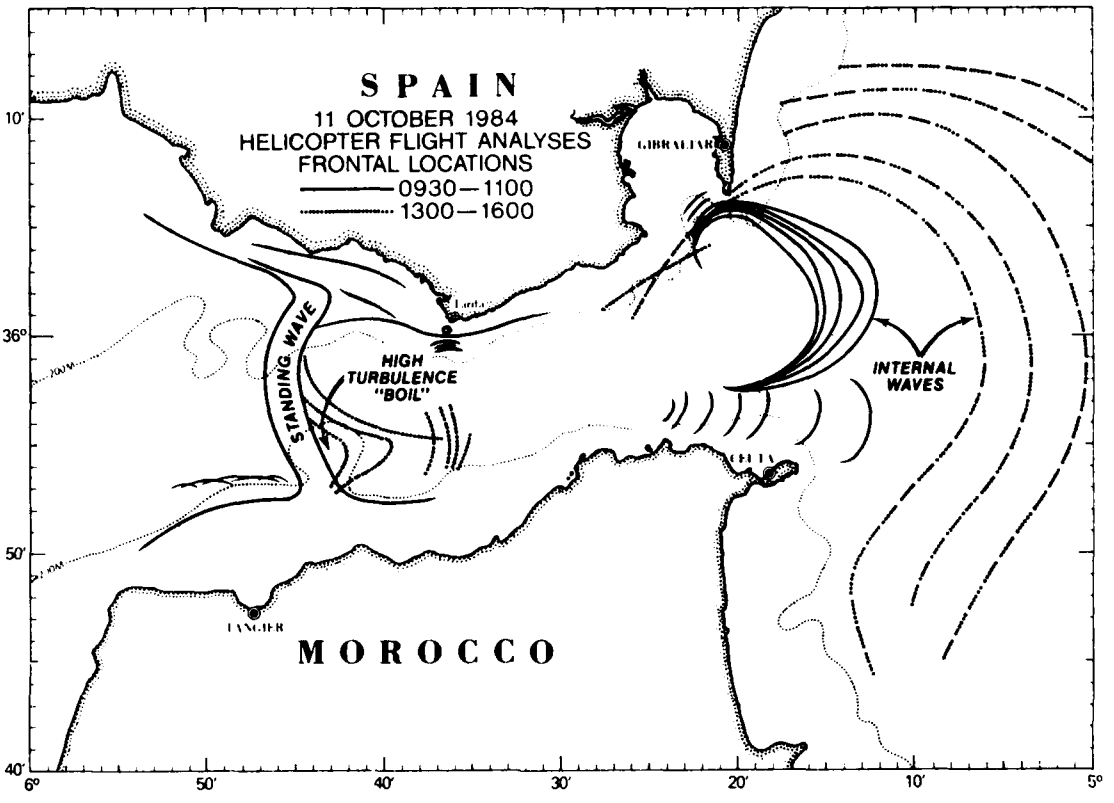
SPAIN
11 OCTOBER 1984
HELICOPTER FLIGHT ANALYSES
FRONTAL LOCATIONS
0930—1100
1300—1600
STANDING WAVE
HIGH TURBULENCE "BOIL"
INTERNAL WAVES
TANGIER
MOROCCO
10'
36°
50'
40'
6°
50'
40'
30'
20'
10'
5°

XXIXth Congress and Plenary Assembly, Lucerne, October, 11-19, 1984
Physical Oceanography Committee

EFFECTS OF WIND VERSUS HYDRAULIC FORCING ON THE DYNAMICS OF THE WESTERN MEDITERRANEAN SEA

George W. Heburn
Naval Ocean Research and Development Activity
NSTL, Mississippi, 39529, USA

SUMMARY

A numerical model is used to examine the relative effects of wind versus hydraulic forcing on the dynamics of the upper layer circulation within the western Mediterranean Sea.

RESUME

Les effets relative du vent et hydraulique sur la circulation de la Mer Mediterranee de l'ouest sont examiner avec un modele numerique.

INTRODUCTION

There are many physical factors which exert an influence on the circulation dynamics of the western Mediterranean; wind stress, hydraulic forced flow (inflow/outflow through the Straits of Gibraltar and Sicily), thermohaline circulation, etc.. The purpose of this study, as an initial step in an investigation of the hydrodynamics of the western Mediterranean, is to examine the relative importance of and interaction between the directly forced responses to the two possibly strongest forcing mechanisms, those being the wind stress and hydraulic forced flow. These two mechanisms are relatively easy to study using a simple reduced gravity, hydrodynamic numerical model.

Many features of the general surface circulation of the western Mediterranean Sea (Allain, 1960; Bethoux, 1980; Ovchinnikov, 1966) appear to be either a hydraulic forced flow, e.g. the North African current, or wind driven currents, e.g. the circulations in the Tyhrennian, Ligurian and Balearic Seas and in the Provencal and northern Algerian basins. While it is true that the thermodynamic effect of excess evaporation over precipitation and river runoff plays an important role in the Mediterranean, this effect is much more important in the eastern Mediterranean than the western half. Thus the western half of the Mediterranean, divided at the Strait of Sicily, is more amenable to use of a purely hydrodynamic approach.

MODEL

The numerical model used in these experiments is a one-active layer, reduced gravity, hydrodynamic, primitive equations model on a β-plane. The one-active layer reduced gravity model is the simplest model which can reproduce prominent upper ocean features and is designed to simulate the first internal baroclinic mode. The term reduced gravity is derived from balance of vertical forces in which the downward force due to the acceleration of gravity, g, is reduced by the upward bouyancy force, $g(\rho_2 - \rho_1)/\rho$. It has an active upper layer separated from an infinitely deep, inert lower layer by an impermeable interface. The interface represents the main pycnocline across which a density contrast is specified. Thermodynamics and interfacial mixing are neglected. The governing equations in the vertically integrated mass transport form in a right-handed coordinate system are:

$$\frac{\partial \vec{V}}{\partial t} + (\nabla\cdot\vec{V} + \vec{V}\cdot\nabla)\vec{v} + \hat{k} \times f\vec{V} = -h\nabla\eta_1 + \left(\frac{\vec{\tau}_w}{\rho}\right) + A\nabla^2\vec{V}$$

$$\frac{\partial h}{\partial t} + \nabla\cdot\vec{V} = 0$$

where

$$\nabla = \frac{\partial}{\partial x}\hat{i} + \frac{\partial}{\partial y}\hat{j} \qquad g' = \frac{(\rho_2 - \rho_1)\, g}{\rho}$$

$$f = f_o + \beta(y - y_o) \qquad \vec{\tau}_w = \tau_w^x \hat{i} + \tau_w^y \hat{j}$$

$$\vec{V} = h\vec{v} = h(u\hat{i} + v\hat{j})$$

$\hat{i}$ and $\hat{j}$ are unit vectors in the x and y directions respectively (see table 1 for a list of symbols).

The model equations are solved using an explicit version of the Hurlburt and Thompson (1980) semi-implicit model with two other important modifications: 1) the ability to handle realistic coastline geometry add by A. Wallcraft (personal communication) and 2) the outflow boundary condition used at the Strait of Sicily is changed to a modified Orlanski (1976) radiation boundary condition.

The Orlanski boundary condition is modified as follows for use in this version of the model. The phase velocities are calculated locally to detect the presence of high speed waves such as Kelvin or internal gravity waves. If these are not present then a global mean outward advective velocity is determined using a mass continuity integral constraint.

The realistic irregular model geometry was created using the Synthetic Bathymetric Profiling System (SYNBAPS) (Vanwyckhouse, 1973; 1979) data set of bottom topography. The bottom topographic height values were interpolated from the 10 minute resolution of the data set to the 0.1° by 0.05° resolution of the model.

Table 2 lists the parameters used in each of the experiments in this study. Based on observations (Ovchinnikov, 1966; Lanoix, 1974; and Katz, 1972), a 200 meter mean at rest layer depth is chosen to represent the upper layer (layer above the main thermocline) of the western Mediterranean. Since the main purpose of this study is to examine only the directly forced responses, the value of the eddy viscosity coefficient was selected to restrict the development of hydrodynamic flow instabilities.

FORCING MECHANISMS

The model was driven by specifying the inflow through the Strait of Gibraltar, or by applying monthly mean wind stresses or a combination of both. The inflow velocity was chosen to yield an inflow volume transport on the order of 1.6 Sv (Sv = 10^6 m^3/sec). Estimations (based on observations) of the volume transport entering the Strait of Gibraltar range from 1.2 to 1.68 Sv (Bethoux, 1979; Lacombe and Richez, 1982; Lanoix, 1974) while the transport exiting the Strait of Sicily is around 1.21 Sv (Bethoux, 1979; Garzoli and Maillard, 1976). Therefore, considering the variations of the transport estimates, for simplicity and to prevent the model from unrealistically gaining mass, the present experiments require the outflow to match the inflow.

The wind forcing is derived from climatogical wind stresses obtained from twenty years (1950-1970) of ship observations in the Mediterranean (May, 1982). Individual stresses were estimated from ship observations of wind speed and direction using a quadratic aerodynamic drag law with a drag coefficient dependent on the wind speed and stability. Monthly averages of the wind stresses were then calculated by averaging the individual wind stress estimates from each month on a one degree latitude by one degree longitude grid. These monthly averages were then bilinearly interpolated to the model grid. The wind forcing is cyclic with a period of one year.

The most prominent and persistent feature in these wind stress fields (fig. 1) is the northwesterly wind blowing through the gap between the Pyrenees and the Alps out over the central western Mediterranean. These wind stresses are strongest in the winter and weaken considerably during the summer months.

RESULTS

Three experiments were conducted to study the relative effects of and interactions between wind stress and hydraulic forcing of the Mediterranean circulation in the layer above the main thermocline. The first experiment used only hydraulic forcing and the second used only wind stress. The third experiment used both forcing mechanisms.

The results for experiment one (fig. 2) reveal a steady source/sink flow entering at the Strait of Gibraltar flowing through the Alboran Sea arcing up along the Spanish coast then turning abruptly eastward through the Algerian basin along the north African coast and finally exiting through the Strait of Sicily. The remainder of the western Mediterranean is relatively quiescent. An enlarged view of the Algerian basin, i.e. the North African Current region, is presented in figure 3 for later comparison with the results from the wind only and combined forcing experiments. This figure shows the flow as it exits the Alboran with part of the flow deflected into the Balearic Sea while the majority of the flow turns eastward through the Algerian basin.

Conservation of absolute vorticity appears to be the dynamical driving mechanism for the path of the current. If the amplitude of constant absolute vorticity (CAV) trajectories (see Haltiner and Martin, 1957 pp 353-356) were calculated based on the current velocity as it exits the Alboran Sea (@ 35.5°N 1.0°W), the northernmost penetration would be to approximately 38°N. The northward penetration of the current (figs. 2 and 3) is to around 37.5°N. The along stream velocity divergence in conjunction with the relatively high eddy viscosity could act to damp the downstream fluctuations as can be seen in the flow through the Algerian basin.

The results from experiment two, shown in figures 4 (full western Mediterranean basin) and 5 (Algerian basin), reveal quasiperiodic solutions in response to the annual cycle of the wind forcing. The four panels of figures 4 and 5 depict the depth averaged upper layer current velocities for a) spring (day 810), b) summer (day 900), c) fall (day 990) and d) winter (day 1080). The variations in the circulations patterns can be closely related to the wind stress curl variations (fig. 6). As can be seen, during the winter when the Mediterranean is covered primarily by positive wind stress curl, strong cyclonic flow dominated the western Algerian basin, the Tyhrennian, Ligurian and Balearic Seas and the Gulf of Lions, while in the Alboran Sea the flow is weakly cyclonic. Of particular note is the cyclonic eddy in the western Algerian basin and the associated strong current along the north African coast since this is in the same area as the current seen in the hydraulic forced case. During the summer when most of the Mediterranean is covered by negative wind stress curl, the cyclonic circulations weaken significantly and in some instances, i.e. in the Tyhrennian and Balearic Seas and the Gulf of Lions, the flow becomes weakly anticyclonic. In the Alboran Sea, the circulation becomes moderately anticyclonic. Again of particular note is the cyclonic eddy in the western Algerian basin and

the current along the north African coast. Both the eddy and the current weaken substantially and the eddy contracts in size.

Figures 7 (full western Mediterranean basin) and 8 (Algerian basin) show the results from the third experiment. The solutions are essentially the same as the wind only experiment in the Tyhrennian, Ligurian and Provencal basins, while in the Alboran Sea and the Sardinian and Sicilian Straits, the solutions are very similar to the hydraulic forcing only experiment.

The strongest interactions between the responses due to the two forcing mechanisms can be seen in the Algerian basin. The steady source/sink flow from the hydraulic forcing is modulated by the periodic responses to the wind stress forcing. Most notable is the interaction between the hydraulically forced current as it attempts to arc northward along the Spanish coast and the wind driven eddy in the western Algerian basin. During the winter when the wind driven flow is at its strongest, the flow exiting the Alboran Sea is forced down onto the north African coast and the North African Current is intensified. Also note that the center of the eddy is displaced approximately 60 km northeast of its location in the wind forced only experiment. During the summer as the wind driven flow weakens, the hydraulically forced current tends to arc more northward in an attempt to follow a CAV trajectory both upstream and downstream of the eddy.

Weaker interactions are observed in the Alboran and Balearic Seas. In the Alboran, the wind driven flow enhances the anticyclonic circulation of the Alboran gyre during the summer and impedes it during the winter. In the Balearic Sea the wind driven response dominates with a strong cyclonic flow, while during the summer the flow becomes weakly anticyclonic under the influence of the hydraulically forced flow.

CONCLUSIONS

A simple one-active layer reduced gravity numerical model has been used to study the directly forced hydrodynamic responses due to hydraulic and wind forcing on the western Mediterranean Sea. The results of this study suggest that wind stress is the dominant driving mechanism in the Tyhrennian, Ligurian and Provencal basins, while hydraulic forcing is the dominant factor in the Alboran Sea and Sardinian/Sicilian Straits region for the directly forced solutions. The flow through the Algerian basin along the North African coast (the North African Current) is significantly affected by both of the forcing mechanisms.

Further investigation into the hydrodynamics of the Mediterranean will require the examination of other flow regimes within the physical parameter space of the problem. In particular, the eddy viscosity must be reduced in order to allow for the possibility of hydrodynamic flow instabilities. Then a similar series of experiments as discussed here needs to be conducted and the results analyzed to determine where and when flow instabilities are significant.

REFERENCES

Allain, C., 1960. Topographie dynamique et ourants gereraux dans le bassin occidental de la Mediterranee. Revue des Travaux de L'Institut des Peches Maritime, 24(1), 121-145.

Bethoux, J.P.,1979. Budgets of the Mediterranean Sea. Their dependence on the local climate and on characteristics of the Atlantic waters. Oceanol. Acta., v. 2, 137-163.

Bethoux, J.P.,1980. Mean water fluxes across sections in the Mediterranean Sea, evaluated on the basis of water and salt budgets and of observed salinities. Oceanol. Acta., v. 3, 79-88.

Garzoli S., and C. Maillard, 1976. Hydrologie et circulation hivernales dans les canaux de Sicile et de Sardaigne. Rapport Interne de Laboratoire d'Oceanographie Physique du Museum National d'Histoire Naturelle, Paris.

Haltiner, G.J. and F.L. Martin, 1957. Dynamical and Physical Meteorology. McGraw-Hill Book Co., 470pp.

Hurlburt, H.E. and J.D. Thompson, 1980. A numerical study of loop current intrusions and eddy shedding. J. Phys. Ocenaogr., 10, 1611-1651.

Katz, E.J., 1972. The Levantine intermediate water between the Strait of Sicily and the Strait of Gibraltar. Deep Sea Res., 19, 507-520.

Lacombe, H. and C. Richez, 1982. The regime of the Strait of Gibraltar, in Hydrodynamics of semi-enclosed seas, edited by J.C.J. Nihoul, Elsevier, Amsterdam, 13-74.

Lanoix, F., 1974. Project Alboran etude hydrologique dynamique de la Mer d'Alboran. Tech. report 66, M. Atl. Treaty Org. Brussels, p. 39.

May, P.W., 1982. Climatological flux estimates in the Mediterranean Sea: Part I. Winds and wind stress. Naval Ocean Research and Development Activity, NSTL Station, MS. NORDA Technical Report 54, p. 56.

Orlanski, I., 1976. A simple boundary condition for unbounded hyperbolic flows, J. of Comp. Phys., 21, 251-269,

Ovchinnikov, I.M., 1966. Circulation in the surface and intermediate layers of the Mediterranean. Oceanology, 6, 48-59.

Vanwyckhouse, R.J., 1973. Synthetic Bathymetric Profiling System (SYNBAPS). Naval Oceanographic Office, Washington, D.C. Technical Report 233, p. 138.

Vanwyckhouse, R.J., 1979. SYNBAPS, Volume I - Data sources and data preparation. Naval Ocean Research and Development Activity, NSTL Station, MS. NORDA Technical Note 35.

List of symbols for Model Equations

Symbol	Definition
A	horizontal eddy viscosity
f	Coriolis parameter
g	acceleration due to gravity
g'	reduced gravity, $g(\rho_2 - \rho_1)/\rho$
h	instantaneous local thickness of the upper layer
H	initial thickness of the upper layer
t	time
u	x-directed component of current velocity
v	y-directed component of current velocity
$\vec{V}$	$h\vec{v}$
x,y,z	tangent plane Cartesian coordinates: x positive eastward, y positive northward, z positive upward
β	differential rotation, df/dy
Δt	time increment in the numerical integration
$\Delta x, \Delta y$	horizontal grid increments
η_1	free surface anomaly; height of the free surface above its initial uniform elevation; $\eta_1 = h - H$
ρ, ρ_1, ρ_2	densities of sea water
τ_w^x, τ_w^y	x and y directed tangential wind stresses at the top of the upper layer

Table 1

Model Parameters

Parameter	Definition	Value
A	eddy viscosity	300 m^2 sec
beta	(df/dy)	1.8×10^{-11} m^{-1} sec^{-1}
f	Coriolis parameter	8×10^{-5} sec^{-1}
g'	reduced gravity due to stratification	0.02 m sec^{-2}
H	undisturbed upper layer depth	200 m
$\Delta x \times \Delta y$	horizontal grid resolution	0.1° x 0.05° (7.5 x 5 km)
Δt	time step	15 mins
v_{in}	inflow velocity	40 cm sec^{-1}

Table 2

Figure 1. Monthly mean wind stress vectors and magnitude contours for a) January, b) April, c) July, and d) October. Contour interval is 0.25 dynes/cm^2.

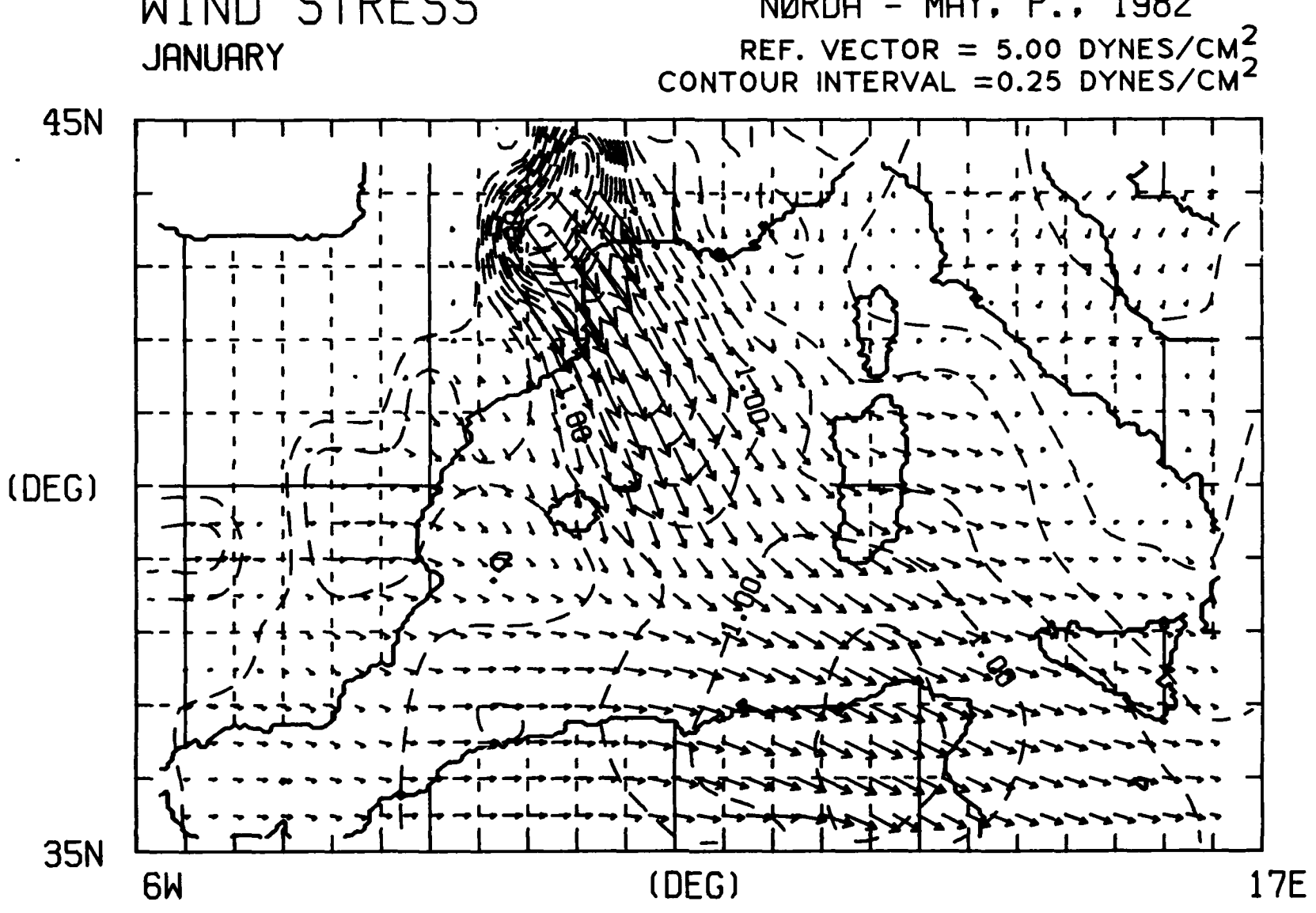
WIND STRESS
JANUARY
NØRDA - MAY, P., 1982
REF. VECTOR = 5.00 DYNES/CM2
CONTOUR INTERVAL =0.25 DYNES/CM2
45N
(DEG)
35N
6W
(DEG)
17E
1.00
1.00
.00
.00
.00
MAX PLOTTED STRESS = 3.64 DYNES/CM2
MAXIMUM VECTOR

Fig. 1a

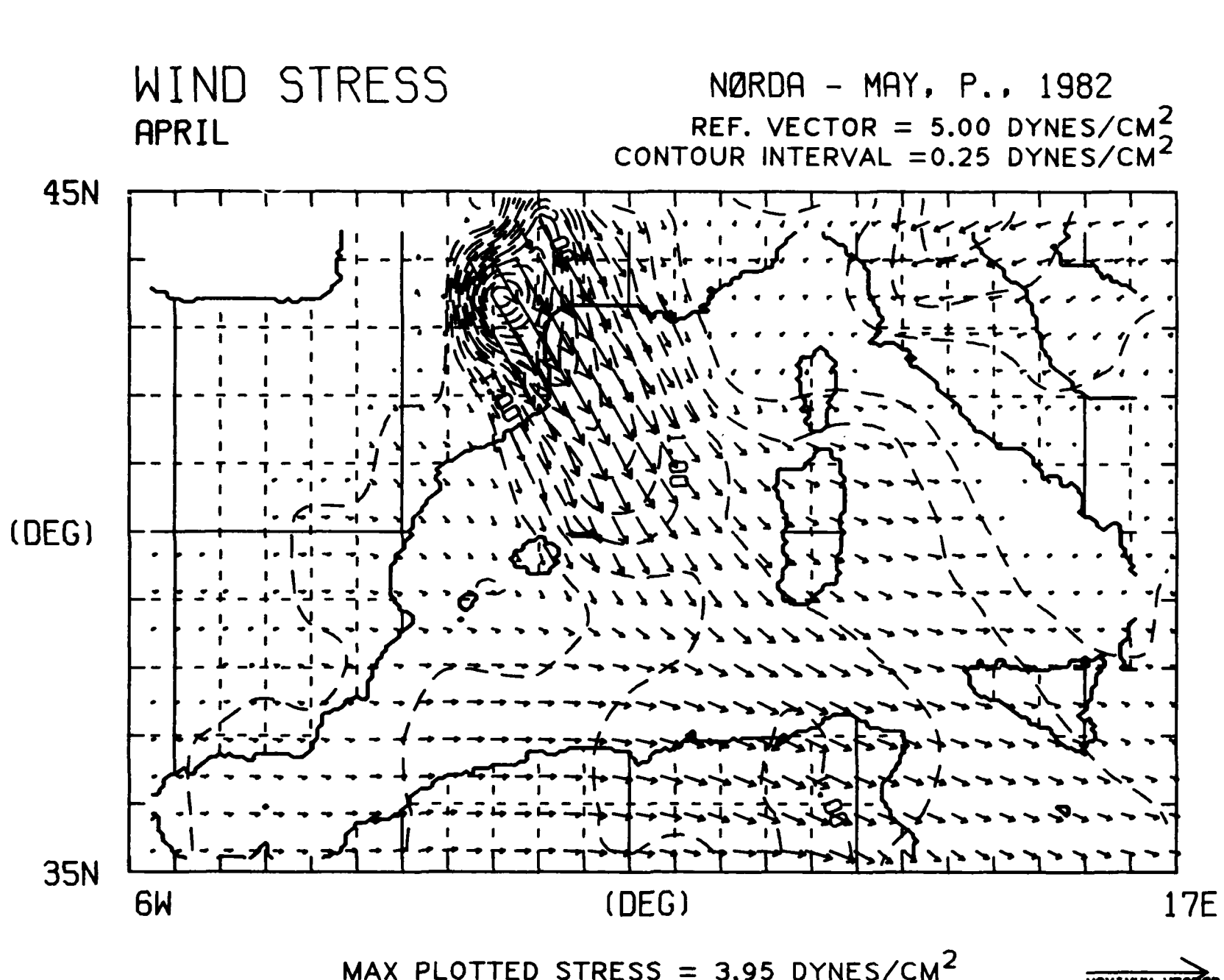
WIND STRESS
APRIL
NØRDA - MAY, P., 1982
REF. VECTOR = 5.00 DYNES/CM2
CONTOUR INTERVAL =0.25 DYNES/CM2
45N
(DEG)
35N
6W
(DEG)
17E
MAX PLOTTED STRESS = 3.95 DYNES/CM2
MAXIMUM VECTOR

Fig. 1b

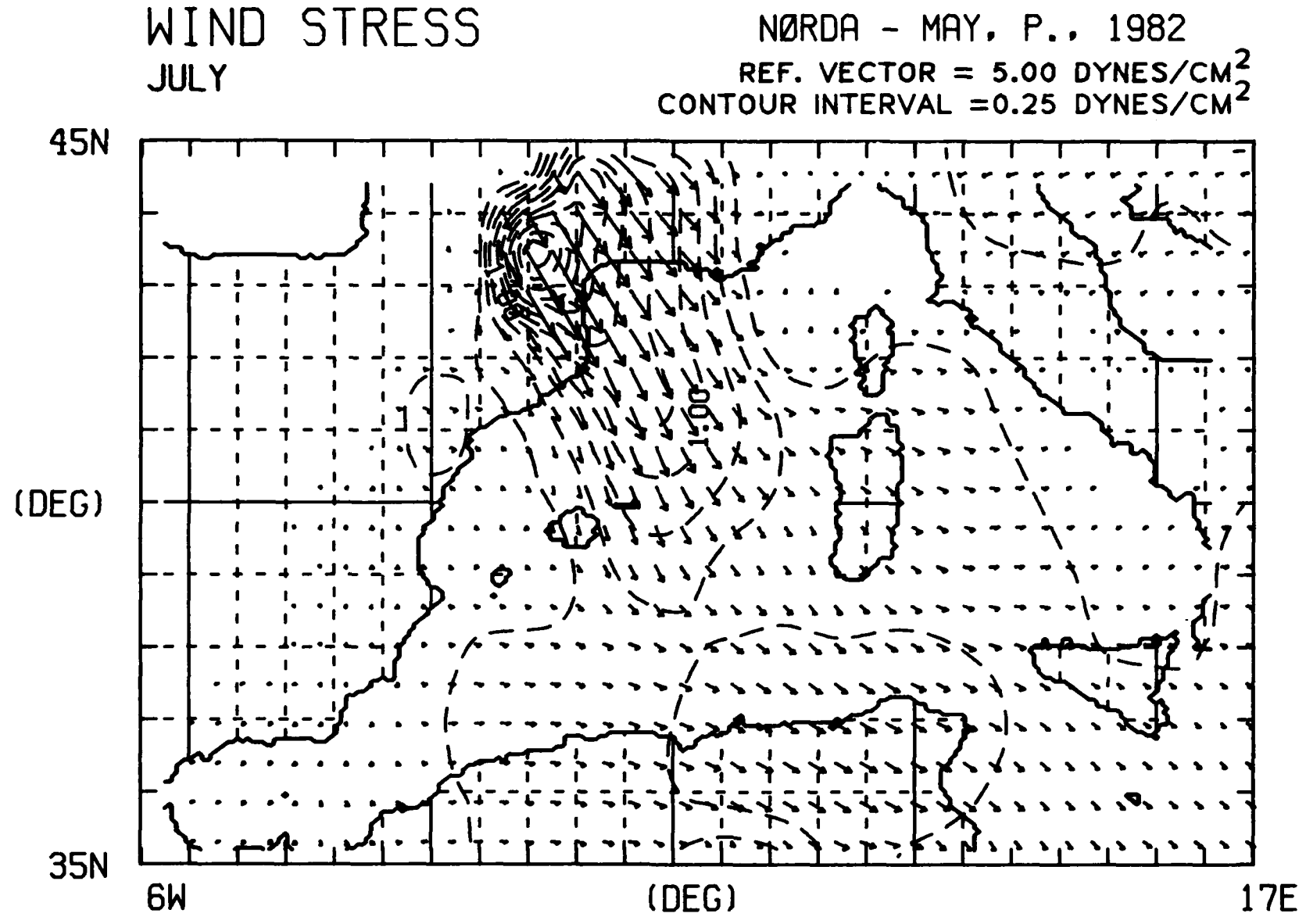
WIND STRESS
JULY
NØRDA - MAY, P., 1982
REF. VECTOR = 5.00 DYNES/CM2
CONTOUR INTERVAL =0.25 DYNES/CM2
45N
(DEG)
35N
6W
(DEG)
17E
MAX PLOTTED STRESS = 2.95 DYNES/CM2
MAXIMUM VECTOR

Fig. 1c

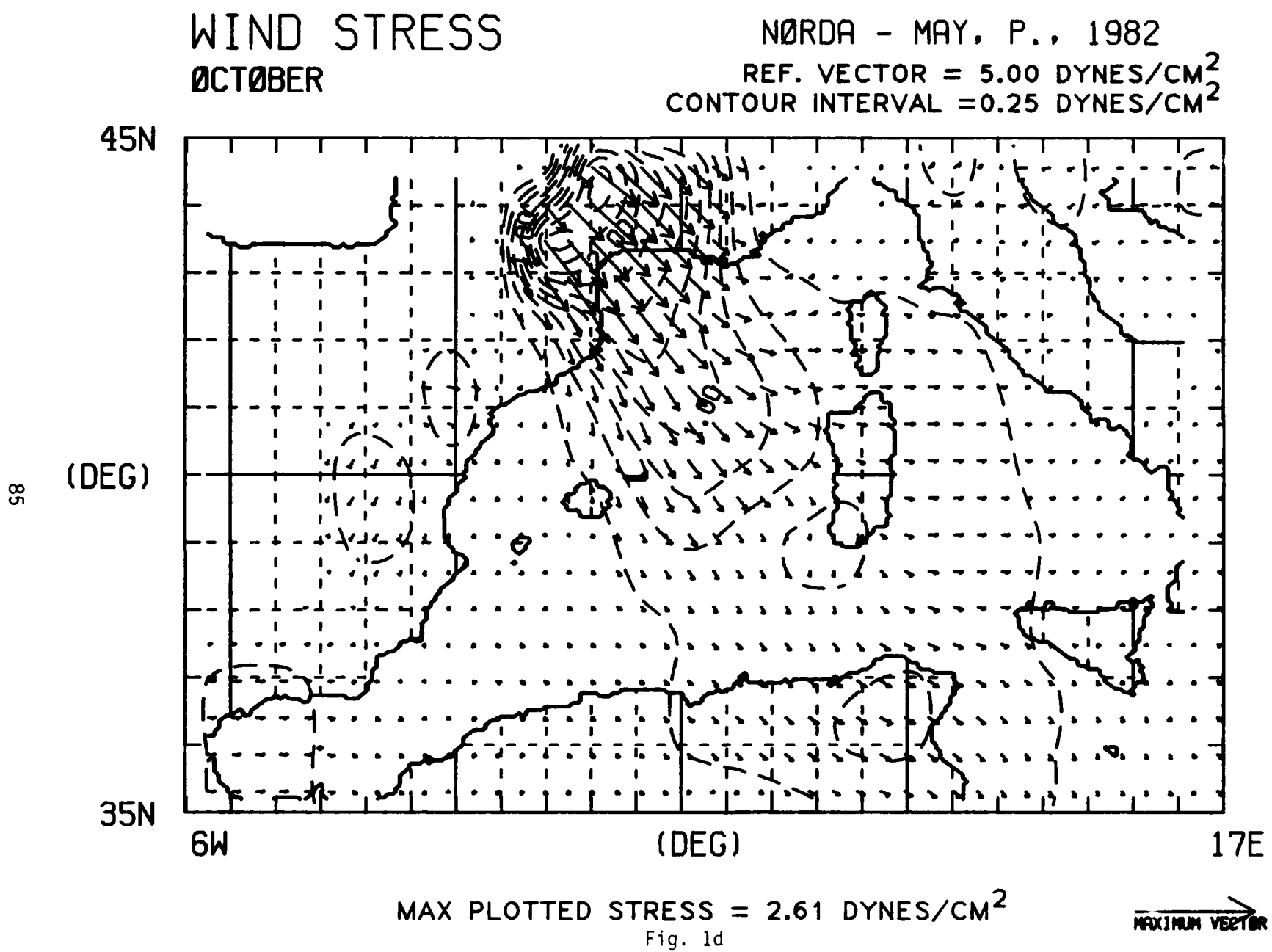
WIND STRESS
ØCTØBER
NØRDA - MAY, P., 1982
REF. VECTOR = 5.00 DYNES/CM2
CONTOUR INTERVAL =0.25 DYNES/CM2
45N
(DEG)
35N
6W
(DEG)
17E
MAX PLOTTED STRESS = 2.61 DYNES/CM2
MAXIMUM VECTOR

Fig. 1d

Figure 2. Upper layer current vectors for day 1080 from the hydraulic forcing only experiment for the full western Mediterranean basin. Vectors are plotted every third grid point in regions of relatively strong flow and every sixth point in regions of relatively weak flow.

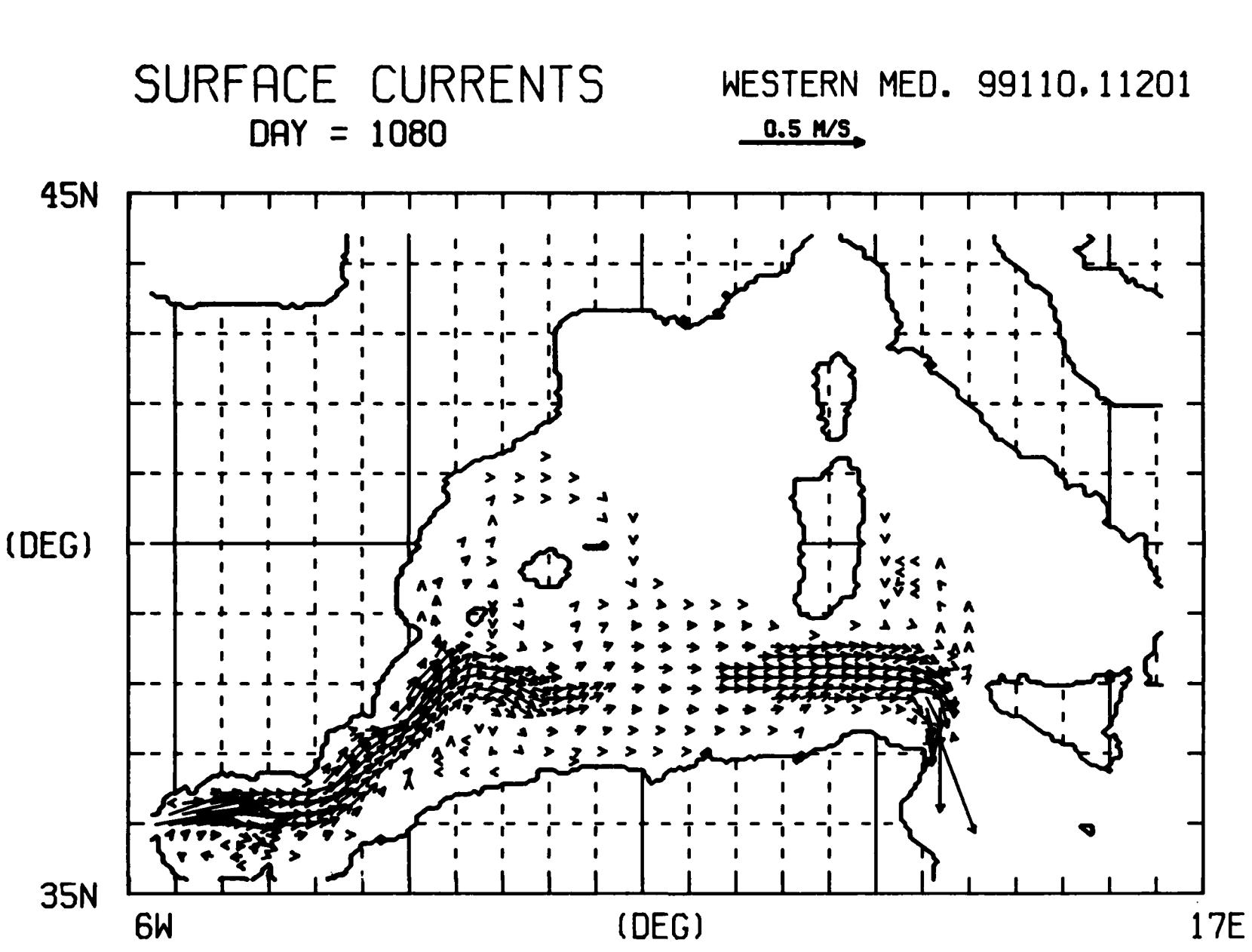
SURFACE CURRENTS
DAY = 1080
WESTERN MED. 99110.11201
0.5 M/S
45N
(DEG)
35N
6W
(DEG)
17E
MAX PLØTTED SPEED = 0.41 (M/SEC)

Fig. 2

Figure 3. Upper layer current vectors for day 1080 from the hydraulic forcing only experiment for the Algerian basin. Vectors are plotted every second grid point in regions of relatively strong flow and every fourth point in regions of relatively weak flow.

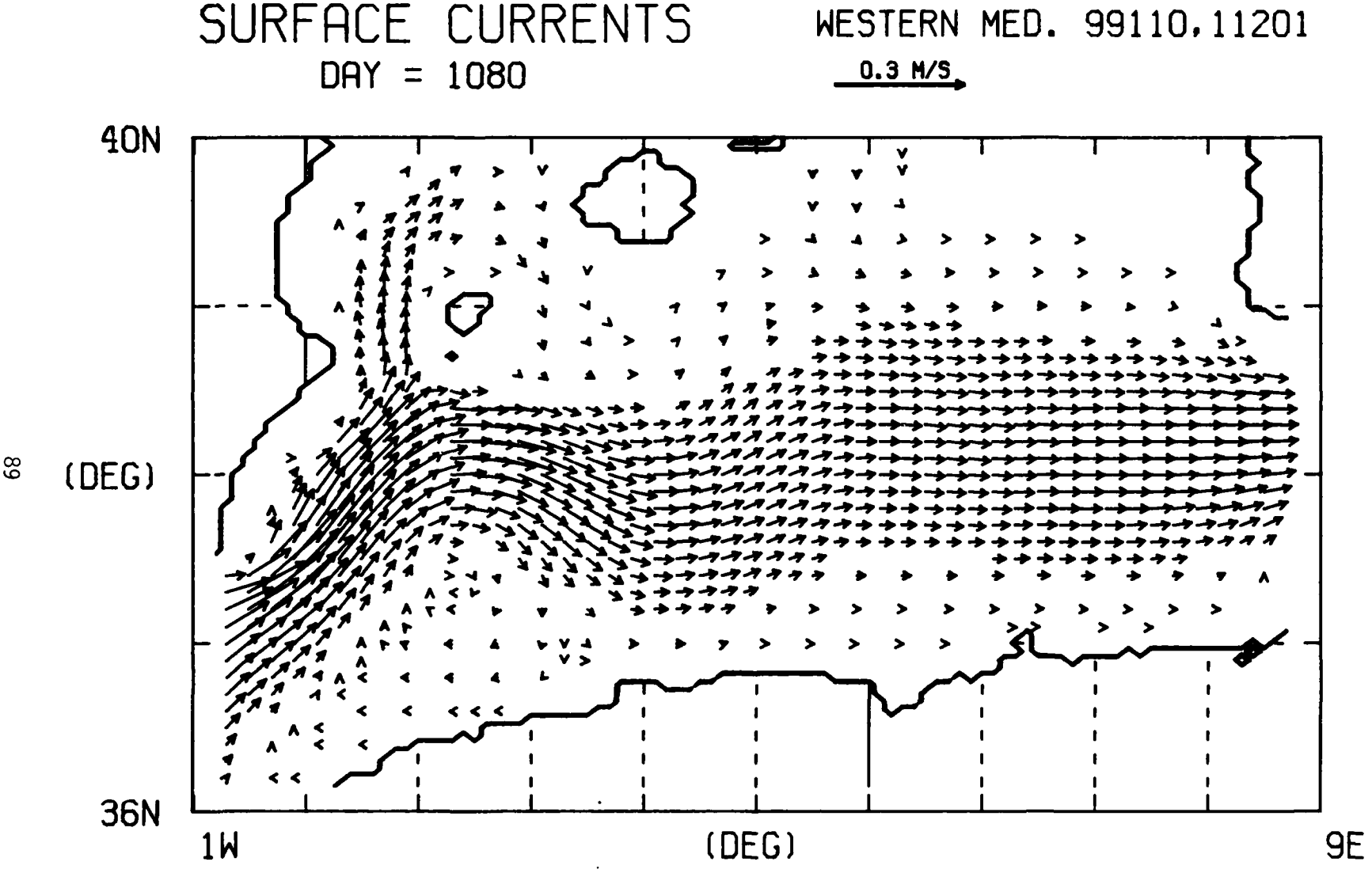
SURFACE CURRENTS
DAY = 1080
WESTERN MED. 99110,11201
0.3 M/S
40N
(DEG)
36N
1W
(DEG)
9E
MAX PLØTTED SPEED = 0.15 (M/SEC)

Fig. 3

Figure 4. Upper layer current vectors for a) day 810 (spring), b) day 900 (summer), c) 990 (fall), and d) day 1080 (winter) from the wind stress forcing only experiment for the full western Mediterranean basin. Vectors are plotted every third grid point in regions of relatively strong flow and every sixth point in regions of relatively weak flow.

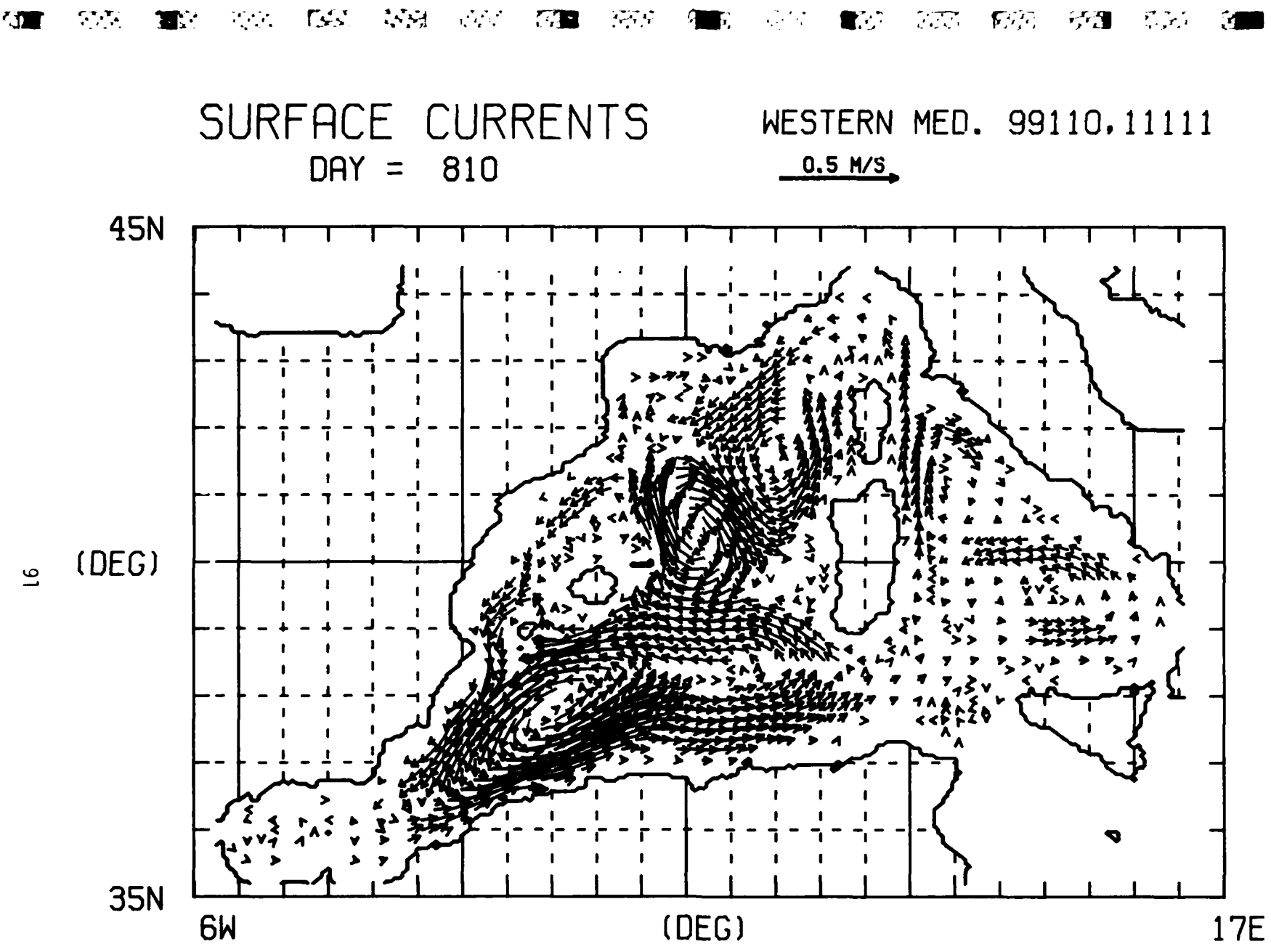
SURFACE CURRENTS
DAY = 810
WESTERN MED. 99110,11111
0.5 M/S
45N
(DEG)
35N
6W
(DEG)
17E
MAX PLØTTED SPEED = 0.25 (M/SEC)

Fig. 4a

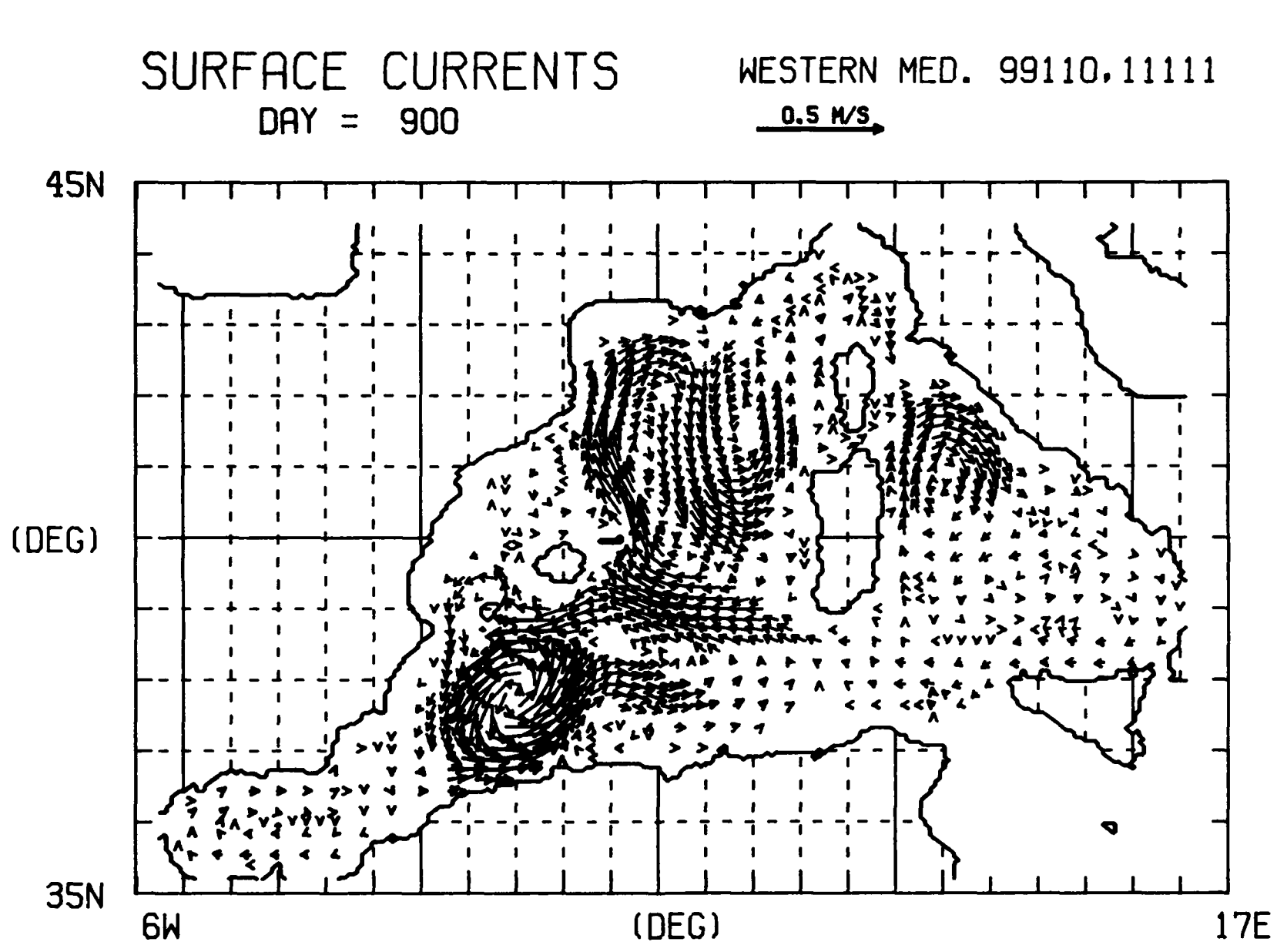
SURFACE CURRENTS
DAY = 900
WESTERN MED. 99110,11111
0.5 M/S
45N
(DEG)
35N
6W
(DEG)
17E
MAX PLØTTED SPEED = 0.21 (M/SEC)

Fig. 4b

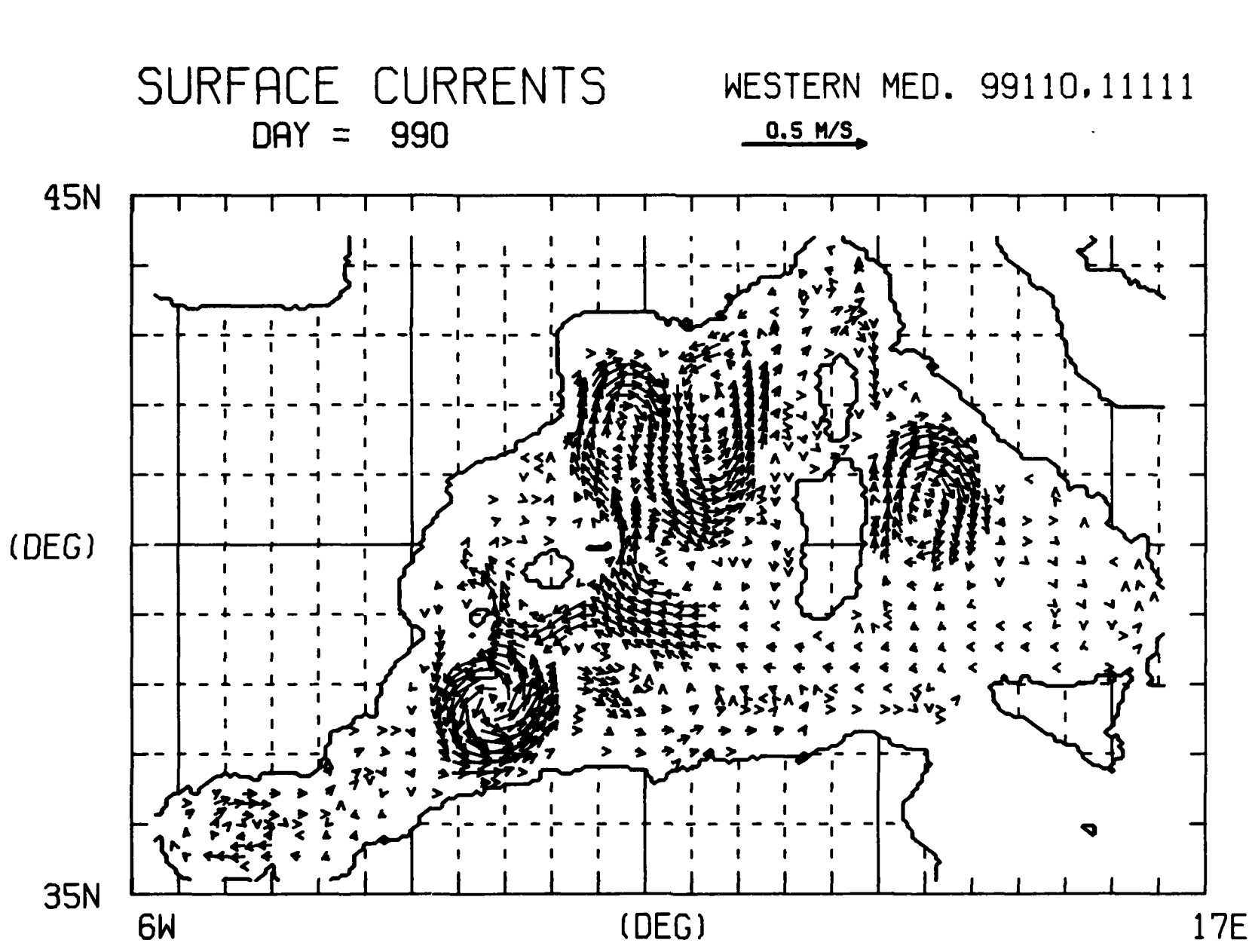
SURFACE CURRENTS
DAY = 990
WESTERN MED. 99110,11111
0.5 M/S
45N
(DEG)
35N
6W
(DEG)
17E
MAX PLØTTED SPEED = 0.15 (M/SEC)

Fig. 4c

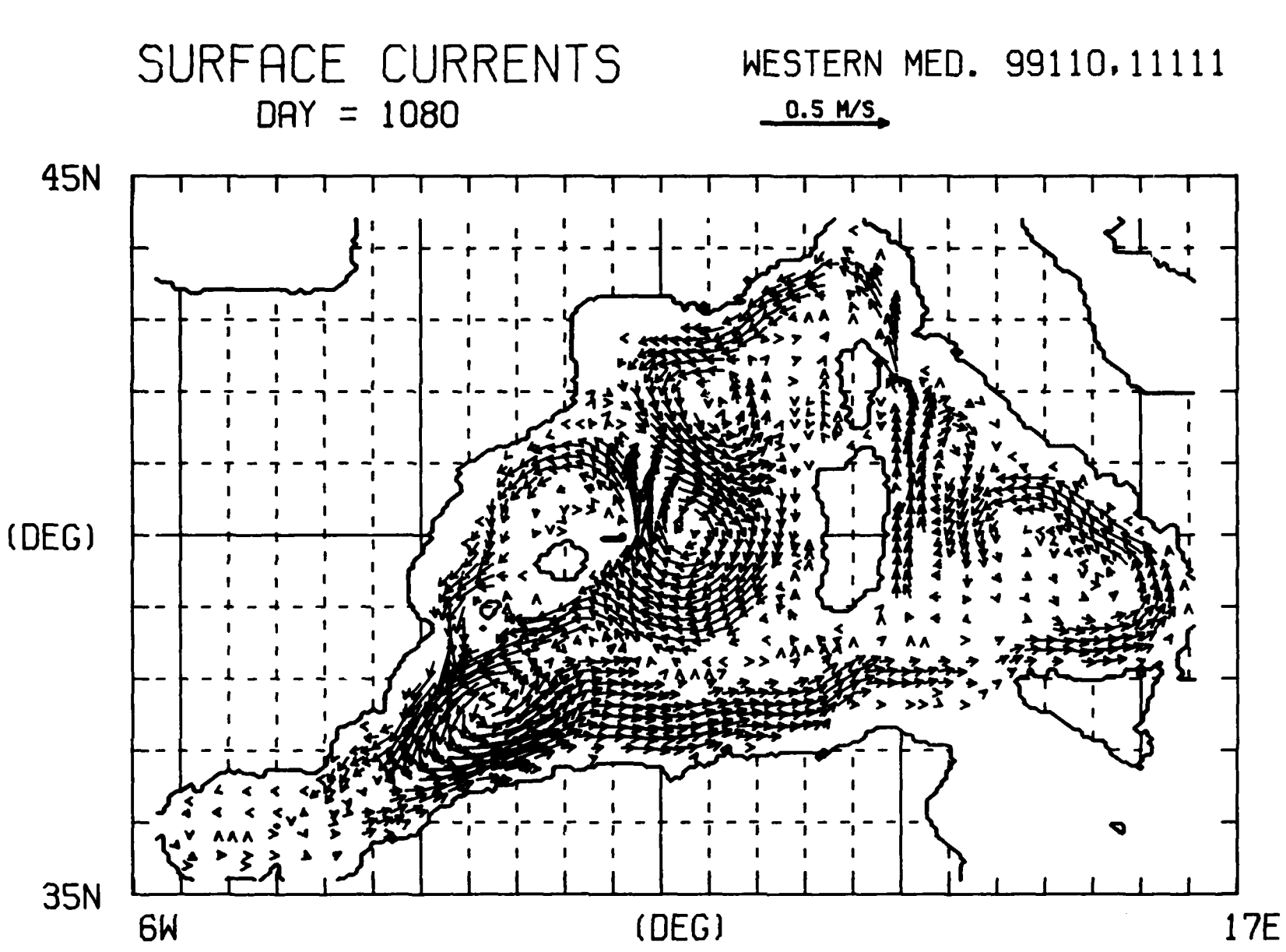
SURFACE CURRENTS
DAY = 1080
WESTERN MED. 99110,11111
0.5 M/S
45N
(DEG)
35N
6W
(DEG)
17E
MAX PLØTTED SPEED = 0.21 (M/SEC)

Fig. 4d

AD-A162 019 CONTRIBUTIONS TO THE OCEANOGRAPHY OF THE WESTERN ALBORAN SEA(U) NAVAL OCEAN RESEARCH AND DEVELOPMENT ACTIVITY NSTL STATION MS R ARNONE ET AL APR 85 2/2

UNCLASSIFIED NORDA-TN-315 F/G 8/3 NL

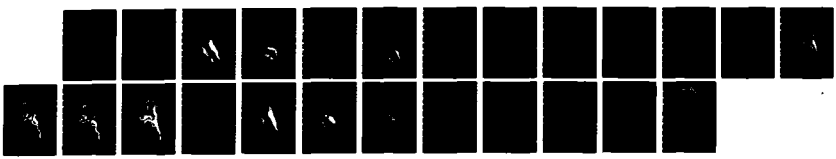

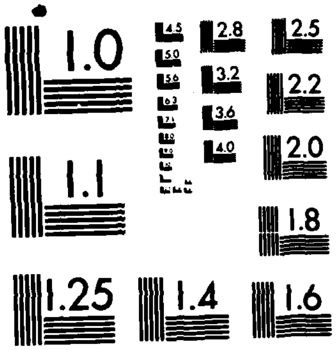

MICROCOPY RESOLUTION TEST CHART
NATIONAL BUREAU OF STANDARDS-1963-A

Figure 5. Upper layer current vectors for a) day 810 (spring), b) day 900 (summer), c) 990 (fall), and d) day 1080 from the wind stress forcing only experiment for the Algerian basin. Vectors are plotted every second grid point in regions of relatively strong flow and every fourth point in regions of relatively weak flow.

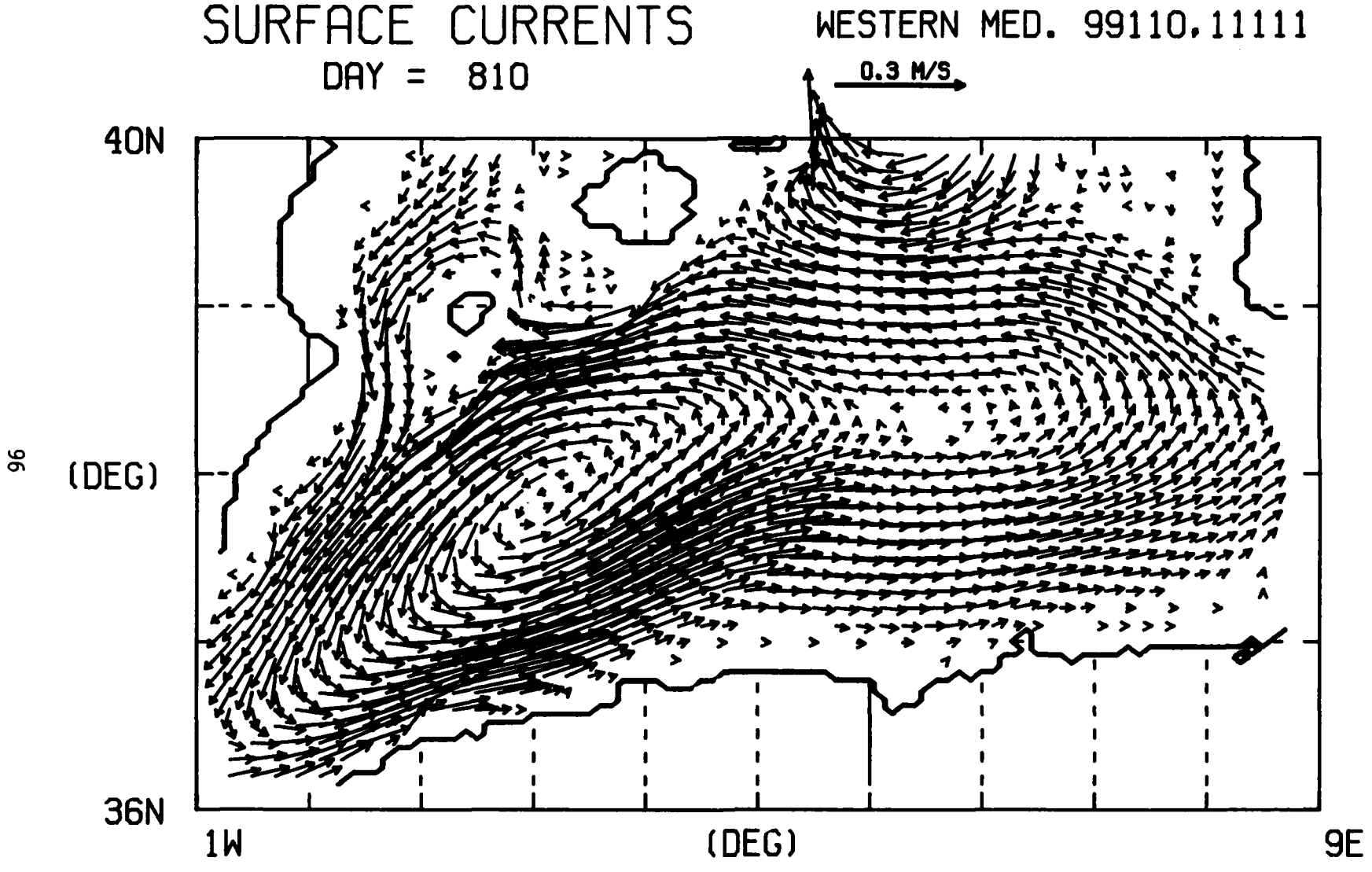

MAX PLØTTED SPEED = 0.25 (M/SEC)

Fig. 5a

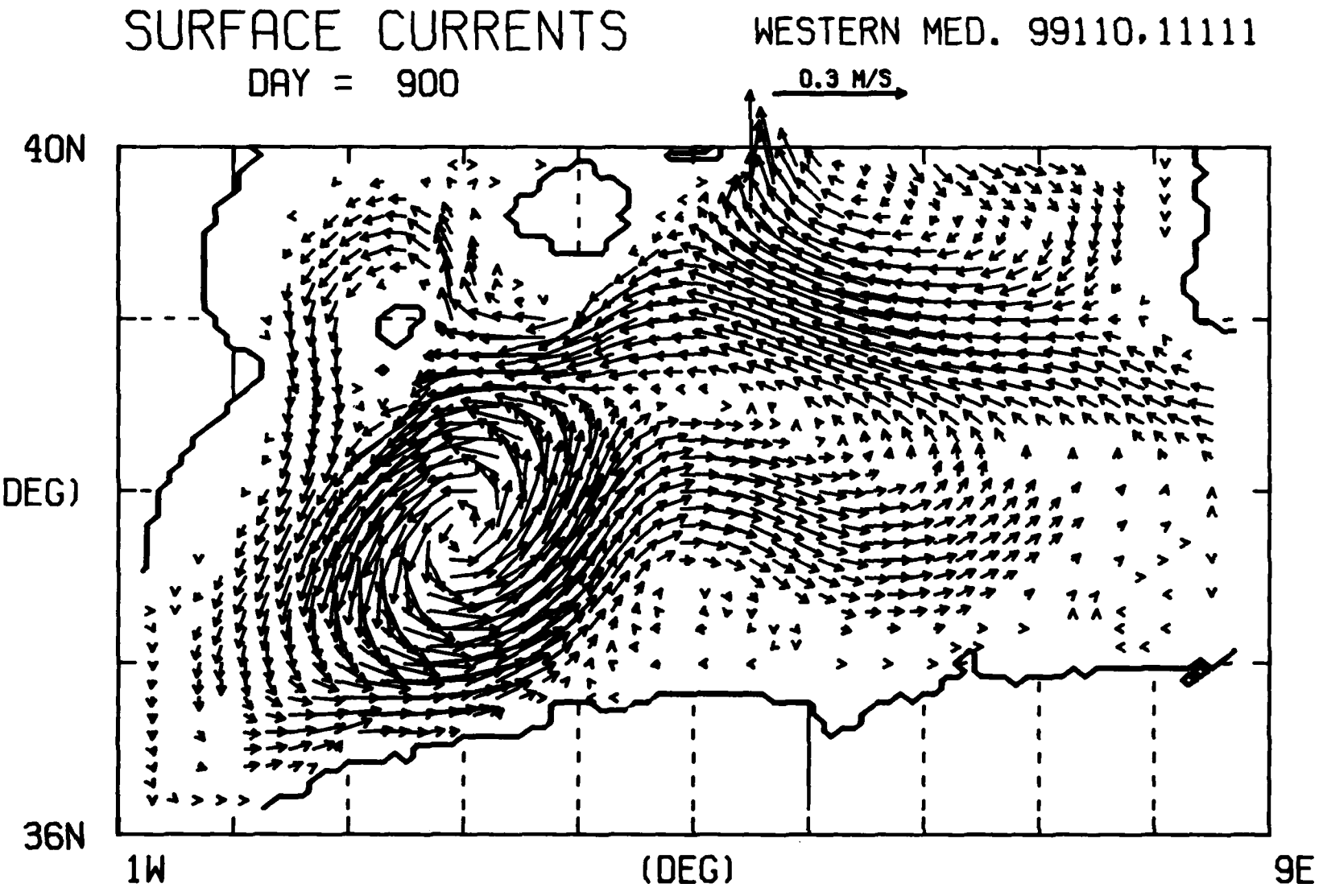
SURFACE CURRENTS
DAY = 900
WESTERN MED. 99110.11111
0.3 M/S
40N
(DEG)
36N
1W
(DEG)
9E
MAX PLØTTED SPEED = 0.21 (M/SEC)

Fig. 5b

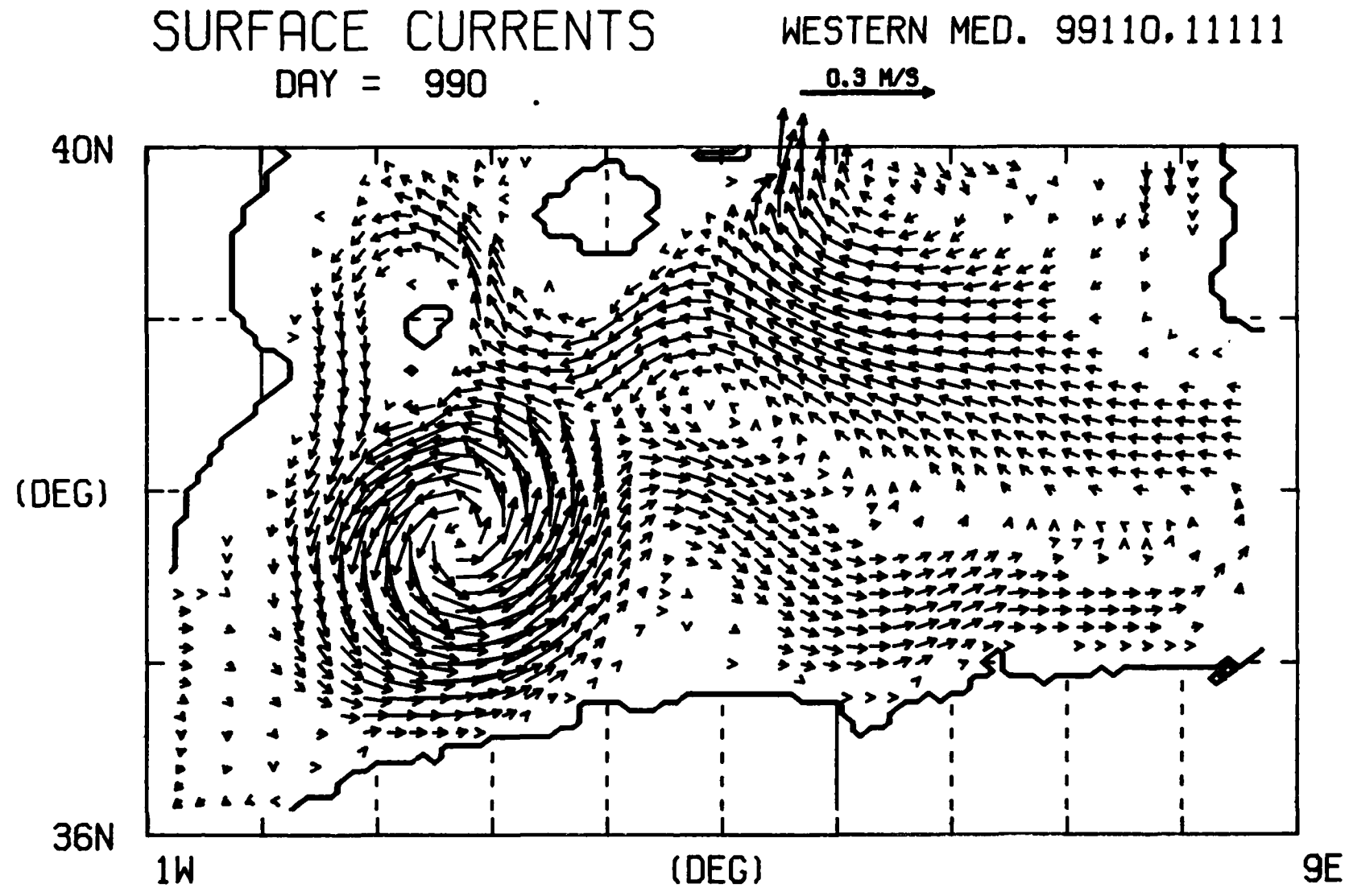
SURFACE CURRENTS
WESTERN MED. 99110.11111
DAY = 990
0.3 M/S
40N
(DEG)
36N
1W
(DEG)
9E
MAX PLØTTED SPEED = 0.15 (M/SEC)

Fig. 5c

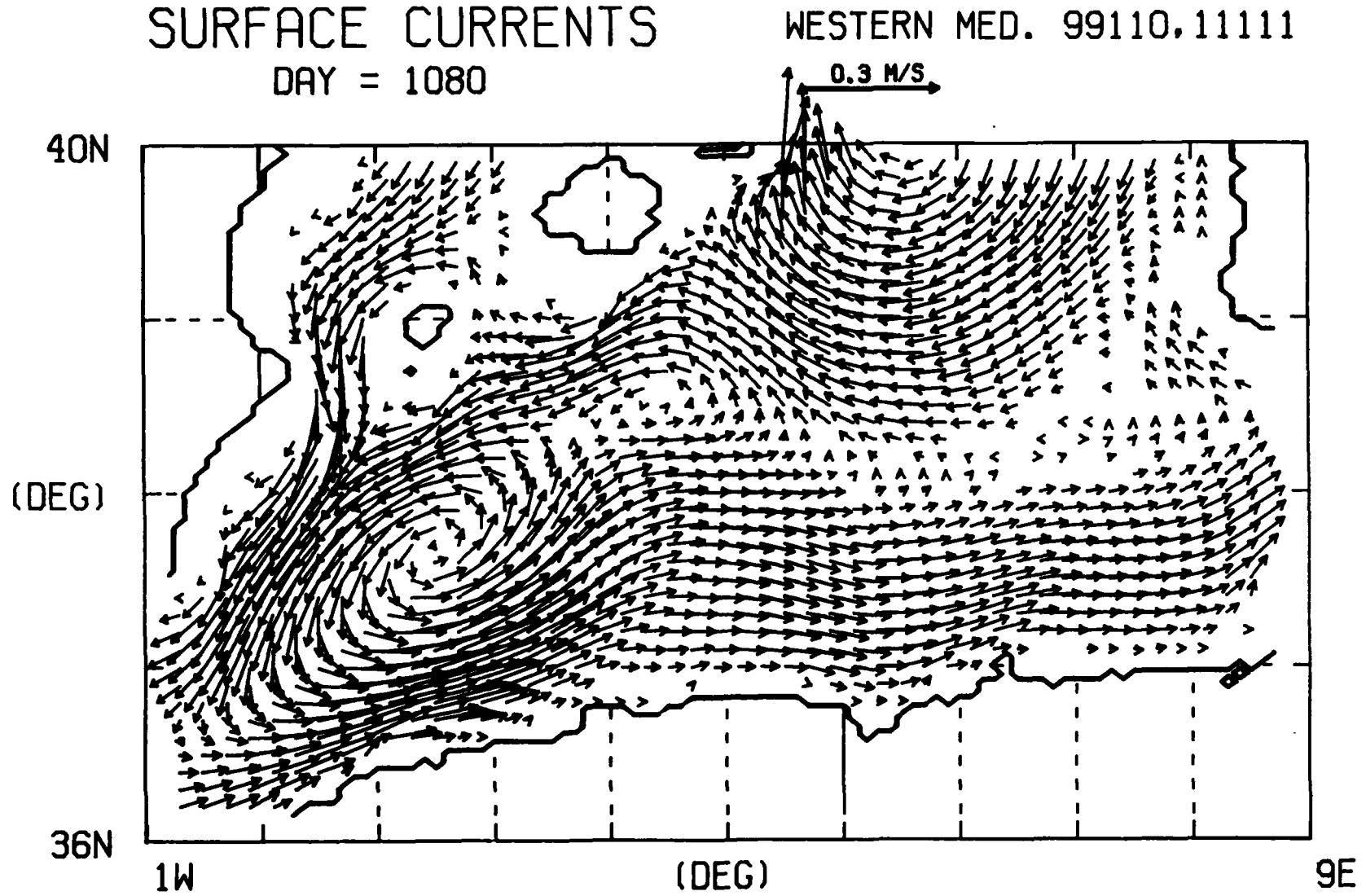
SURFACE CURRENTS
DAY = 1080
WESTERN MED. 99110,11111
0.3 M/S
40N
(DEG)
36N
1W
(DEG)
9E
MAX PLØTTED SPEED = 0.21 (M/SEC)

Fig. 5d

Figure 6. Monthly mean wind stress curl for a) January, b) April, c) July, d) October. Contour interval is 0.2×10^{-8} dynes/cm^3.

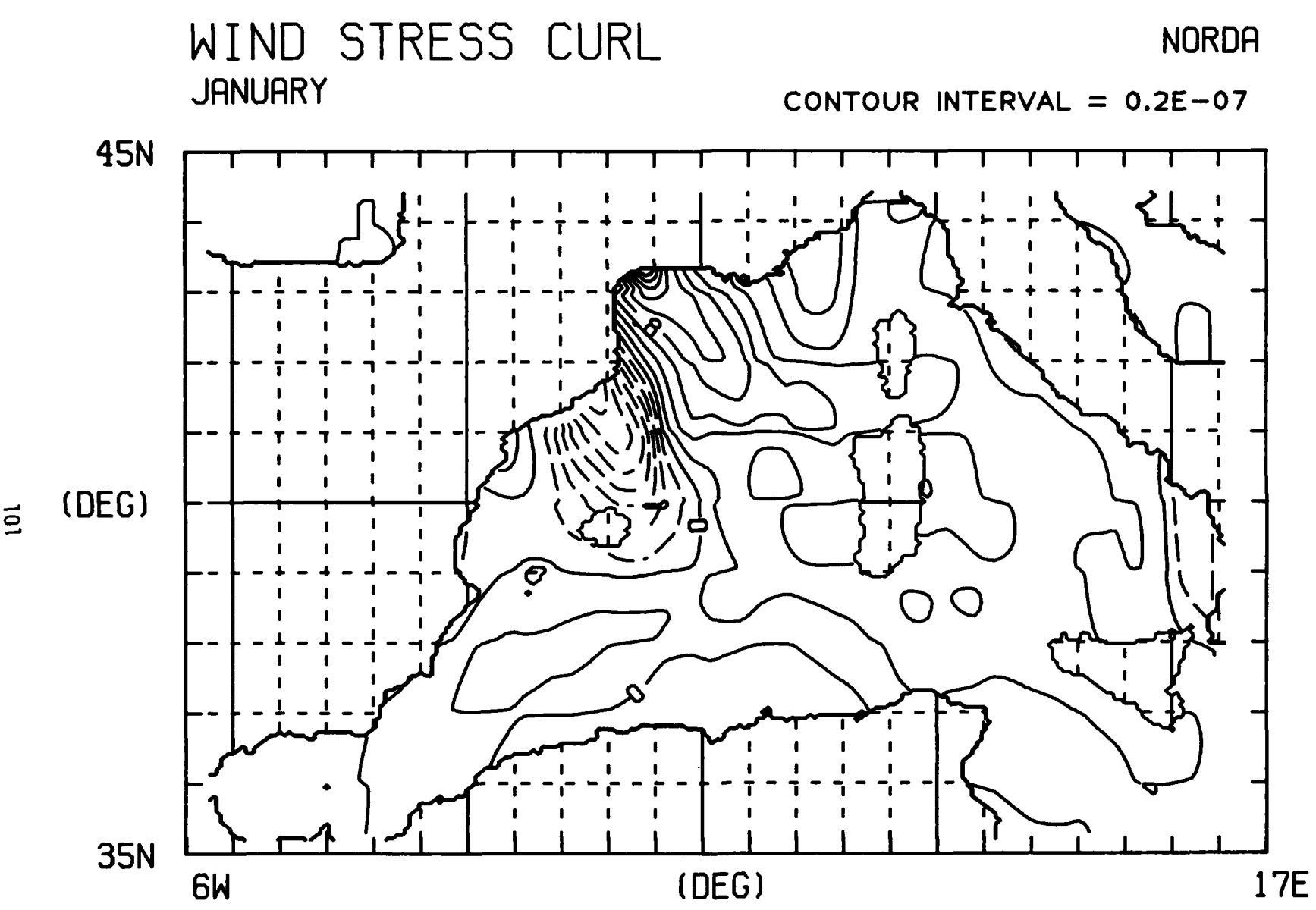
WIND STRESS CURL
NORDA
JANUARY
CONTOUR INTERVAL = 0.2E-07
45N
(DEG)
35N
6W
(DEG)
17E
RANGE IS -0.4E-06 TO 0.4E-06

Fig. 6a

WIND STRESS CURL

NORDA

APRIL

CONTOUR INTERVAL = 0.2E-07

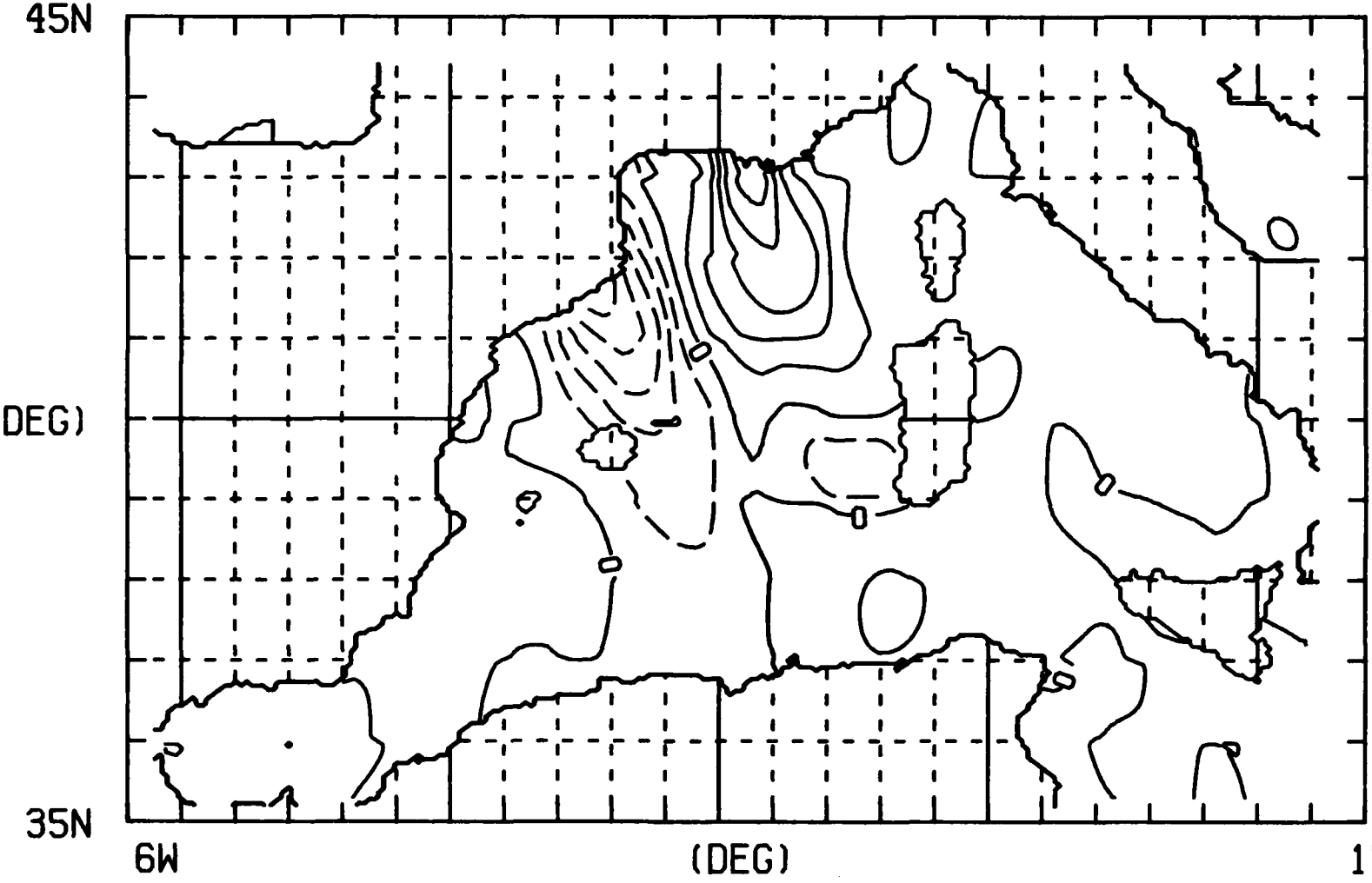

RANGE IS -0.3E-06 TO 0.2E-06

Fig. 6b

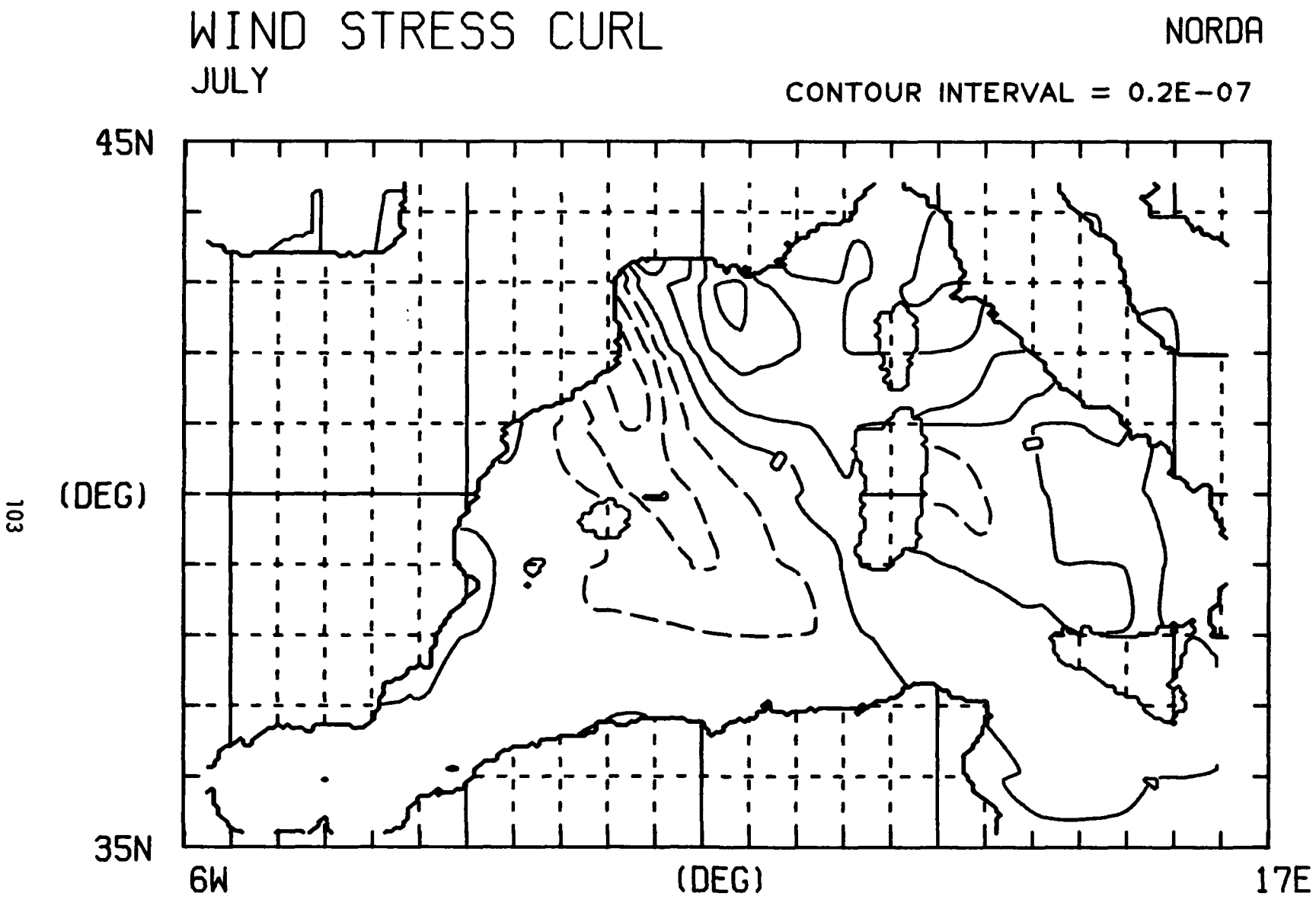
WIND STRESS CURL
NORDA
JULY
CONTOUR INTERVAL = 0.2E-07
45N
(DEG)
35N
6W
(DEG)
17E
RANGE IS -0.1E-06 TO 0.2E-06

Fig. 6c

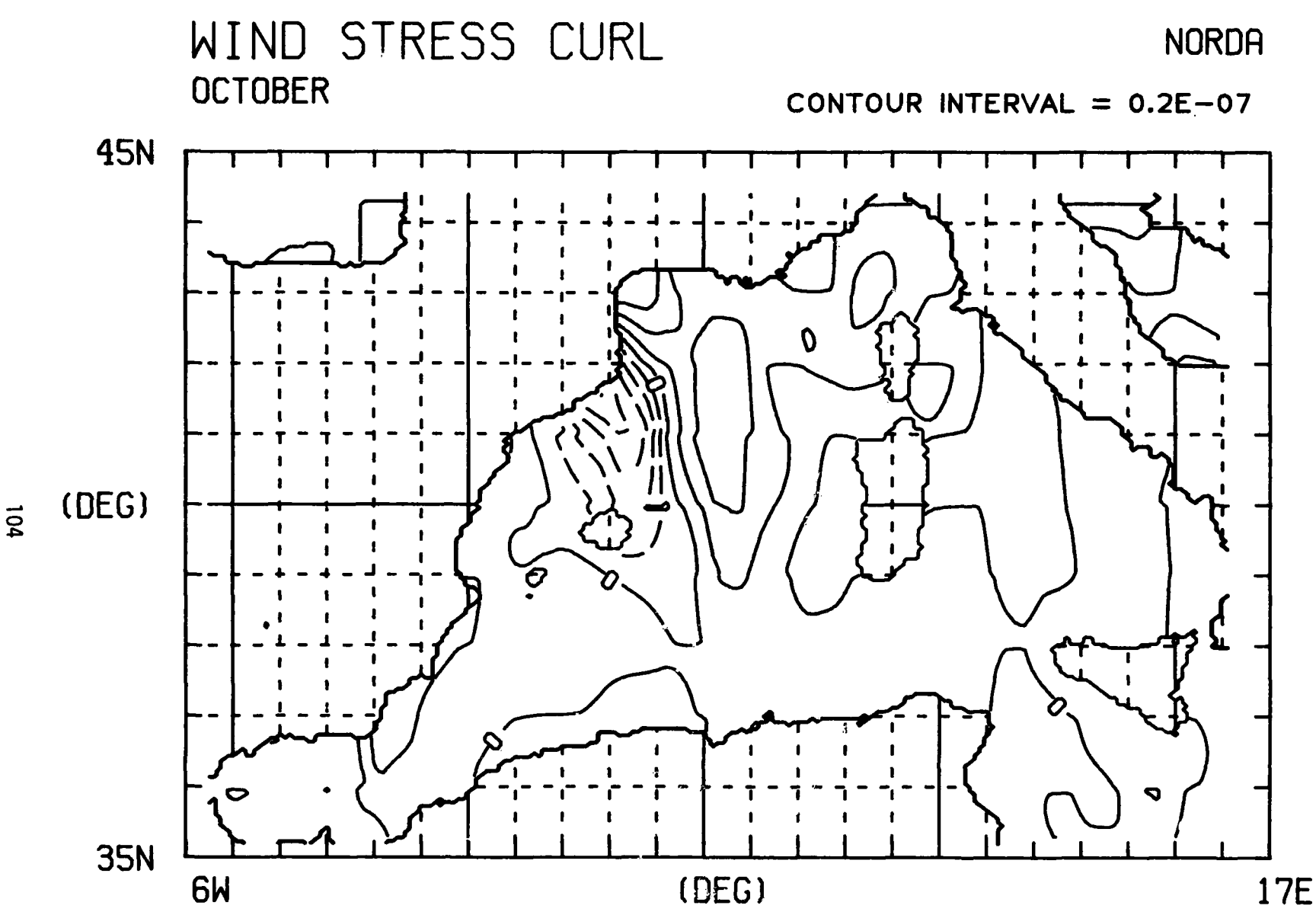
WIND STRESS CURL
NORDA
OCTOBER
CONTOUR INTERVAL = 0.2E-07
45N
(DEG)
35N
6W
(DEG)
17E
RANGE IS -0.3E-06 TO 0.2E-06

Fig. 6d

Figure 7. Upper layer current vectors for a) day 810 (spring), b) day 900 (summer), c) 990 (fall), and d) day 1080 (winter) from the combined forcing experiment for the full western Mediterranean basin. Vectors are plotted every third grid point in regions of relatively strong flow and every sixth point in regions of relatively weak flow.

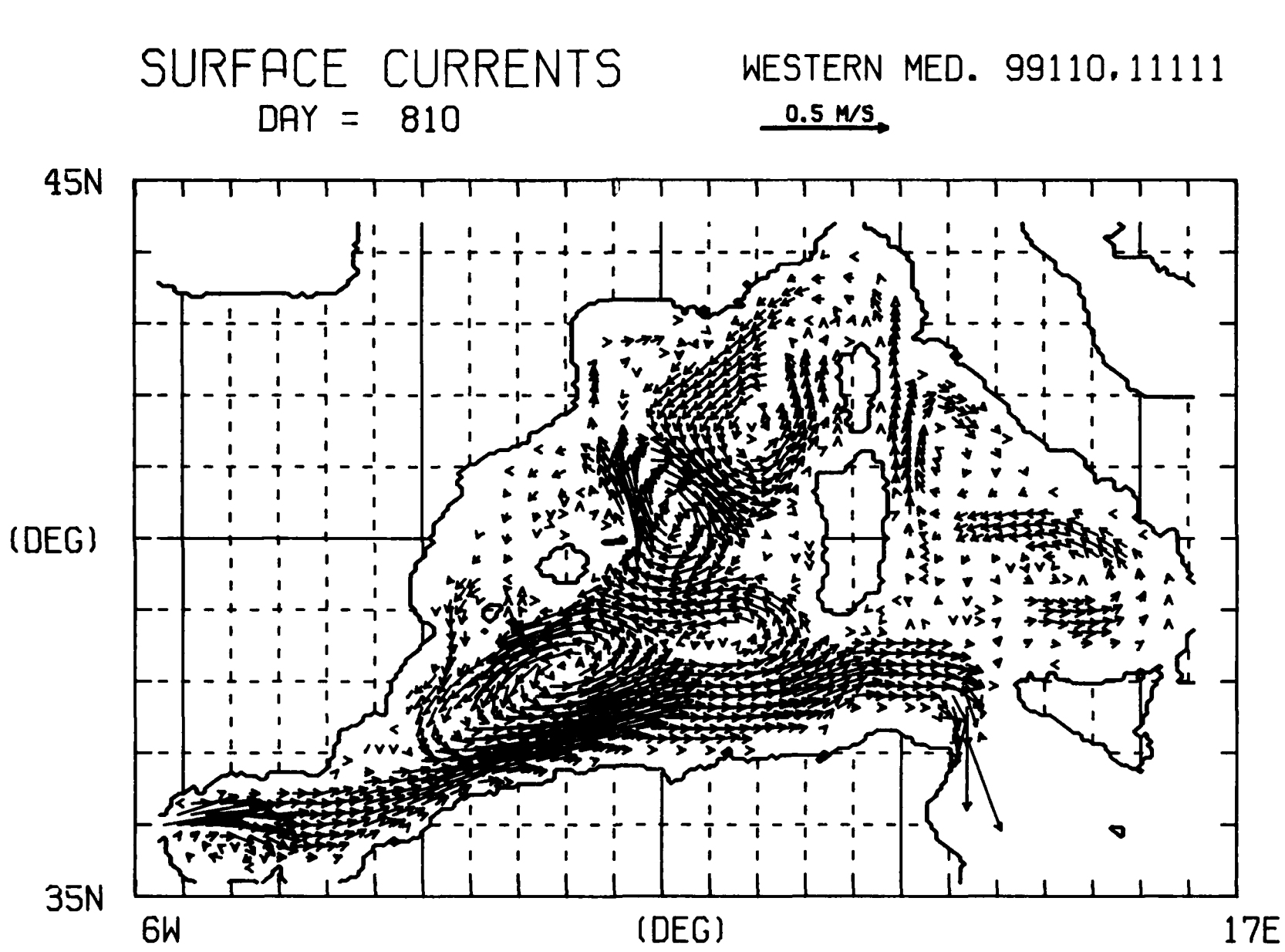
SURFACE CURRENTS
DAY = 810
WESTERN MED. 99110.11111
0.5 M/S
45N
(DEG)
35N
6W
(DEG)
17E
MAX PLØTTED SPEED = 0.39 (M/SEC)

Fig. 7a

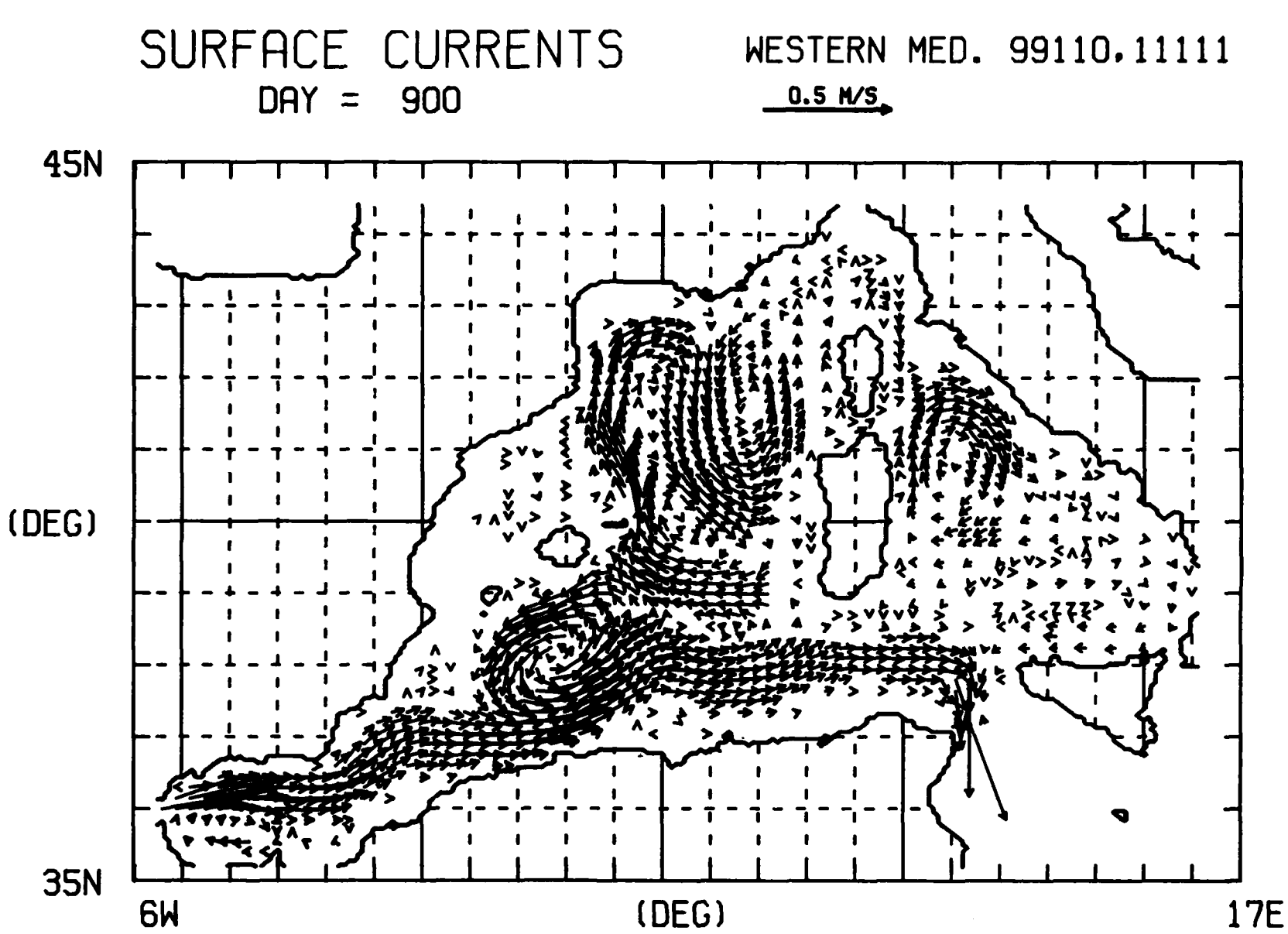
SURFACE CURRENTS
DAY = 900
WESTERN MED. 99110.11111
0.5 M/S
45N
(DEG)
35N
6W
(DEG)
17E
MAX PLØTTED SPEED = 0.41 (M/SEC)

Fig. 7b

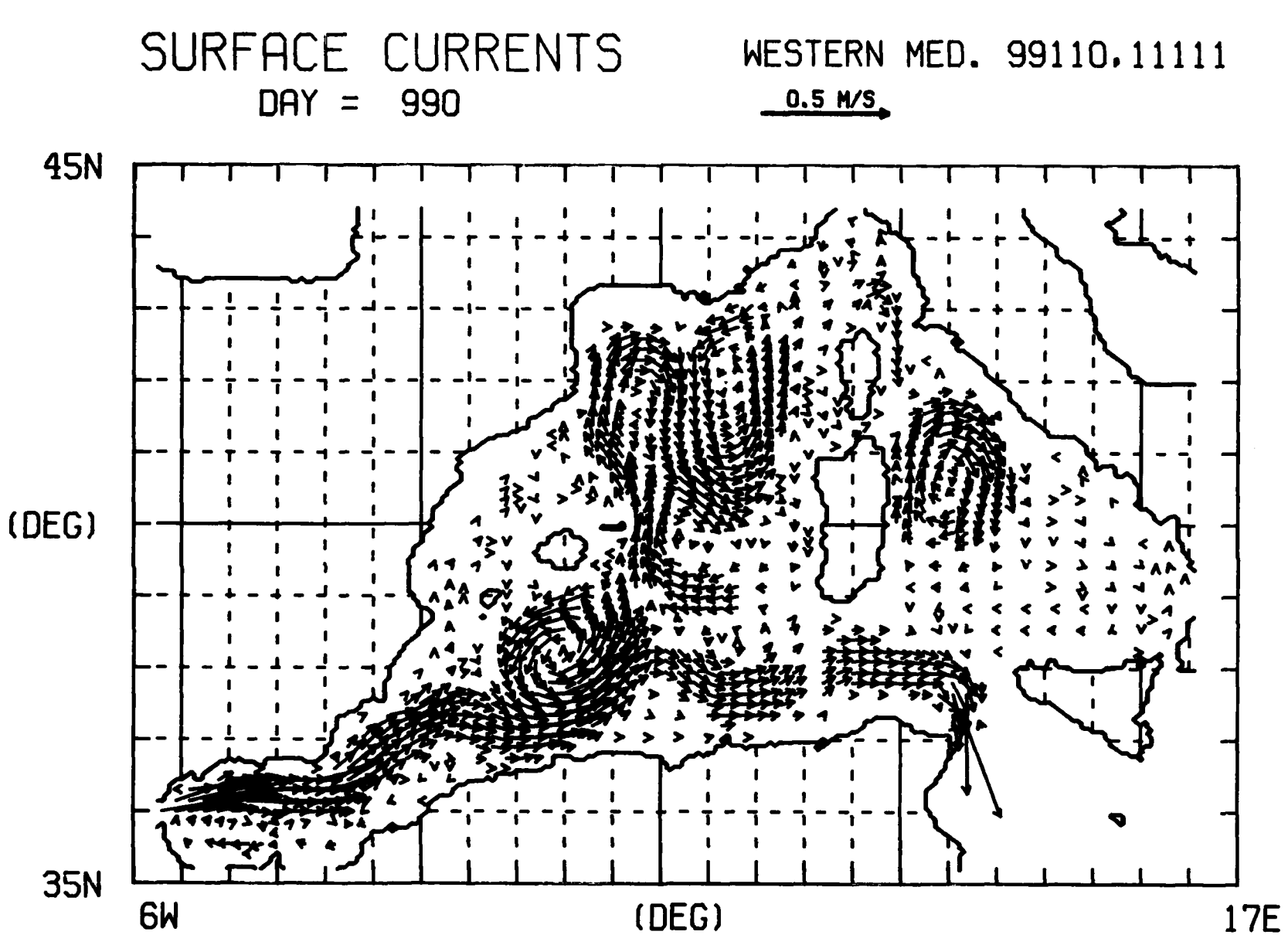
SURFACE CURRENTS
DAY = 990
WESTERN MED. 99110.11111
0.5 M/S
45N
(DEG)
35N
6W
(DEG)
17E
MAX PLØTTED SPEED = 0.39 (M/SEC)

Fig. 7c

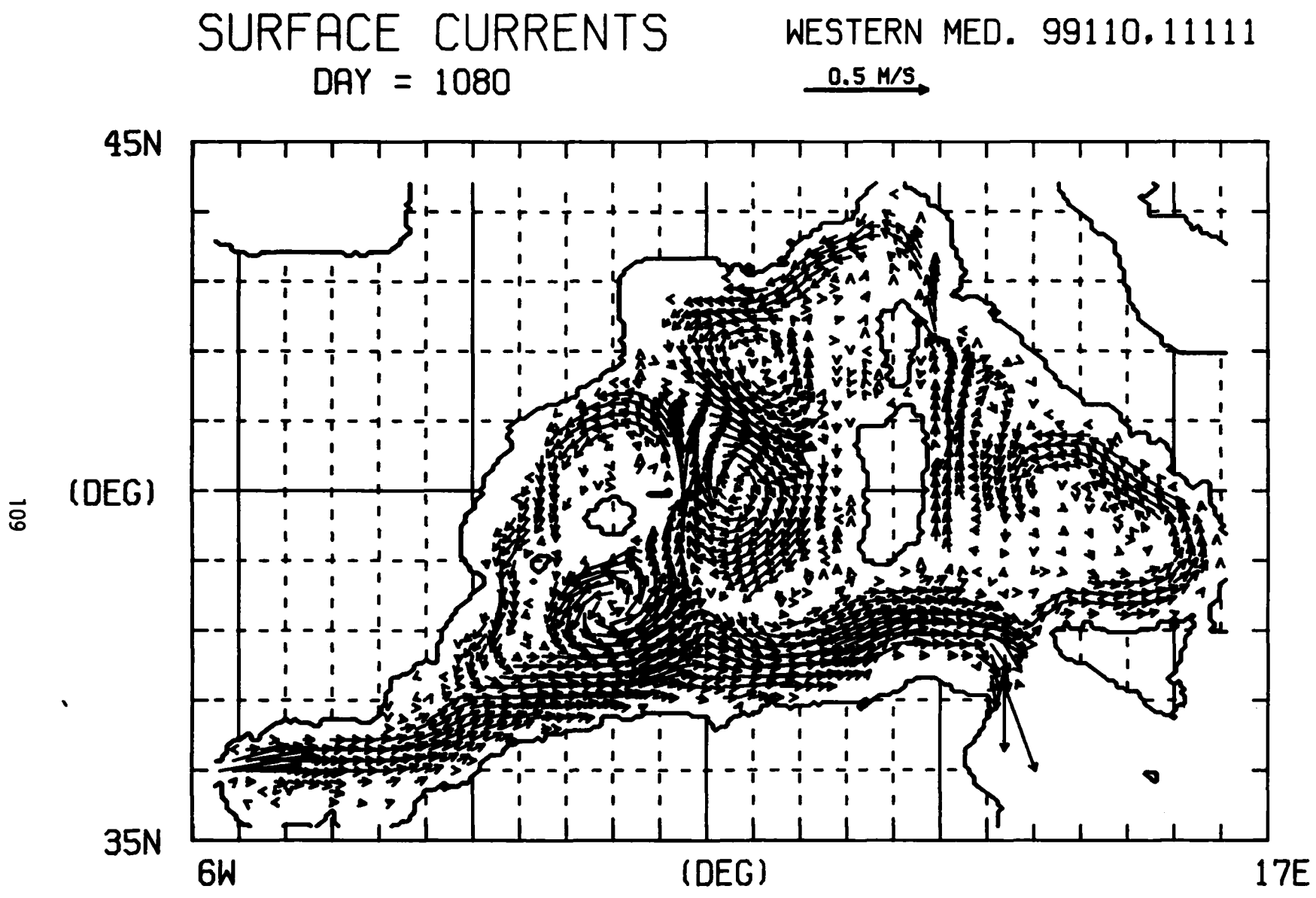
SURFACE CURRENTS
DAY = 1080
WESTERN MED. 99110.11111
0.5 M/S
45N
(DEG)
35N
6W
(DEG)
17E
MAX PLØTTED SPEED = 0.38 (M/SEC)

Fig. 7d

Figure 8. Upper layer current vectors for a) day 810 (spring), b) day 900 (summer), c) 990 (fall), and d) day 1080 from the combined forcing experiment for the Algerian basin. Vectors are plotted every second grid point in regions of relatively strong flow and every fourth point in regions of relatively weak flow.

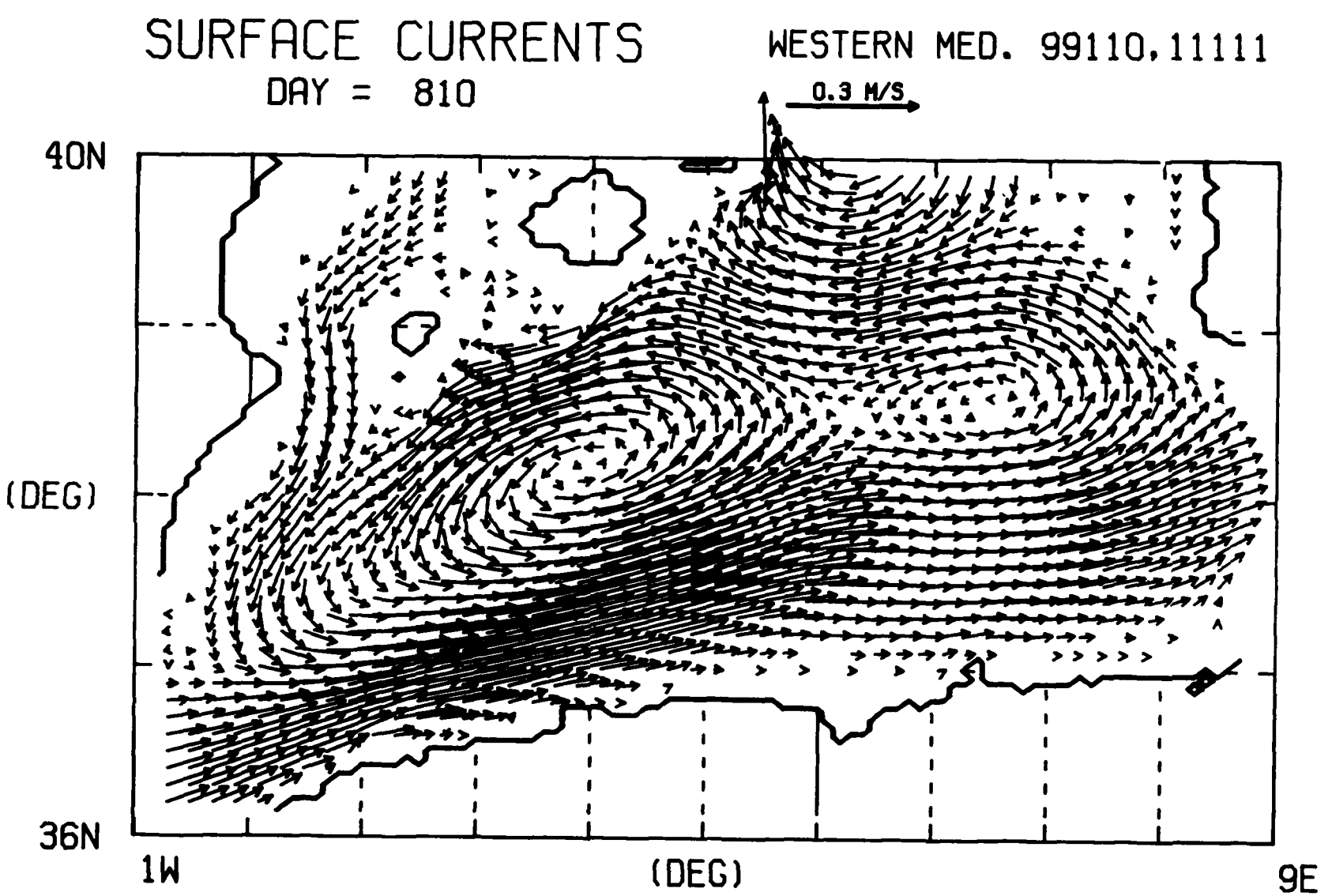
SURFACE CURRENTS
WESTERN MED. 99110,11111
DAY = 810
0.3 M/S
40N
(DEG)
36N
1W
(DEG)
9E
MAX PLØTTED SPEED = 0.24 (M/SEC)

Fig. 8a

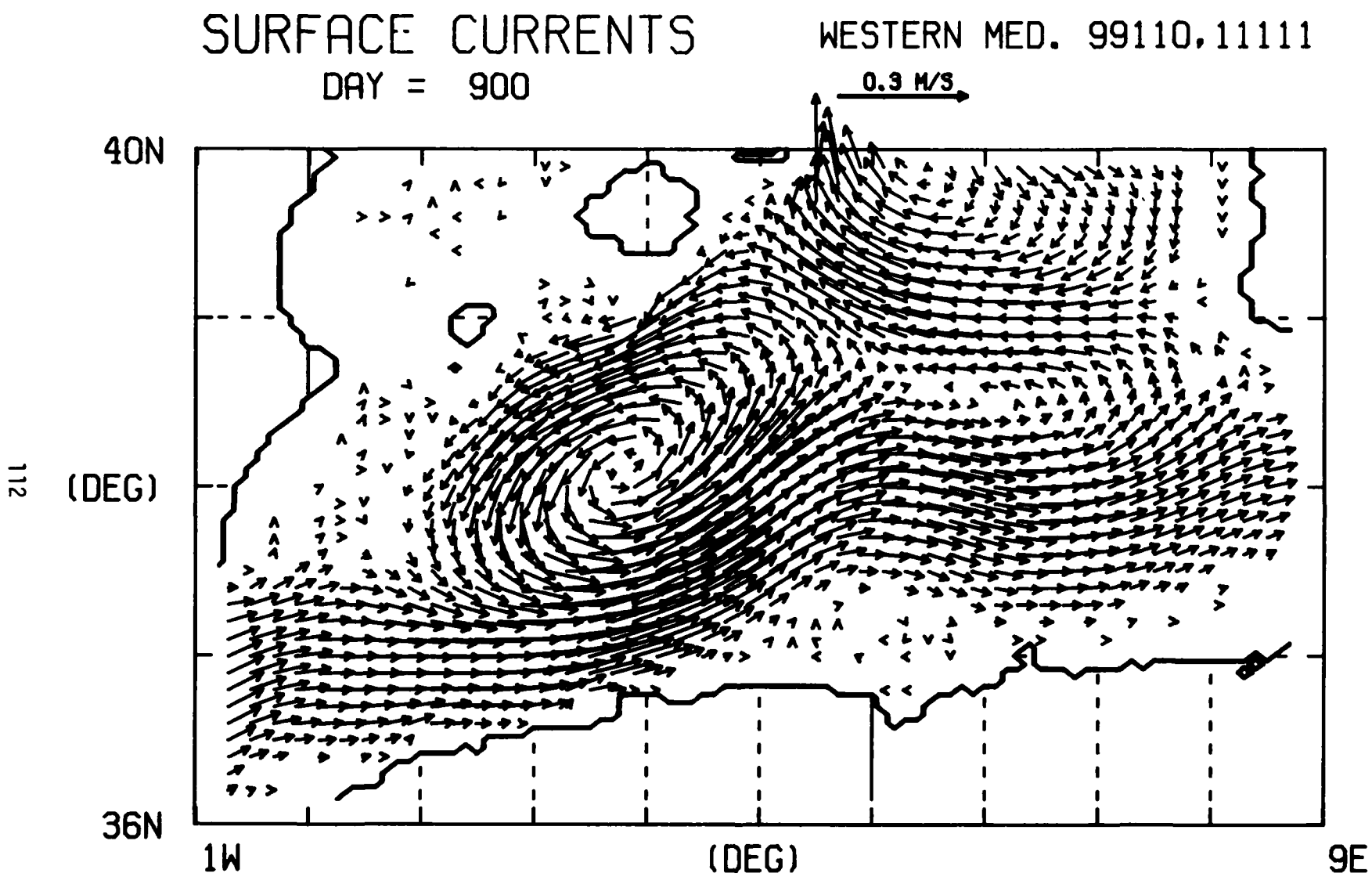
SURFACE CURRENTS
WESTERN MED. 99110,11111
DAY = 900
0.3 M/S
40N
(DEG)
36N
1W
(DEG)
9E
MAX PLØTTED SPEED = 0.20 (M/SEC)

Fig. 8b

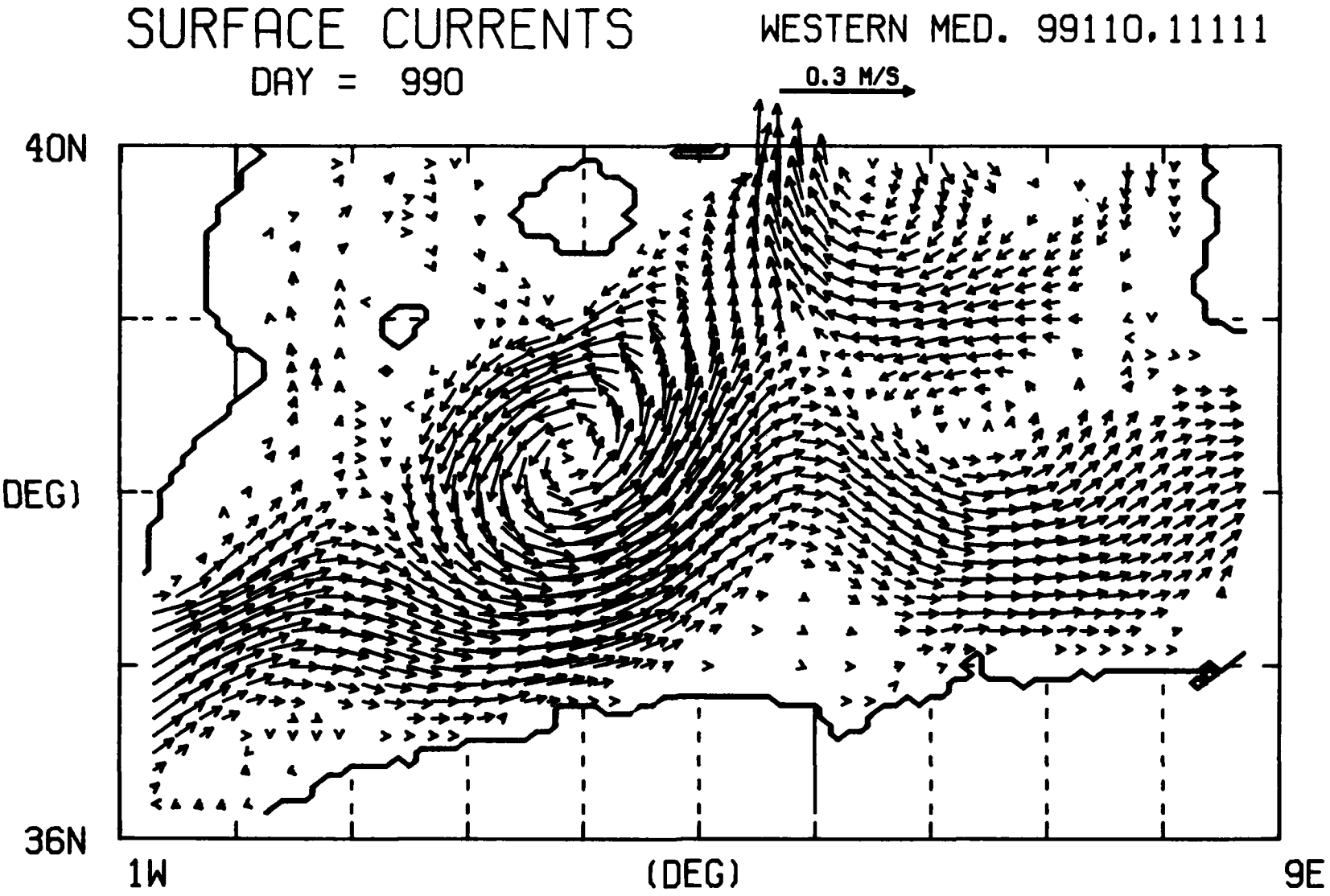
SURFACE CURRENTS
WESTERN MED. 99110.11111
DAY = 990
0.3 M/S
40N
(DEG)
36N
1W
(DEG)
9E
MAX PLØTTED SPEED = 0.16 (M/SEC)

Fig. 8c

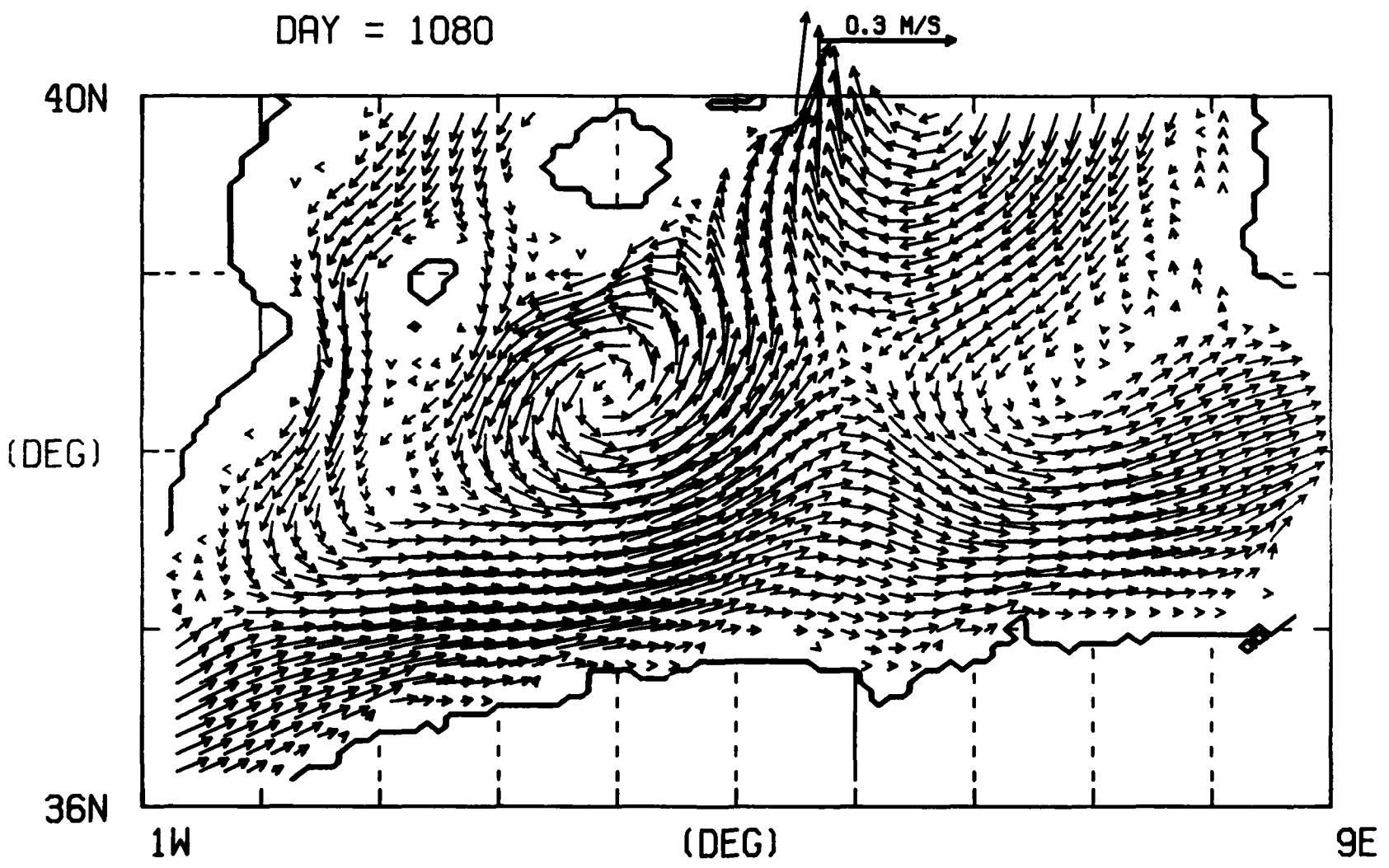

MAX PLØTTED SPEED = 0.22 (M/SEC)

Fig. 8d

This paper is not to be cited without prior reference to the authors

XXIXth Congress and Plenary Assembly, CIESM
Lucerne, October 11-19, 1984
Physical Oceanography Committee

Computational Methods for Two Problems in Air-Sea Interaction

B. Edward McDonald, S. A. Piacsek, and Gretchen Dawson
Naval Ocean Research and Development Activity
NSTL Station, MS 39529, USA

Abstract. This paper addresses mathematical - computational techniques currently under development for solving elliptic equations in the investigation of wind - driven ocean dynamics in large and small scale limits.

Resume. Cette communication concerne les techniques mathematiques et numeriques en voie de developement pour la solution des equations elliptiques rencontrees dans les investigations de l'evolution dynamique des oceans soumis a l'action des vents dans la limite des grandes et petites echelles d'espace.

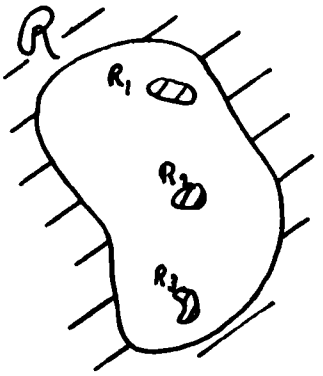

The large scale problem under consideration calls for solution of an elliptic equation for the mass transport stream function Ψ in a multilayer rigid lid formulation [1] of mesoscale wind driven circulation in a basin of irregular shape containing islands. For constant depth one must solve $\nabla^2\Psi = \omega$ in the basin $\mathcal{R}$ with $\omega = 0$ in the interior of each island R_n. (The constant depth case is shown for purposes of illustration. In our rigid lid model[2], topography introduces variable coefficients into the equation and requires special attention to layer intersections with the sloping bottom). Boundary conditions are $\Psi = 0$ on the basin boundary $\partial\mathcal{R}$ and $\Psi = \Psi_n =$ constant on each island boundary ∂R_n, corresponding to free slip. The Ψ_n values must be such that the circulation around each island will agree with circuit integrals of the momentum equations. When applied formally, this condition leads to a capacitive matrix model which, in its entirety, is expensive to use. We offer an iterative technique in which no circuit integral monitoring is necessary. Our method generates sheet vorticity along each shoreline such that the proper circulation and free slip conditions are met. The technique uses a symmetry which arises in a particular solution for two dimensional flow past a circular cylinder:

$$\tilde{\Psi} = \sum_m a_m (r/r_0)^{\pm m} e^{im\theta}$$

where $+m$ is used for $r<r_0$ and $-m$ for $r>r_0$. This solution describes a vortex sheet on the surface $r = r_0$ of the cylinder with no flow at

infinity. With properly chosen expansion coefficients, this solution may be superimposed upon an arbitrary streamfunction Ψ_o whose vorticity is zero inside r_o to give the free slip condition at r_o, no flow interior to r_o, and leave the flow unchanged at infinity. The symmetry which can be exploited is that the radial derivative of $\tilde{\Psi}$ changes sign but not magnitude at r_o. This means that when $\Psi_o + \tilde{\Psi}$ = const for $r<r_o$, the sheet vorticity at $r = r_o$ is exactly <u>twice</u> that which would be created by setting to zero the interior flow due to Ψ_o. With this brief justification, one argues for a simple iterative prescription for the multiple island problem with an overrelaxation factor of two. One starts with a solution for arbitrary sheet vorticity at shorelines and computes velocities everywhere including land areas. One then computes the vorticity created when velocities are set to zero on land. Exactly twice this vorticity is added to the forcing term ω and the iteration is repeated until convergence is obtained.

The small scale problem concerns the solution of Poisson's equation for the velocity potential for finite amplitude deep water waves with boundary values given on the surface (vorticity is assumed to reside in a thin surface sheet). A generalized Bernoulli equation[3] is used to forecast the tangential component of surface velocity from known or prescribed surface stresses. One solves for the velocity potential in the underlying flow.

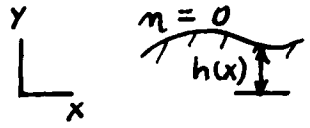

This calls for solution of a Dirichlet problem with values given on the arbitrarily wavy surface. A new iteration proceedure allows rapid solution via fast Fourier transform after conformal mapping to a flat surface. The mapping[4] is

$$x+iy = \xi+i\eta + \sum_{k\geq 0} A_k\, e^{-ik(\xi+i\eta)}$$

where $\eta = 0$ on the wavy surface $y = h(x)$. The coefficients A_k are obtained in the following iteration which converges for wave slopes less than unity. $\xi_n = (n-1)\,\delta\xi$, $A_k = 0$

$$\begin{cases} x_n = \xi_n + Re \sum A_k e^{-i\xi_n} \\ y_n = h(x_n) \quad \text{by interpolation} \\ A_k = FFT^{-1}(x+iy-\xi), \quad \text{de-aliased.} \end{cases}$$

1. W. R. Holland and L. B. Lin, J. Phys. Oceanog. 5, 642, 1975.
2. B. E. McDonald, P. W. May, S. A. Piacsek, and R. H. Preller, CIESM 1982.
3. B. E. McDonald and J. M. Witting, J. Comp. Phys. 56, 1984.
4. E. A. Caponi, B. Fornberg, D. D. Knight, J. W. McLean, P. G. Saffman, and H. C. Yuen, J. Fluid Mech. 124, 347, 1982.

UNCLASSIFIED

SECURITY CLASSIFICATION OF THIS PAGE

AD-A162019

REPORT DOCUMENTATION PAGE

1a REPORT SECURITY CLASSIFICATION Unclassified	1b RESTRICTIVE MARKINGS None
2a SECURITY CLASSIFICATION AUTHORITY	3. DISTRIBUTION/AVAILABILITY OF REPORT Approved for public release; distribution is unlimited.
2b DECLASSIFICATION/DOWNGRADING SCHEDULE	
4 PERFORMING ORGANIZATION REPORT NUMBER(S) NORDA Technical Note 315	5. MONITORING ORGANIZATION REPORT NUMBER(S) NORDA Technical Note 315
6 NAME OF PERFORMING ORGANIZATION Naval Ocean Research and Development Activity	7a NAME OF MONITORING ORGANIZATION Naval Ocean Research and Development Activity
6c ADDRESS (City, State, and ZIP Code) Ocean Science Directorate NSTL, Mississippi 39529-5004	7b ADDRESS (City, State, and ZIP Code) Ocean Science Directorate NSTL, Mississippi 39529-5004
8a NAME OF FUNDING/SPONSORING ORGANIZATION Naval Ocean Research and Development Activity 8b OFFICE SYMBOL (If applicable)	9 PROCUREMENT INSTRUMENT IDENTIFICATION NUMBER
8c ADDRESS (City, State, and ZIP Code) Ocean Science Directorate NSTL, Mississippi 39529-5004	10 SOURCE OF FUNDING NOS. PROGRAM ELEMENT NO. / PROJECT NO. / TASK NO. / WORK UNIT NO.

11 TITLE (Include Security Classification)
Contributions to the Oceanography of the Western Alboran Sea

12 PERSONAL AUTHOR(S)
Henry Perkins, editor

13a TYPE OF REPORT	13b TIME COVERED	14 DATE OF REPORT (Yr., Mo., Day)	15. PAGE COUNT
Final	From _____ To _____	April 1985	118

16 SUPPLEMENTARY NOTATION

17 COSATI CODES			18 SUBJECT TERMS (Continue on reverse if necessary and identify by block number)
FIELD	GROUP	SUB. GR.	Mediterranean Sea, Alboran Sea, gyre, ocean fronts

19 ABSTRACT (Continue on reverse if necessary and identify by block number)

This volume includes papers presented during the XXIXth Congress and Plenary Assembly of the International Commission for the Scientific Study of the Mediterranean Sea (CIESM) in Lucerne, Switzerland October 11-19, 1984. The authors are a loose association of scientists from the Donde Va? project and from NORDA. The papers will also be reported in the Rapports et Process-Verbaux of CIESM, where they will be condensed to meet the prescribed two-page limit of that report. Their format here is enlarged primarily by the inclusion of the figures that accompanied the original presentations.

20 DISTRIBUTION/AVAILABILITY OF ABSTRACT	21. ABSTRACT SECURITY CLASSIFICATION	
UNCLASSIFIED/UNLIMITED ☐ SAME AS RPT ■ DTIC USERS ☐	Unclassified	
22a NAME OF RESPONSIBLE INDIVIDUAL Henry Perkins	22b. TELEPHONE NUMBER (Include Area Code) (601) 688-4736	22c. OFFICE SYMBOL Code 331

DD FORM 1473, 83 APR EDITION OF 1 JAN 73 IS OBSOLETE

UNCLASSIFIED

SECURITY CLASSIFICATION OF THIS PAGE

END

FILMED

1-86

DTIC